SAPIENZA
UNIVERSITÀ DI ROMA

SCUOLA DI DOTTORATO "VITO VOLTERRA"
DOTTORATO DI RICERCA IN FISICA – XXII CICLO

Equilibrium and off-equilibrium mechanisms for slow dynamics in glass-forming liquids

THESIS SUBMITTED TO OBTAIN THE DEGREE OF
DOCTOR OF PHILOSOPHY ("DOTTORE DI RICERCA") IN PHYSICS
OCTOBER 2009

BY

Chiara Cammarota

Program Coordinator
Prof. Enzo Marinari

Thesis Advisors
Prof. Enzo Marinari
Dr. Andrea Cavagna

Contents

Introduction

Two parts compose this Ph.D. thesis. Both of them concern the most significant feature of glass-forming liquids, namely the impressive growth of the relaxation time on lowering the temperature.

Once the supercooled phase is reached and crystallization avoided, the relaxation time starts to increase very sharply with decreasing temperature. It soon exceeds the experimental time scale. When this happens the equilibrium of the liquid cannot be achieved and the material, although structurally disordered, behaves mechanically like a solid. It is a glass. Conventionally, the quite sharp turning point in temperature where this change takes place has been called glass transition, T_g.

Many competing theories have been developed to explain the mechanism involved in such spectacular growth of the time scale. There have been mean field models, microscopic and phenomenological approaches, dynamical and thermodynamical theories. Still a full agreement on this problem has not been reached yet.

While the largest part of the theoretical effort has been devoted to the comprehension of the equilibrium issue, a large amount of experimental data on the non-equilibrium dynamics has been gathered. The non-equilibrium dynamics phenomenology is the most easily available piece of phenomenology of glass-forming liquids, simply because of the very large relaxation time they show.

In the low temperature non-equilibrium regime a kind of covariance emerges. The time, t_w, that the system has spent out-of-equilibrium, influences the phenomenology. The system ages. In this aging regime very interesting phenomena like memory and rejuvenation effects have emerged. This has attracted the attention to the non-equilibrium dynamics of glasses too.

As in the case of the study of equilibrium, many theories has been proposed to enlighten the aging mechanism. Still, the full comprehension of the non-equilibrium dynamics is not attained.

In this thesis we report our numerical and theoretical contribution to the comprehension of the equilibrium and non-equilibrium dynamics of glass forming liquids.

The first part is devoted to the study of the equilibrium problem.

A common idea is that the growth of the relaxation time scale should be connected to the simultaneous growth of a length scale. This is true for critical phe-

nomena: in proximity of the transition point the relaxation time τ grows as a power law of the correlation length ξ: $\tau \sim \xi^z$. The idea of cooperativity has often been suggested also in the study of disordered systems both in dynamical approaches (e.g. dynamical heterogeneity) and in different thermodynamical theories (e.g. the Mosaic theory that we will see in detail, the frustration-limited-domain theory, and the Voronoi defects theory). In this case the role played by activation lead us to expect an exponential law instead of a power law: $\tau \sim \exp(\xi^\psi/T)$.

An interesting picture is provided by the Mosaic theory. This theory is also known as the Random First Order Transition theory for it has been inspired by the paradigm of nucleation of first order theory. In the following we will always refer to this theory as to the Mosaic theory. The Mosaic is a purely thermodynamic theory which explains the mechanism of the slowing down of the dynamics. According to this theory the low temperature equilibrium phase of a liquid is dominated by an extensively large number of amorphous states. The logarithm of this number per unit volume is called configurational entropy. Readapting an argument of Adam and Gibbs, the Mosaic claims that the smaller the configurational entropy, the larger is the typical size of the cooperative regions. In this way an increasing length scale is introduced in the equilibrium dynamics of the system. Thus, the growth of the relaxation time is explained in terms of this increasing correlation length. The Mosaic theory recovers a generalized version of the Voghel-Fulcher-Tamman law, i.e. the most famous phenomenological law for the relaxation time growth.

We want to remark here that the Mosaic lies in a theoretical framework which suggests the existence of a downright thermodynamic transition between the liquid phase and a thermodynamic glassy phase. The direct experience of this putative transition point, i.e. discontinuities in the thermodynamic variables or in their derivatives, is not possible. This is one of the major objections to this theoretical framework. In fact, if this theory described only an unattainable transition point, it would be quite useless. The reply is that the core of the Mosaic theory is in the mechanism it proposes for the explanation of the dynamical arrest. The existence of an underlying possible thermodynamic transition is only a byproduct. If the configurational entropy vanished at finite temperature, the cooperative length scale should diverge and the configurational entropy should be discontinuous to not further decrease. This would signal a thermodynamic transition. Otherwise no thermodynamic transition would be implied. On the contrary, the connection between time and length scale and the mechanism for the enlarging of the cooperative regions is the core of the theory. It provides a description of the low temperature equilibrium dynamics in the temperature range where the equilibrium phenomenology can be directly experienced.

The very interesting theoretical results of this theory in explaining the slowing down of the dynamics are based on the existence of different metastable states. The problem is: what a metasteble state is? When we can in fact define metastable states in real systems? When the description of the system as a simple liquid fails? When the multi-state description provided by the Mosaic theory is justified? Only the landscape of the potential energy can account for the possible presence of mi-

nima deep enough to slow down the dynamics. However, in the real space it is not present any structural indication of the difference between two states. If metastable states really existed, they would look equally amorphous.

In the case of coexistence between two traditional phases, e.g. crystal and liquid, the order parameter distinguishes the spatial regions in the two different phases. Nevertheless the fingerprint of the coexistence is the surface tension. The free-energy density cost of the interface between the two phases. In the same way we can operatively define the existence of different amorphous states as long as the interface cost of their contact is nonzero.

Imagine to choose two decorrelated configurations belonging to the high temperature liquid state. We can put them in contact with each other. We expect that the stress due to the contact between them does not remain localized at the interface. The configurations can freely rearrange to find a perfect matching at the boundary so to pay nothing. On the other hand; two low temperature configurations belonging to different amorphous states experience an higher rigidity in the reorganization and they do not relax the interface stress: in this case there is a finite surface tension. The first part of this thesis deals with the direct investigation of what we have just sketched. We will develop in detail the consequences of our results finding an estimate of the surface tension between distinct amorphous configurations. We will also study the distribution of the surface tension between different pairs of states and the large time relaxation of the interfaces at finite temperature.

An introductory part on the phenomenology is in the first chapter. The second chapter is a review of the most important theories for the slowing down of the dynamics. The original part of our work is presented in the third chapter, where a description of the numerical methods and of our set-up for the measure of the surface tension is given. Then, the zero temperature analysis is developed giving the results on the zero temperature surface tension value at different temperatures and its distribution. In the analysis of the interfaces emerges the roughening phenomenon certifying the physical meaning of the configurations we study. Finally, a finite temperature analysis is performed where a confirmation of the results at zero temperature is found. In this context the relaxation of the interfaces is studied in the activated picture and the scaling of the activation barriers with the linear size of interfaces is obtained. The final result of the finite temperature study is the recovering of the Voghel Fulcher Tamman law.

In the second part, we focus on the non-equilibrium problem.

Two different frameworks have emerged in the study of aging in disordered system. The first picture has been obtained from the exact solution of the dynamics of mean-field models. The non-equilibrium dynamics after a quench of the system from high temperature, T_i, to a value T_f below the dynamic transition temperature, T_c, can be described as a slower and slower, never ending, descent in the energy landscape. This descent takes longer and longer time as the systme go down in energy, since as the energy landscape flattens, the downhill directions are fewer and fewer. In this first picture the activated dynamics does not play a role

since mean field models have infinite barriers in the thermodynamic limit. On the contrary, the second framework is centered on activation. An activation mechanism for the dynamics is invoked in the case of coarsening in disordered system, in a real space approach. Activation is at the basis of a phenomenological approach in phase space, the trap-model proposed by J. P. Bouchaud.

It has been pointed out that the trap-model is a schematic model for a quite universal aging mechanism. The Bouchaud's trap model is the simples example of the so called *arcsine law* of the aging. Other more common models like the REM model and the p-spin model seem to belong to this universality class. However, the mathematical proof of this has only been obtained in the case of an unusual rule for the dynamics. According to this rule, the waiting time in a configuration is only influenced by its energy depth. A more common and physically sounder dynamics is the Metropolis dynamics. Its single step between two configurations is determined by the difference between the initial and the final energy level. A very interesting issue is to check whether the change in the rules of the dynamics influence the aging mechanism as to let it deviate from the arcsine law.

In the second part of this thesis we will report our numerical observations of the aging mechanism in the REM-like trap model of Bouchaud and in p-spin model to numerically re-obtain what has been mathematically proven. We will also try to extend the universal aging result to models with a more standard Metropolis dynamics.

In the fourth chapter, a phenomenological and theoretical introduction to the aging is given with particular attention to the Bouchaud's trap model. The results of our numerical study of the aging mechanism in two models and with two different dynamic rules are in the fifth chapter.

The results collected here have been published in:

- Chiara Cammarota, Andrea Cavagna, Giacomo Gradenigo, Tomas S. Grigera, Paolo Verrocchio. *Surface tension fluctuations and a new spinodal point in glass-forming liquids,* arXiv:0906.3868
- Chiara Cammarota, Andrea Cavagna, Giacomo Gradenigo, Tomas S. Grigera, and Paolo Verrocchio. *Numerical determination of the exponents controlling the relationship between time, length, and temperature in glass-forming liquids,* J. Chem. Phys. **131**, 194901 (2009)

Part I

Equilibrium dynamics

Chapter 1

Glasses and supercooled liquids

1.1 The glass

1.1.1 A definition of glass

A glass is a material as disordered as liquids, that behaves mechanically like a solid.

Solids have a crystalline structure. The molecules are arranged in a regular lattice and shows a well defined long range order. On heating the solid, the molecules vibrates around their position in the lattice until the crystal breaks at the melting point. The molecules then have a disordered arrangement. It is the liquid phase. There is a sharp distinction between the solid and the liquid state, i.e. the distinction between structural order and disorder.

As liquids, the microscopic structure of a glass is disordered, it looks exactly the same as a liquid. As an example we consider the radial distribution function $g(r)$. It accounts for the probability of finding a particle at distance r from a reference particle:

$$g(r) = \frac{1}{N}\frac{1}{4\pi r^2 \rho}\left\langle \sum_i^N \sum_{j\neq i} \delta(r - r_{ij}) \right\rangle , \tag{1.1}$$

where N is the number of particles, ρ the density, and r_{ij} the distance between the particle i and the particle j. The radial distribution function $g(r)$ is good at reveal the microscopic structure of a particle system: the higher the degree of order in the system, the more the $g(r)$ is structured in term of peaks.

In Fig.1.1 examples of $G(r)$ are shown for a solid and a liquid. In a crystal the peaks are sharp and do decay slowly with increasing r. On the contrary, in a liquid and in a glass as well, the function shows broad peaks corresponding to consecutive shells around the reference particle. These peaks soon become weaker and broader the larger r, for the system lacks long range order.

The mechanical behaviour of a solid is characterized by elastic response to an external shear. The application of a shear to a solid along the *x-axis* produces a displacement, $u(x, y)$, proportional to the distance y from the level where the solid is kept fixed. In solids $u(x, y)$ is also independent from x. The shear strain, $s(x, y)$,

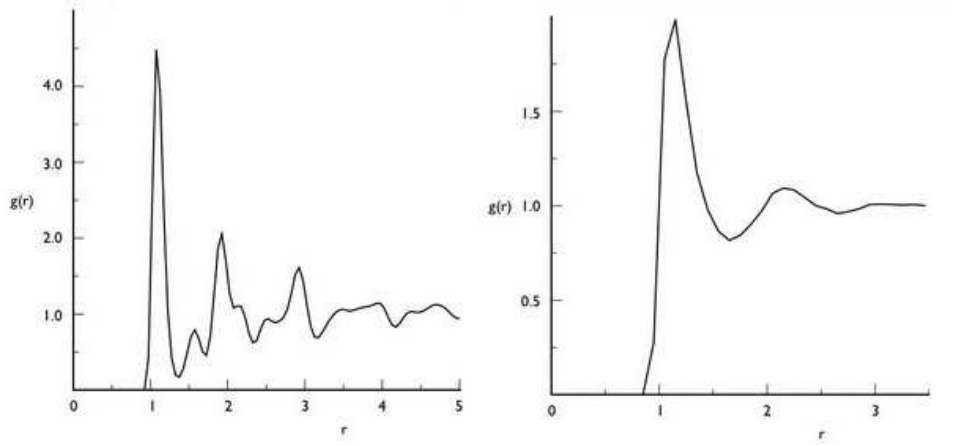

Figure 1.1. The radial distribution function for a solid (left panel) and a liquid (right panel).

defined as follows

$$s(x,y) = \frac{\partial u(x,y)}{\partial y} \,, \tag{1.2}$$

is thus constant in a solid and we will call it γ. Moreover solids respond elastically to a step shear strain. A stress σ arises proportional to the strain according to a factor G called elastic shear modulus:

$$\sigma = Gs(x,y) = G\gamma \,. \tag{1.3}$$

On the contrary the response of a liquid can be described by introducing a time-dependent shear modulus, the linear stress-relaxation function, $G(t)$. In time translation invariance (TTI) regime and using linear approximation, a step shear at time $t' = 0$ produces the following stress σ at time t

$$\sigma(t) = G(t)\gamma \,. \tag{1.4}$$

The important point is that the stress-relaxation function $G(t)$ in (1.4) is a decaying function of t. Thus for enough short time, liquids respond elastically to shear. The time scale below which liquids behave like solids is the so called shear relaxation time τ_R. Therefore, according to our initial definition of glasses, every liquid is a glass provided that it is observed for short enough times. However, commonly a material at low temperature is said to be a glass when its shear relaxation time is of the order or larger than the typical duration of an experiment. Thus we can rephrase the definition of a glass saying that a glass is a disordered material like a liquid that behave mechanically like a solid on a time scale comparable to the experimental one. The very distinctive phenomenological trait of the materials showing glassy behaviour at low temperature is in fact the impressive growth of the shear relaxation time without any remarkable change in the microscopic structure. The typical τ_R of a liquid is about 10^{-13} sec at high temperature but it can become of the order of $10 - 100$ sec after lowering the temperature by only a factor 2.

The most common quantity used to account for the increasing of the shear relaxation time is the viscosity, η. To introduce its definition we consider an arbitrary shear strain $\gamma(t)$ rather than a step strain. The produced stress is the consequence of many steps of strain:

$$\delta\sigma = G(t-t')\delta\gamma(t') \; . \tag{1.5}$$

If the strain is zero for $t < 0$, the total stress is

$$\sigma(t) = \int_0^t dt' G(t-t')\dot{\gamma}(t') \; . \tag{1.6}$$

When the shear strain is linear, $\dot{\gamma}$ is constant with time and (1.6) becomes

$$\sigma(t) = \dot{\gamma}\int_0^t ds G(s) \; . \tag{1.7}$$

The viscosity η is defined as the ratio of shear stress to linear shear strain in the asymptotic regime $t \to \infty$:

$$\eta = \frac{1}{\dot{\gamma}} \lim_{t\to\infty} \sigma(t) = \int_0^\infty ds G(s) \; . \tag{1.8}$$

In a normal liquid the stress-relaxation function decays faster than $1/s$ and the viscosity is finite. The classical connection between viscosity and shear relaxation time is recovered for Maxwell liquids. Maxwell proposed the simplest form of the stress-relaxation function:

$$G(t) = G_\infty \exp(-t/\tau_R) \; , \tag{1.9}$$

where G_∞ is the infinite frequency shear modulus. Using (1.9) in (1.8) we have in the Maxwell model

$$\eta = G_\infty \tau_R \; . \tag{1.10}$$

More in general the viscosity is related by (1.8) to the time scale on which the stress-relaxation function decays.

Recalling our last definition of a glass, we can introduce the glass transition (or dynamic glass transition) and the glass transition temperature T_g. T_g is the temperature at which the relaxation time exceeds the experimental time, t_{exp},

$$\tau_R(T < T_g) > t_{exp} \; . \tag{1.11}$$

Thanks to equation (1.10), it is common use to refer to the viscosity η for an equivalent definition of T_g:

$$\eta(T < T_g) > \frac{t_{exp}}{G_\infty} \; . \tag{1.12}$$

This definition can seem a bit strange, for it seems to depend on the experimental protocol. However in many glass forming liquids the increase of the relaxation time is so sharp that also a huge effort of experimentalists' patience cannot change significantly the position of T_g. For this reason it makes sense to define a glass transition. Conventionally a threshold in the relaxation time and thus in the equivalent viscosity was fixed to uniquely define T_g:

$$\tau_R(T_g) \sim 10^2 \,\text{sec} \qquad \eta(T_g) \sim 10^{13} \,\text{P} \; . \tag{1.13}$$

1.1.2 Beyond the crystal: glasses and supercooled liquids

How can we operatively avoid the crystal? The rapid slowing down of the dynamics can be experienced by lowering the temperature of the system below the melting temperature, T_m. In particular T_g usually occurs at about $\frac{2}{3}T_m$. However in most of the cases crystallization intervenes unless a specific cooling protocol is followed. A small digression on the crystallization process [1,2] will help us to find the proper cooling strategy, if any.

Below the melting temperature the crystal phase is the stable one. Its free energy density is lower than the free energy density of the liquid phase. The supercooled liquid is in its metastable phase. In this regime any crystal nucleus of linear size l formed by thermal fluctuations is less energetically costly than the same amount of particles in the liquid phase. Let δg be the free energy density difference between the liquid and the crystal, so that the bulk free energy gain is $\delta g l^d$. At the same time, the mismatch between the two different phases along the interface produces also a surface free energy cost, σl^{d-1} where σ is the surface tension. The total free energy change, $\Delta G(l)$, is

$$\Delta G(l) = \sigma l^{d-1} - \delta g l^d \, . \tag{1.14}$$

Small nuclei have the surface cost larger than the bulk gain, while the opposite is true for large enough ones. As such, the total free energy change has a maximum. The size l for which ΔG is maximum is the definition of the critical nucleus size l_{max}:

$$l_{max} = \frac{d-1}{d}\frac{\sigma}{\delta g} \, . \tag{1.15}$$

Nuclei with size larger than l_{max} are thermodynamically favored to enlarge. They originate the crystallization of the system. Finally the total free energy cost at the critical size is the barrier that the system have to overcome to crystallize. It reads as follows:

$$\Delta G(l_{max}) = \left(\frac{d-1}{d}\right)^{d-1} \frac{\sigma^d}{\delta g^{d-1}} \, . \tag{1.16}$$

In (1.14), (1.15), and (1.16) we disregarded irrelevant dimensionless geometric factor.

The time scale involved in the crystallization process can be obtained simply invoking the Arrhenius formula of activation. As we saw, the barrier is represented by the free energy involved in the formation, i.e. nucleation, of a critical nucleus of size l_{max}. Thus the leading time scale is the nucleation time:

$$\tau_N = \tau_0 \exp\left(\frac{\Delta G(l_{max})}{k_B T}\right) = \tau_0 \exp\left(\frac{(d-1)^{d-1}}{d^{d-1}} \frac{\sigma^d}{k_B T \delta g^{d-1}}\right) \, , \tag{1.17}$$

where k_B is Boltzmann's constant and τ_0 is a prefactor including the system's volume term. A wrong, but harmless assumption for the time being is that τ_0 does not depend on T. We also note that σ mildly changes with the temperature, especially around T_m. Thus the temperature dependence of τ_N comes only from δg and the

explicit term T in the exponential. By definition of melting point, i.e. the point at which the liquid and the crystalline phase have the same free energy, we have $\delta g = 0$ at T_m. The nucleation time diverges at $T = 0$ and at $T = T_m$, and it has a minimum, τ_{min}, at an intermediate temperature, T_{min}. At T_{min}, the crystallization process takes the smallest time, and therefore this is the most delicate point. In practice, for a good cooling protocol we have to stay well below the time τ_{min} in reaching the temperature T_{min}.

A cooling protocol is defined by its cooling rate, $r(T)$, the temperature variation per unit time:

$$r(T) = \frac{dT}{dt} \, . \tag{1.18}$$

Using a linear cooling rate, the constant r has to be larger than roughly the inverse of the minimum nucleation time, τ_{min}. Indeed a slower cooling process would leave to the system enough time to crystallize. From a theoretical point of view the crystallization is thus avoided if the cooling is fast enough. However, the realization have to deal with experimental limits and the fact that measuring τ_{min} is far from trivial.

Hitherto, we focused only on glasses, materials out of equilibrium. Deepening our study of glassy phenomenology and the theoretical questions about glasses reveals very interesting physics in the supercooled equilibrium phase. We listed the difficulties which arise in the experimental study of glasses, but the equilibrium of the supercooled phase is even harder to detect, and sometimes impossible.

First of all a remark on metastability and equilibrium is required. In principle it should be unfair to talk about equilibrium properties of a metastable phase like the supercooled liquid. The 'by definition' equilibrium phase is only the stable one. However as far as, after a small 'equilibration' time, time translational invariance (TTI) holds, we will talk about equilibrium also in supercooled liquids. Only crystallization would unveil metastability. In other words, the measurements have to be performed during TTI regime and before crystallization. The definition of equilibrium for the metastable phase is possible only if $\tau_N \gg \tau_R$. Under this condition it is always possible to measure the equilibrium properties of the system as long as $\tau_R \ll t \ll \tau_N$.

The validity limit of metastable equilibrium is the kinetic spinodal point. The spinodal temperature T_{sp} is defined as follows,

$$\tau_N(T_{sp}) \sim \tau_R(T_{sp}) \, . \tag{1.19}$$

Below T_{sp} no equilibrium measurements can be performed on the system. The only equilibrium phase is the crystal and the only amorphous phase is the off-equilibrium one: the glass.

The formation of the supercooled phase is quite complicated [3]. Firstly, the simple linear cooling protocol inevitably fails to keep the system in the supercooled phase. To avoid crystallization the cooling rate has to be higher than the τ_{min}^{-1}. However, the relaxation time τ_R increases when the temperature is decreasing. Thus the fast cooling protocol will sooner or later push the system out of equilibrium. Only a non linear route with a fast initial rate and a slower cooling

for low temperatures can avoid both crystallization and falling off-equilibrium. Secondly the existence in some cases of the spinodal point prevents from any equilibrium measurement below T_{sp} simply because the metastable equilibrium cannot be defined.

We remark that the spinodal point exists only in some cases. If it was the converse, at very low temperature only the crystal phenomenology would be accessible and the existence of an amorphous deep-cooled phase would clearly be a figment of our imagination. On the contrary, the existence of a cool amorphous phase is perhaps the most debated question in the glass community.

Kauzmann was the first to suggested the spinodal point as solution of this question in the late 40s [4]. In fact some theoretical arguments were developed taking into account the kinetic origin of the nucleation prefactor [1,2]. As result, the proof of an unavoidable spinodal point has not been achieved. On the other hand, the study of elastic properties of supercooled liquids has revealed a mechanism that can inhibit nucleation [5, 6]. When $\tau_N \sim \tau_R$ the formation of a crystal nucleus with typically different specific volumes carries an extra energetic price due to the elastic response of the liquid ($G(\tau_N) \neq 0$). As a consequence the thermodynamic drive to nucleation is depressed and the nucleation time increases. In this way the kinetic spinodal can be completely suppressed. Therefore, in some systems the supercooled liquid phase is well defined at whatever low temperature.

1.2 Phenomenology of glass-forming liquids

1.2.1 The glass transition

As we saw, the distinctive phenomenological trait of glass-forming liquids is the remarkably fast growth of the relaxation time upon lowering temperature. This feature was firstly revealed looking at the volumetric behaviour of liquids during linear cooling. The system is pushed out of equilibrium as the relaxation time becomes larger than the inverse cooling rate hence the volumetric behaviour changes.

In Fig.1.2 a picture of the volume contraction with isobarically lowering temperature is shown. In a narrow temperature range the slope of the volume-temperature curve rapidly changes. The temperature slope at lower temperature is generally smaller than the liquid one and comparable to that of a solid. Something similar to as a solidification process intervenes. However, it has very different features with respect to the crystallization process: $\alpha_p = V^{-1}(\partial V/\partial T)_p$ changes in a narrow but finite range of temperatures, the temperature at which the solidification intervenes does depend on the cooling rate, and also the final solid phase depend on its cooling history. The sudden change of the expansion coefficient is the glass transition.

As already mentioned, the linear cooling protocol is not able to keep the system in equilibrium as the relaxation time increases. In other words, the crossover temperature revealed by the α_p change was the T_g we already defined and the off-equilibrium solid-like state is the glass. The conventional definition of the glass

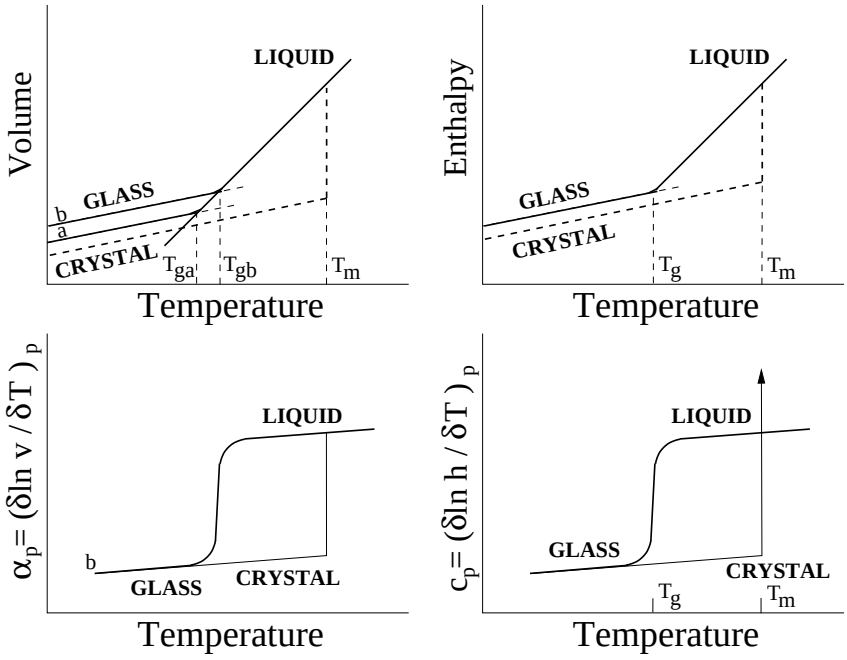

Figure 1.2. Left panel: volume contraction on lowering temperature. Below the correspondent thermal coefficient α_p. Right panel: Enthalpy diminution with temperature decreasing. Below the heat capacity. (Figure from [7]).

transition in (1.13) has its roots in the abrupt change of static quantities upon linear cooling.

A rescaling of the temperature by T_g reveals two ends of the dynamical slowing down, i.e. of the the viscosity growing, in liquids. The Angell plot, in Fig.1.3, shows the logarithm of the viscosity *vs.* T_g/T for different substances. The so-called *strong* liquids are purely Arrhenius:

$$\eta = \eta_0 \exp\left(\frac{\Delta}{T}\right) \tag{1.20}$$

Their viscosity increase is exponential with the inverse of temperature and no particular features are present at T_g. *Fragile* liquids, on the other hand, show a steepening of the viscosity just before T_g. Indeed the definition of a fragility parameter, f, is given at T_g as

$$f = \left(\frac{d\log(\eta/\eta_0)}{d(T_g/T)}\right)_{T=T_g} . \tag{1.21}$$

A classic way to describe the viscosity increase especially at intermediate and low temperatures is the so called Vogel-Fulcher-Tammann (VFT) law:

$$\eta = \eta_0 \exp\left(\frac{A}{T-T_0}\right) . \tag{1.22}$$

The virtue of the VFT law is in the classification of the liquids it achieves. Indeed

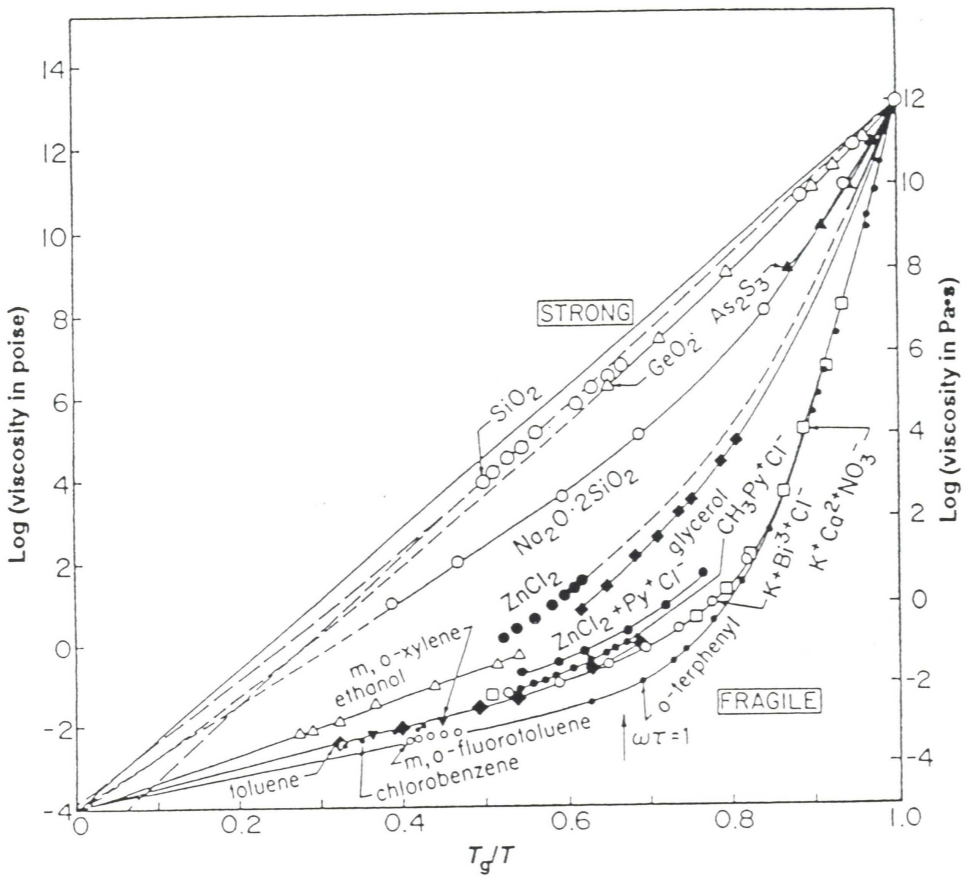

Figure 1.3. Viscosity increase on lowering temperature of many glass-formers. The variable T_g/T is on the x-axis.

within this parametrization, the fragility reads

$$f = k\left(1 + k\frac{T_0}{A}\right) , \tag{1.23}$$

where $k = \log(\eta(T_g)/\eta_0)$. Strong liquids correspond to the special case $T_0 = 0$ or have very small ratio T_0/A. Instead fragile liquids data seem to indicate a divergence of η at a finite temperature T_0. Moreover they have an high fragility value f.

The VFT law also produces the inspiring suggestion of free-energy barriers Δ diverging at finite temperature. Indeed, for T_0 quite larger than zero, the trend of (1.20) with $\Delta \sim 1/(T - T_0)$ is similar to the one of (1.22). In this picture the glass transition at T_g would be the secondary consequence of a diverging of the relaxation barriers.

Other descriptions of the growing viscosity have been proposed. For example at little larger temperature, the data lie quite well on a power law with a divergence at finite temperature, T_c. This fit fails at lower temperature simply because it predicts a divergence at $T_c > T_g$, where the relaxation time are very large but

still finite. We will see that this kind of description is the result of a dynamical theoretical frame, i.e. the Mode Coupling theory.

Summing up the feeling is that especially in fragile liquids something new is happening near the glass transition. The very fast slowing down around T_g seems the visible consequence of non trivial underlying change.

1.2.2 The dynamic correlation function

More light on this topic come from the observation of the dynamic correlation functions. The viscosity is the integral of a dynamic correlation function, i.e. the shear relaxation function, by (1.8). However a function contains much more information than its integral. The correlation functions detect how correlations decay with time. For $\phi_i(t)$ be an observable of the particle i at time t, the dynamical correlation function reads as follows

$$C(t', t'') = \frac{1}{N} \sum_{j=1}^{N} < \phi_j(t')\phi_j(t'') > \ . \tag{1.24}$$

In TTI regime $C(t', t'') = C(t)$ where $t = t' - t''$. At high temperature the system decorrelates over an intrinsic time scale τ following a simple exponential decay

$$C(t) = C_0 \exp(-t/\tau) \ . \tag{1.25}$$

As we saw, the time scale of the shear relaxation function rapidly increases with lowering temperature. Besides, a qualitative more important change develops. In Fig.1.4, the intermediate incoherent scattering function $F_s(q, t)$ is shown at different temperatures. This function is obtained replacing $\phi_j(t)$ with $\delta\rho_j(\mathbf{q}, t) = \exp(-i\mathbf{q}\mathbf{r}_j(t))$ in the (1.24). It corresponds to the Fourier transform of the self part of the Van Hove function

$$G_s(r, t) = \frac{1}{N} \sum_{j=1}^{N} \langle \delta(r - |\mathbf{r}_j(t) - \mathbf{r}_i(0)|) \rangle \ . \tag{1.26}$$

The functions in Fig.1.4 are the $F_s(q, t)$ at the wave-vector q of the main peak in the static structure factor $S(q)$, i.e. the Fourier transform of the radial distribution function $g(r)$ mentioned on the first section. Typically, at low temperature the time dependence of the correlation function has a plateau. Upon decreasing the temperature the simple exponential decay changes into a two step relaxation with a stretched exponential tail. In this regime, a first fast decay approaches the plateau and a second slow decay leaves the plateau. The former is the β relaxation, the latter strongly depends on the temperature and is called α relaxation.

The time scale leading to the increasing of the viscosity is the α relaxation one. But the correlation function has revealed the development of new features close to T_g. At first, the glass transition was defined by convention on the basis of the remarkable slowing down of dynamics. No thermodynamics is implied simply because some systems get off-equilibrium on human available time-scales. Now, separation of time-scales and non exponential relaxation of the tail are genuine

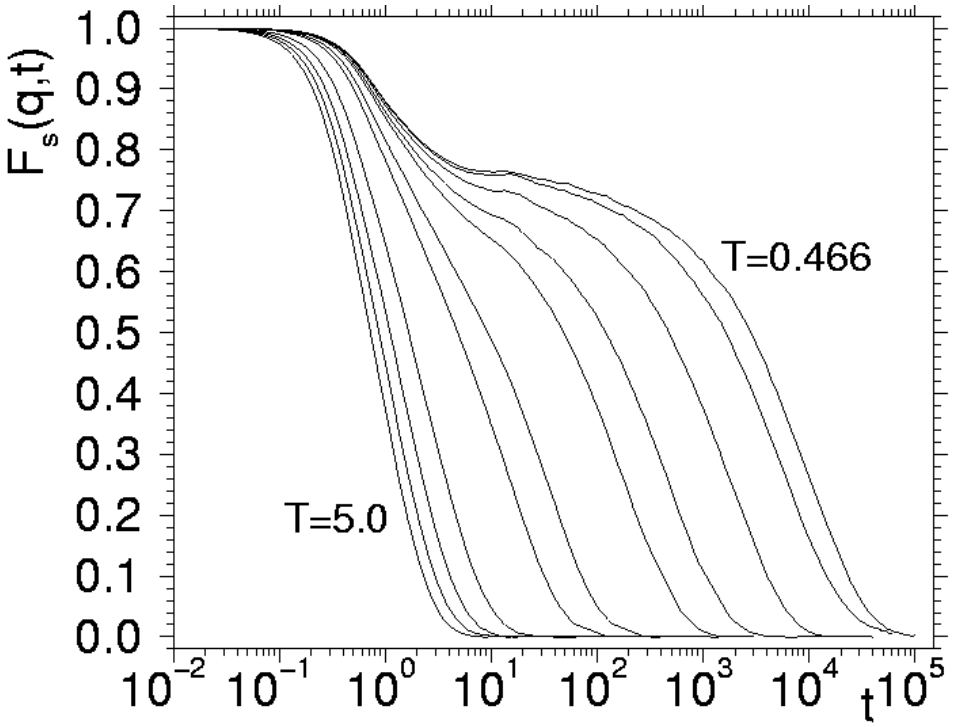

Figure 1.4. Time dependence of the incoherent intermediate scattering function of a mixture of Lennard-Jones particles during numerical simulation. (Figure from [8]).

equilibrium properties and they arise just before the glass transition. However, on the one hand, the only change in the equilibrium dynamical correlation function is continuous: it does not pinpoint any transition temperature. On the other hand, the glass transition appears to be something more than a kinetic consequence of the dynamical slowing down.

1.2.3 Kauzmann paradox

Kauzmann in 1948 [4] asked what should happen if an infinitely slow cooling protocol would be realized. This is not possible. However, an extrapolation of the equilibrium data of the liquid phase can be performed and compared with the crystalline features. Kauzmann focused its speculation on the specific heat. The thermal behaviour of the system under linear cooling is very similar to the volumetric behaviour (see Fig.1.2 right panels). The enthalpy changes continuously across T_g but its slope $c_p = (\partial h/\partial T)_p = T\,(\partial S/\partial T)_p$ has an abrupt change when the system falls in off-equilibrium regime. The observation of the specific heat reveals the entropy variation of the liquid. Following Kauzmann, we can look at the extrapolation of the equilibrium entropy results. For $T < T_m$,

$$S_{lq}(T) = S_{lq}(T_m) + \int_{T_m}^{T} \frac{c_{p,lq}(T')}{T'}\, dT' \tag{1.27}$$

$$S_{cr}(T) = S_{cr}(T_m) + \int_{T_m}^{T} \frac{c_{p,cr}(T')}{T'}\, dT' \,, \tag{1.28}$$

where lq stands for liquid and cr for crystal phase. The entropy difference thus reads

$$\Delta S(T) = \Delta S_m + \int_{T_m}^{T} \frac{\Delta c_p(T')}{T'}\, dT' \,, \tag{1.29}$$

provided $S_m = S(T_m)$. $\Delta S/\Delta S_m$ *vs.* T/T_m is shown in Fig.1.5. The extrapolated

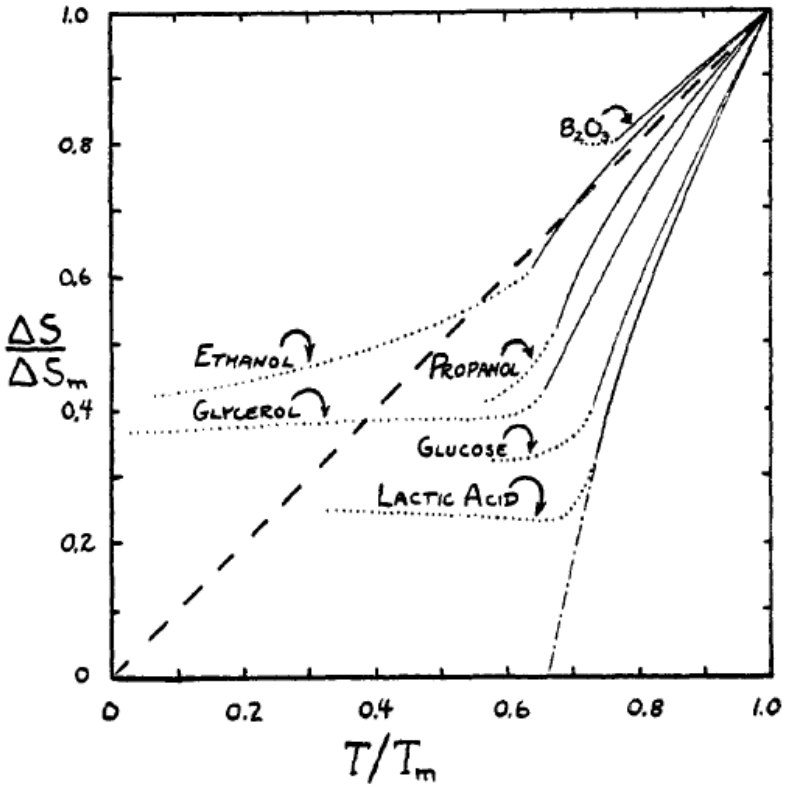

Figure 1.5. Extrapolation of the excess entropy of many substances by Kauzmann. (Figure from [4]).

excess entropy seems to vanish at non-zero temperature. If the extrapolation really held, there should exist a finite temperature T_k such that $\Delta S(T_k) = 0$:

$$0 = \Delta S_m + \int_{T_m}^{T_k} \frac{\Delta c_p}{T}\, dT \,. \tag{1.30}$$

Moreover at any $T < T_k$ the entropy of the supercooled liquid should be smaller than the solid one.

The same argument holds for the specific volume. However liquid's volume smaller than crystal is somewhat more likely than smaller entropy. Thus the phe-

nomenon of zero excess entropy at T_k was called entropy crisis or Kauzmann paradox. Kauzmann himself did exclude the occurrence of this strange phenomenon invoking the spinodal temperature before the entropy crisis. Today we know it is not true that the spinodal does always prevent the Kauzmann paradox. Only a hidden slackening of the entropy diminution at lower temperature would avoid the problem failing the extrapolation. But this dynamic-like transition is exactly what the equilibrium curve should not to do [4]. Thus the paradox still holds.

A very intriguing fact is that the Kauzmann temperature is often very close to the Vogel temperature T_0. This coincidence suggests the existence of a very low temperature thermodynamic transition at $T_k = T_0$ [9]. This equilibrium singularity should also control the dynamical phenomena. In any case, even without attributing all the dynamical glassy features to a singularity at T_k, the rapid decrease of the entropy towards the crystal value seems to be related to the dynamical slowing down.

1.2.4 The mean square displacement

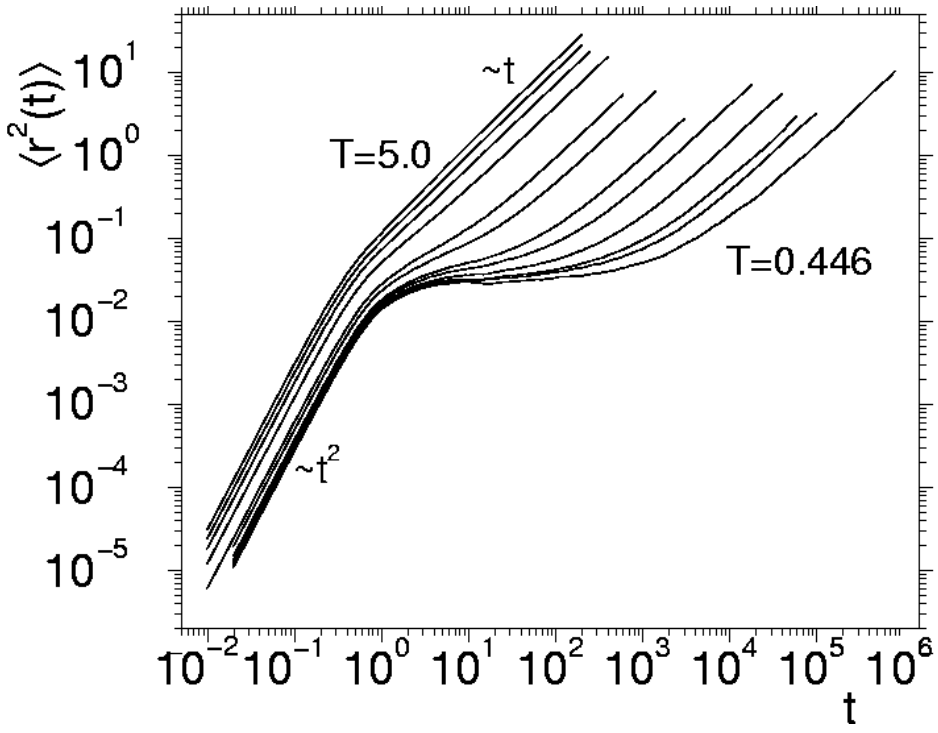

Figure 1.6. The mean square displacement of particles during computer simulations of a mixture of Lennard-Jones particles. (Figure from [8]).

In Fig.1.6, we report the mean square displacement (MSD) of a tagged particle:

$$\langle r^2(t)\rangle = \frac{1}{N}\sum_{i=1}^{N} |\mathbf{x}_i(t) - \mathbf{x}_i(0)|^2 \ . \tag{1.31}$$

At each temperature the small time regime is ballistic: the MSD grows with t square. At high temperatures this ballistic regime is followed by a diffusive regime for which $\langle r^2(t)\rangle \sim t$. On supercooling, between those two regimes a plateau develops. For intermediate times after an almost free motion, each particle remains confined in a finite region of the space. At the plateau the covered distance is smaller than the interparticle distance. Once again two time scales have emerged at low temperature. This phenomenon is strictly connected with the two step decay of the correlation function but it has a more direct physical meaning.

An explanation is given by thinking that each particle is trapped in a cage formed by its neighbors. After the ballistic motion, the particle starts to vibrate within the cage till it does find a way out. Later, the same trapping-escaping mechanism will repeat but on the log scale we can only appreciate the diffusive motion and not the trapping interplay. Also at high temperature the first neighbors surround the tagged particle but only at low temperature the cage effect influences the particle motion. The problem is why the cage is becoming harder upon lowering the temperature. Moreover how the particle can cross the neighbors wall? Does it find an entropic passage or does it push the other particles to let it move? We will see that both mechanisms play a role even if each will dominate in a different temperature regime.

1.2.5 Dynamical heterogeneities

Another remarkable feature of supercooled liquids is heterogeneity. The non exponential decay of the correlation function tail can be related to a homogeneous non-exponential relaxation of the system but also to many exponential relaxations involving different time scales. We cannot exclude the first explanation since spin glass mean field models reveals non exponential and, by definition, homogeneous relaxation. However heterogeneity in glassy system can be directly experienced revealing that the two mechanisms can be both involved in the real relaxation.

The heterogeneity also is a mobility feature. It cannot be observed in a single configuration of the liquid sample but only looking at two configurations separated by a time interval t. Provided that t is intermediate between the ballistic regime and the structural relaxation time, the heterogeneity emerges. In the second configuration with respect to the first, some particles have moved significantly more and other less than the average mobility. Moreover the highly mobile particles are grouped: patches with different mobility cover the system.

The same phenomenon can be observed following the motion of a single particle. The square displacement $|\mathbf{r}_i(t) - \mathbf{r}_i(0)|^2$ of a single particle i is a sequence of jumps and long periods during which the particle vibrates around a fixed position. We already observed the MSD of the particles, i.e. the average of this single particle signal. However the MSD cannot account for the wide distribution of the jumps during time. In fact, the distribution of the particle displacements is quantified just by the self part of the Van Hove function, $G_s(\mathbf{r}, t)$, defined in (1.26). It is the real space counterpart of the self intermediate scattering function, i.e. the function which shows the two step relaxation. In an isotropic Gaussian diffusive

process the Van Hove function depends only on the modulus of $\mathbf{r}$ and self part $G_s(r,t)$ reads

$$G_s(r,t) = \frac{1}{(4\pi D_s t)^{3/2}} \exp\left(-\frac{r^2}{4D_s t}\right) , \tag{1.32}$$

where D_s is the diffusion coefficient. On the other hand in deep supercooled liquids, the rare large jumps produce in the $G_s(r,t)$ fat tails better described by exponential decay

$$G_s(r,t) \sim \exp\left(-\frac{r}{\lambda(t)}\right) . \tag{1.33}$$

Again the fat tails enhance the qualitative difference between the relaxation of a viscous liquid and a normal liquid with Gaussian diffusion.

We can thus follow the single particle in space and time: it firstly vibrates into its cage then rapidly changes position. This happens typically in the meanwhile its neighbors reveal an high mobility. What is the mechanism behind such a heterogeneous relaxation mechanism is still not completely understood. What is clear is that, as we anticipated, the heterogeneity at intermediate time scales contributes to the stretched exponential relaxation. Moreover it introduces the question about cooperativity. The presence of clusters of highly mobile particles suggests that the particle in the clusters are correlated in some way. This sets the basis for the definition of a dynamical correlation length which also grows with lowering temperature. We will come back on this topic later on.

The last important phenomenon we mention is the failure of the Stokes-Einstein (SE) relation at low temperatures. At high temperature, the validity of the SE relation ($D_s\eta/T = \text{cost.}$, see also (2.3)) means that the equivalence between different measures of the relaxation time holds. Observing a particle with radius R moving in a fluid the relaxation time τ can be measured in terms of the self diffusion coefficient, D_s, ($\tau \sim R^2/D_s$) and of the viscosity, η ($\tau \sim \eta R^3/T$). At high temperature these two measures give the same relaxation time scale. On decreasing the temperature, D_s does not decreases as fast as the inverse of the viscosity, thus the SE relation fails.

The explanation of this phenomenon is in the heterogeneous dynamics of the system at low temperature. Indeed different observables probe in different way the large distribution of relaxation time scales. The more mobile particles influence the diffusion coefficient while the viscosity reveal the time scale needed to every particle movement. On the other hand, even at low temperature, the SE relation is restored provided that the diffusion is measured using an enough large probe. In this way many heterogeneities are averaged and the homogeneity is restored.

Chapter 2

Theories of the glass transition

2.1 Mode Coupling Theory

One of the most successful dynamical theories of the glass transition is the Mode Coupling Theory (MCT). According to MCT the glass transition is due to a structural arrest of the system. This result is obtained from the solution of an evolution equation for density fluctuation. There are no thermodynamical implications. The whole theory develops a feedback mechanism involving the viscosity [10]: first, the shear stress relaxation is a consequence of the diffusion in the system. Second, according to the Stokes-Einstein equation, diffusivity is the inverse of the viscosity. Third, the viscosity is proportional to the shear stress relaxation time, thus closing the feedback.

We describe at a phenomenological level the loop starting from the last condition. We recall equation (1.10):

$$\eta = G_\infty \tau_R \approx G_\infty \tau_{vib} + G_\infty \tau_s \, . \tag{2.1}$$

In (2.1) the shear relaxation time is the sum of vibrational, τ_{vib}, and structural contributions, τ_s. Since $\tau_s \sim D^{-1}$, we have

$$\eta \approx \eta_0(T) + b(T) D^{-1} \, , \tag{2.2}$$

with $\eta_0 = G_\infty \tau_{vib}$ and where $b(T)$ is a non increasing function of the temperature, given that both τ_s with fixed D and G_∞ are non increasing. The diffusion in a viscous liquid is ruled by the Stokes-Einstein relation:

$$D\eta = \frac{k_B T}{Ca} \, , \tag{2.3}$$

with a and C constants dependent on the microscopic details. Invoking (2.3), equation (2.2) becomes

$$\eta \approx \eta_0(T) + \frac{Ca}{k_B T} \, b(T) \eta = \eta_0(T) + B(T) \eta \, . \tag{2.4}$$

Finally we have for the viscosity:

$$\eta = \frac{\eta_0}{1 - B(T)} \, , \tag{2.5}$$

where $B(T) = Ca\, b(T)/k_B T$ decreases with increasing temperature. The feedback mechanism is in (2.5). It predicts a viscosity increase upon cooling and a dynamical divergence: the vitrification of the sample.

MCT develops this phenomenological picture on a more rigorous basis. It sets out similar feedback equations for $F(\mathbf{k}, t)$, i.e. the Fourier Transform of the Van Hove density-density correlation function $G(\mathbf{r}, t)$. As a result, MCT equations are predictive. They require as input only the static structure factor, the zero-time value of $F(\mathbf{k}, t)$. From this single piece of information, they give a good description to the dynamics of the relaxation process. The feedback mechanism enhances the slight changes in the static structure factor with the variation of T and the sample density, ρ.

MCT firstly takes into account the structural arrest shown by the correlation function: it predicts the decay to zero of $F(\mathbf{k}, t)$ for certain choices of T and ρ and the decay to a finite value for other choices of the same parameters. Secondly, the theory describes that the diffusion coefficient, $D(\propto \eta^{-1})$, goes to zero as a power law:

$$D \propto \left(\frac{T - T_c}{T_c}\right)^{\gamma} \propto \left(\frac{\rho_c - \rho}{\rho_c}\right)^{\gamma} . \tag{2.6}$$

According to the theory, relation (2.6) holds for $T > T_c$ (and $\rho < \rho_c$) and predicts the existence of a critical temperature (or critical density) for the structural arrest. Thirdly, the theory predicts even the way the correlation function approaches the plateau and leaves it for $T > T_c$. The two exponents a and b, involved in the predicted functional form of the correlation function, are also related to the exponent γ of D:

$$\gamma = \frac{1}{2a} + \frac{1}{2b} . \tag{2.7}$$

The MCT predictions are numerous and detailed. The theory has found a significant confirmation of its results in numerical and experimental data [11–14]. In particular, the description of the correlation function behaviour is confirmed. The exponent γ governing the growing of the long time-scale of the plateau ($\tau \propto D^{-1}$) agrees with relation (2.7), where a and b are independently obtained. The relaxation time, or the viscosity, follows quite well the power law increase with decreasing temperature predicted by MCT. However, this is true provided the observed temperatures are high enough. Whenever a reasonable subset of the relaxation time data is fitted to a power law, the result is a divergence at a temperature T_c above T_g. However above T_g, experimental data are available which directly negate the existence of any divergence.

The description of the structural arrest, i.e. the divergence of the relaxation time, in purely dynamical terms was the resolution of MCT. Actually this was not obtained. On the other hand, this elegant theory has accomplished the detailed description of the dynamics of liquids at temperature above T_c. This is a very interesting result. It is the highest level of the analytic effort in real liquids. But, it is not enough to explain the experimentally observed arrest of the dynamics.

An explanation of why this theory fails at low temperatures can be searched in the breakdown of the SE relation we introduced in the previous section. Indeed

the SE relation is one of the building block of the feedback mechanism in MCT.

The heterogeneous dynamics, the cage effect and the SE break down, all reveal the emergence of a spatial structure that is non uniform. This local description is what lacks to MCT, which has been also revealed to give the same results of a mean-field approach to spin-glasses, i.e. the p-spin model. Indeed the same self-consistent equations can be obtained via both these two very different approaches to the problem.

Briefly summarizing, MCT describes quite well the two step relaxation feature and the non exponential tail of the correlation function. However, it cannot entirely catch the highly heterogeneous physics of supercooled liquids.

2.2 The Adam-Gibbs-Di Marzio theory

In a finite dimensional system with short range interaction we cannot forget that the dynamics has to be a local process. In particular the relaxation of the system should proceed via the reorganization of finite regions. This phenomenon is emphasized by the heterogeneous dynamics described in section 1.2.

In general, the presence of static cooperative regions in physical systems implies a precise time-length relation. Indeed the larger the number of the particles involved in the rearrangement, the longer is the time for the rearrangement. In critical phenomena this relation is a power law

$$\tau \sim \xi^z \,, \tag{2.8}$$

with ξ the static correlation length. Instead, when activation is present, an exponential law is expected. In this case, the size of cooperative regions is introduced assuming a power law scaling of the barrier with the correlation length:

$$\tau \sim \exp\left(\frac{\xi^\psi}{k_B T}\right) \qquad \Delta = \xi^\psi \,. \tag{2.9}$$

A growing of the correlation length leads to an exponential increase of the relaxation time.

The first theory of supercooled liquids which involves the presence of correlated regions is the Adam-Gibbs-DiMarzio (AGD) theory of the *Cooperative Rearranging Regions* (CRR). This theory was directly inspired by the Kauzmann paradox. Indeed it connects the decrease of ΔS in (1.29) with the increasing size of correlated regions, and it uses (2.9) to link the correlation size with a relaxation time scale.

This AGD theory had one of its best results in the recovering of the VFT law (1.22) for the viscosity increase with lowering temperature. However the very novelty was the prediction of the viscosity growing via a purely thermodynamical theory. In this sense, it was the first thermodynamic theory for the slowing down of the dynamics in supercooled liquids.

In the late 50s, Gibbs and Di Marzio firstly proposed that the vanishing of ΔS, suggested by Kauzmann's extrapolation, was the signal of a thermodynamic second order phase transition [15]. According to his view, the liquid entropy reaches

the crystal one at T_k but it does not fall below the crystal entropy since it has a kink and it no longer decreases. The decrease of the liquid excess entropy and its vanishing at T_k is the unique thermodynamic origin of the dynamical slowing down.

The full argument was successively developed by Adam and Gibbs [16]. The low temperature relaxation proceeds via the reorganization of larger regions of correlated particles, the CRR. A CRR is the smallest region that can be rearranged independently from its surrounding. Hence the number of the available stable configurations in the system, $\mathcal{N}$, is the combinatorial sum of a small number, $\Omega > 1$, of stable configurations in each of the N/n CRRs:

$$\mathcal{N} = \Omega^{N/n} \,, \tag{2.10}$$

where N is the number of particles in the system and n is the typical number of particles in each CRR. The excess entropy with respect to the crystal, ΔS, reads as follows:

$$\Delta S = \frac{1}{N} \log \mathcal{N} \,. \tag{2.11}$$

Adam and Gibbs used the word 'stable configurations' to specify that $\mathcal{N}$ does not account for the vibrations. In other words, they considered ΔS as the excess entropy with respect to the crystal ($\Delta S = S_{lq} - S_{cr}$) since, on the one hand, the vibrational contribution is not present in $\mathcal{N}$ ($\log \mathcal{N}/N \sim S_{lq} - S_{vib}$) and, on the other hand, the vibrations around the stable crystalline configuration is the only contribution to the crystalline entropy ($S_{cr} \sim S_{vib}$).

Using (2.10) in (2.11), we have

$$\Delta S = \frac{\log \Omega}{n} \tag{2.12}$$

and finally

$$n(T) = \frac{\log \Omega}{\Delta S(T)} \,. \tag{2.13}$$

In this purely thermodynamic way Adam and Gibbs explained why the number of cooperatively rearranging particles increases when the excess entropy decreases.

Adam and Gibbs then linked their result to (2.9) fixing the following scaling of the Gibbs free energy barriers

$$\Delta \sim n \sim \xi^d \tag{2.14}$$

where, in this case, ξ is the linear size of the CRR. Thus they finally obtained the divergence of the relaxation time at the Kauzmann temperature where $\Delta S = 0$:

$$\tau = \tau_0 \exp\left(A \frac{n(T)}{k_B T}\right) = \tau_0 \exp\left(\frac{B}{T \Delta S}\right) \,. \tag{2.15}$$

The recovering of the super-Arrhenius increase of the relaxation time as T approaches T_k needs the simple thermodynamical argument we already met some sections ago: the excess entropy ΔS is the integral of the difference of the specific

heat. Integrating between T and the Kauzmann temperature T_k, where by definition $\Delta S = 0$, the (1.29) becomes

$$\Delta S(T) = \int_{T_k}^{T} \frac{\Delta c_p(T')}{T'}\, dT' \,. \tag{2.16}$$

Under the approximation of a small variation of Δc_p with temperature, the excess entropy becomes simply

$$\Delta S(T) = \Delta c_p \, \log\left(\frac{T}{T_k}\right) \sim \Delta c_p \, \frac{T - T_k}{T_k} \,, \tag{2.17}$$

and finally the (2.15) reads

$$\tau = \tau_0 \exp\left(B \frac{T_k}{\Delta c_p T(T - T_k)}\right) \,. \tag{2.18}$$

As we said, the VFT fit of the viscosity and the Kauzmann extrapolation suggest the coincidence between T_k and T_0. The AGD result in (2.18) is the theoretical justification of this finding. According to (2.18), the relaxation time diverges approaching T_k from above. Hence it has to exist an higher temperature (T_g) at which the relaxation time exceeds the experimental time scales. In other words, in the AGD picture the glass transition at T_g is only the high temperature onset of the true thermodynamical transition at lower temperature T_k. Moreover the AGD theory accounts for a further distinction between strong and fragile liquids. Indeed, the factor A in (1.22) is inversely proportional to the specific heat difference Δc_p, as such the fragility in (1.23) depends on the specific heat jump at the glass transition. The larger is the jump the more fragile is the liquid for the larger is the ratio T_0/A.

2.3 The landscape approach

The MCT theory and the AGD theory start from two opposite views of glassy sluggishness. The former excludes any thermodynamical influence on the dynamical slowing down while the latter is of purely thermodynamic origin. The AGD theory indeed explains the enlarging of the relaxation time in terms of activated dynamics and entropy diminution. These two theories seem incompatible. However, they pertain to the same physical picture. A unifying description emerges from the inspection of liquids' potential energy landscape.

In 1969 Goldstein emphasized the description of the system in the phase space [17]. It is the g-dimensional space, where g is the number of the degrees of freedom of the system. Each configuration of the system is a point in the phase space and corresponds to a specific potential energy level. The dynamics of the system is represented by the motion of the point over the potential energy manifold, that is the potential energy landscape.

Goldstein firstly argued that the equilibrium motion (the phase space exploration) of the system at low enough temperature corresponds to a series of activated events between different minima of the potential energy landscape. An

important remark is that the activated jump between two minima corresponds to the local rearrangement of only few particles n. In the meanwhile the surrounding particles are very weakly affected by this process. Hence the activation energy barriers are non-extensive.

We note here that this activation picture strongly influenced the following approach to the glass transition. It was immediately supported by the Arrhenius-like behaviour of the strong glasses. The fragility feature was interpreted as the result of the activation barriers growing with lowering temperature and the AGD theory followed from this way of thinking.

At high temperature, in Goldstein's picture, the thermal energy has to become comparable to the typical energy barrier and the dynamics proceeds no more through activation thus becoming very fluid. In this description, the crossover between activated and non activated dynamics is marked by the temperature T_x which Goldstein did estimate as

$$\tau(T_x) \sim 10^{-9} \text{ s}ec \,. \tag{2.19}$$

At temperatures smaller than T_x the equilibrium dynamics of the system proceeds via jumps and subsequent relaxations. In this picture, the two step feature of the correlation function is due to the vibration within a single minimum of the total potential energy (β relaxation) and to the jumps from minimum to minimum towards the complete decorrelation of the system (α relaxation).

The MCT theory and the p-spin model theory cannot catch the heterogeneity and the spatial structure of a local activated dynamics as the one described by Goldstein. Indeed their failure in the description of the activated dynamics is the reason why they miss the low temperature phenomenology of the system. This is confirmed by the coincidence between the temperature T_c, i.e. the limit of validity of the mean field like description, and the temperature T_x, i.e. the Goldstein crossover between activated and non activated dynamics. It has been verified [18, 19] that the relaxation time at T_c is often of order 10^{-9} sec, just what Goldstein estimated for the relaxation time at T_x.

Therefore Goldstein's picture reconciles the MCT dynamical results with the local activated thermodynamical provided e.g. by the AGD approach. These two regimes both characterize the physics of supercooled liquids in two different ranges of temperature. The common limit of these ranges is $T_c \sim T_x$. This temperature has become a reference temperature for a system approaching glassiness. It is a precursor of T_g: activated dynamics requires longer and longer relaxation times as the temperature decreases. Moreover, T_x is also better defined on a theoretical point of view.

What is still lacking to this picture is a better understanding of the crossover between the activated and non activated regimes. As already discussed introducing MCT, the predicted divergence at T_c is avoided by finite dimensional systems. Moreover both the dynamical and thermodynamical theories describe quite well the two step relaxation of the correlation function although with very different approaches and on mirroring temperature regimes. Therefore, the crossover at T_x is

a very smooth one. Again the topological study of the energy landscape is of great help.

This was firstly performed in the easier p-spin mean-field model [20]. In this system, below the Mode Coupling temperature T_c, equilibrium dynamics is confined within a single minimum. The system cannot jump away for the infinite barriers which surround the basin. In this case a very precise topological study of the minima is possible. For each minimum, it is possible to compute the eigenvalue of the matrix of second derivative, i.e. the Hessian (the first derivatives are zero by definition). A very useful quantity is the spectrum of the eigenvalues, the fraction of the eigenvalue equal to the value λ:

$$\rho(\lambda) = \frac{1}{g} \sum_{i=1}^{g} \delta(\lambda - \lambda_i) \; . \tag{2.20}$$

For each energy density level E, the resulting average spectrum $\rho(\lambda; E)$ has a compact structure which shifts to the left with increasing energy. This means that minima at lower energy density are stiffer than the higher ones having generally larger positive eigenvalue. Moreover it is possible to distinguish the energy at which the lower bound of the spectrum support, λ_{min}, becomes zero [21]. This energy value has been called *threshold* energy, E_{th}.

The importance of the threshold energy is in the fact that it marks the passage between stable minima and unstable saddles, i.e. a stationary point with at least one negative eigenvalue. This is a very significant feature in a mean field system where the stable directions are bounded by infinite barriers. The threshold energy marks the limit of the ergodicity restoration.

This topological transition has important consequences on the low temperature dynamics of the system. At low temperature, the thermal fluctuations bring the system energy, U, to exceed the bottom of the minima, E, it visits by the classical factor $k_B T/2$. Moreover for the highly complex landscape, different temperatures correspond to different density energy level of the bottom well, $E(T)$. In particular, the higher is the temperature, the higher is the level $E(T)$. The very remarkable fact is that the temperature at which the bottom well energy reaches the threshold value is the Mode Coupling temperature T_c [22]:

$$E(T_c) = E_{th} \; . \tag{2.21}$$

In other words, the Mode Coupling transition in the p-spin model is nothing else than the topological transition minima-saddles. The arrest of the dynamics predicted by MCT theory is the ergodicity breaking in a mean field model. Indeed the trapping of the system in only one minimum determines the non-zero infinite-time-limit in the correlation function. This limit is continuously obtained as the temperature approaches T_c from above: at high temperature the typical dynamical configuration lies in the neighborhood of an high energy saddle with many unstable directions. With lowering the temperature, the typical saddle has less and less negative eigenvalues. Therefore the evolution of the system takes longer and longer to find the way out. This increasing time scale is the slow mode of the two

step relaxation of correlation function [23]. Thus the distinction of fast and slow relaxation is not the consequence of an activated mechanism, impossible in a mean field model, but the result of a non-activated dynamics through fewer and fewer channels. This is the very reason why MCT and mean field models catch the two step relaxation of glassiness.

The same conceptual framework is applicable to the description of liquids' physics. Again, above T_c the dynamics is dominated by saddles. This is revealed by the instability index $k(E)$ [24–26]: the fraction of negative eigenvalue of the stationary points with density energy E. It becomes zero at a well defined energy threshold value:

$$k(E_{th}) = 0 \, . \tag{2.22}$$

The correspondence between temperature and energy density of the typical saddles allows the definition of T_{th} and the notable following check:

$$T_{th} \sim T_c \, . \tag{2.23}$$

The main difference, in this case, is the presence of the relaxation channel through activated dynamics. This is the reason why the dynamics is not completely arrested at T_c contrary to what expected by MCT theory. Instead it exists a continuous crossover between non-activated dynamics through very few unstable directions and activated mechanism across yet not-so-high barriers. This transition is not revealed by the correlation function. Indeed it shows a plateau above the MCT transition where the slow decay is due to the presence of few unstable directions rather than barriers. The activated dynamics is only quantitatively revealed by the increasing of the slow relaxation time scale. The two step relaxation can thus be described above and below T_c using non-activated and activated theories.

In the following we will focus to the very low temperature dynamics. In this regime the threshold has been crossed, thus we will need a landscape highly influenced description.

A key concept in the landscape description is the configurational entropy. As we saw, at low temperature, in the Goldstein scenario, the system is in a single amorphous minimum vibrating for long times. On the other hand ergodicity is not broken. Activation allows the phase space exploration through a large number of different minima. Therefore it is useful the distinction between two terms in the entropy of supercooled liquids. The first term accounts for the vibrations within each minimum, S_{vib}. The second term is due to the presence of an exponentially large number of minima: this is the so-called configurational entropy, S_c. This factorization holds on the quite reasonable assumption that the equilibrium dynamics of the system lies in similarly shaped wells. Therefore the number of configurations in liquids results from the product of the configurations within a single well and of the number of the minima, $\mathcal{N}$. Taking the logarithm, the product turns into a sum and the second term is exactly the configurational entropy:

$$S_{lq} = S_{vib} + S_c \, , \tag{2.24}$$

where

$$S_c = \frac{1}{N} \exp(\mathcal{N}) \, . \tag{2.25}$$

The configurational entropy is indeed non-zero if the number of the minima is exponentially large in the size of the system.

A further approximation is usually made. We can consider the vibrational entropy, S_{vib}, of each amorphous minimum not too different from the entropy of the crystal, S_{cr}. Actually they are not the same for the quite different shape of the crystalline minimum with respect to an amorphous one. Moreover, the difference is larger the higher is the temperature since the minima become more and more soft. However, in the deep supercooled regime the approximation

$$S_{vib} \sim S_{cr} \tag{2.26}$$

is acceptable and the (2.24) becomes

$$S_{lq} \sim S_{cr} + S_c \, . \tag{2.27}$$

This rationalization of the liquid entropy is useful to link the excess entropy ΔS, firstly introduced by Kauzmann, to a theoretical counterpart. Indeed from (2.27) we have

$$\Delta S = S_{lq} - S_{cr} \sim S_c \, . \tag{2.28}$$

We already met this theoretical picture of the liquid excess entropy in the AGD theory. Moreover it is one of key passages of other thermodynamic theories inspired by the seminal work of Adam and Gibbs.

2.4 The mean-field approach

A striking theoretical development with regards to the configurational entropy comes from the study of mean field models. In this context the description of the landscape complexity is more natural. In particular the very concept of metastable states as basins of the free energy is well defined. In finite dimensional systems, on the other hand, only the potential energy has a well defined complex landscape. There are important conceptual difference between a description in terms of free-energy and a description in terms of potential energy. Indeed, the free-energy landscape changes with the temperature variation while the potential profile does not. Moreover, the very basins structure of the potential energy is only partially reflected in the more physically interesting free-energy. In mean field, the infinite connectivity assures infinitely high barriers in the thermodynamical limit. Thus below the threshold the separation of the entropy in a vibrational and a configurational term is sharp.

For all these reasons, mean field models provide an easier and sharper understanding compared to the finite dimensional models.

The main lines of the thermodynamic approach to the mean field models like the p-spin [20] read as follows. The free energy of the system,

$$F = -\frac{1}{\beta N} \log Z \tag{2.29}$$

with

$$Z = \sum_{\sigma} \exp(-\beta H(\sigma)) \ , \tag{2.30}$$

can be rewritten in terms of single basin free-energies. Indeed, defining f_α as

$$f_\alpha = -\frac{1}{\beta N} \sum_{\sigma \in \alpha} \exp(-\beta H(\sigma)) \ , \tag{2.31}$$

where $\sigma \in \alpha$ indicates every configuration within the minimum α, we can re-write the (2.30) as follows:

$$Z = \sum_{\alpha=1}^{\mathcal{N}} \sum_{\sigma \in \alpha} \exp(-\beta H(\sigma)) = \sum_{\alpha=1}^{\mathcal{N}} \exp(-\beta N f_\alpha) \ . \tag{2.32}$$

In the previous equations, σ runs over all the configurations of the system, N is the number of spins, $\mathcal{N}$ is the number of metastable states, and $\beta = 1/k_B T$. In terms of the generic density free energy f of single basin, (2.32) becomes

$$Z = \int df \exp(-\beta N f) \sum_{\alpha=1}^{\mathcal{N}} \delta(f - f_\alpha) \ . \tag{2.33}$$

Finally, the last equation can be rewritten introducing the configurational entropy S_c,

$$S_c(f) = \frac{1}{N} \log \mathcal{N}(f) \ , \tag{2.34}$$

where

$$\mathcal{N}(f) = \sum_{\alpha=1}^{\mathcal{N}} \delta(f - f_\alpha) \ : \tag{2.35}$$

$$Z = \int df \exp(-\beta N f + N S_c(f)) \ . \tag{2.36}$$

In the thermodynamic limit, the saddle-point method simplify the integral on f. The total free energy of the system thus reads as follows:

$$F = -\frac{1}{\beta N} \log Z = \min_f \{ f - S_c(f)/\beta \} = f_{eq} - S_c(f_{eq}) \ . \tag{2.37}$$

The first remark here is that the global free energy of the system is smaller or equal than the equilibrium single basin free energy. The inequality strictly holds when the configurational entropy is non-zero. In other words, when $S_c \neq 0$, the free energy of a single basin is not the equilibrium free energy. It is higher than the equilibrium energy ($f_{eq} > F$) thus the contribution to the partition function of each metastable state individually taken is irrelevant. Only the collective contribution to the partition function of the large number of states at the same free-energy level f_{eq} gives the right free-energy result.

Relation (2.34) can be exactly computed in p-spin model [20]. The resulting S_c is a function which increases with f. It also becomes zero at the free-energy density f_0 of the lowest metastable state. Moreover, it has a negative second derivative,

thus dS_c/df increases with decreasing f. The first derivative is also finite at f_0. The single basin free energy, f_{eq}, which solves the (2.37) is fixed by the equation

$$\left.\frac{dS_c}{df}\right|_{f_{eq}} = \beta \, . \tag{2.38}$$

This means that with lowering temperature, i.e. increasing β, the growing of the derivative of S_c causes the single basin equilibrium free energy, f_{eq}, to decrease. As usual, on lowering the temperature the weight of the entropic term decreases. In this case this pushes the system to lower and fewer minima, i.e. the configurational entropy itself decreases. The total free-energy finally reads

$$F(T) = f_{eq}(T) - TS_c(f_{eq}(T)) \, . \tag{2.39}$$

$F(T)$ ceases to be different from $f_{eq}(T)$ at T_k such that $f_{eq}(T_k) = f_0$. Indeed at f_0, the configurational entropy is zero and no lower minima can be found. Moreover the value of T_k is finite since the slope of the configurational entropy is finite at f_0. For the finite temperature range $[0 : T_k]$, the total free energy corresponds to the single minimum equilibrium free energy $F(T) = f_{eq}(T)$. Very few and low states dominate the partition function and the system free energy decreases only for the smaller and smaller vibrational entropy.

The mean field approach provides a rigorous definition of the entropy separation in a configurational and a vibrational contribution. Indeed in each metastable state the free energy contains the vibrational entropy: $f_{eq}(T) = e_{eq}(T) - TS_{vib}(T)$. Hence equation (2.39) reads

$$F(T) = e_{eq}(T) - TS_{tot}(T) \, , \tag{2.40}$$

where e_{eq} is the density energy of the bottom of each equilibrium minimum and

$$S_{tot}(T) = S_{vib}(T) + S_c(f_{eq}(T)) \, . \tag{2.41}$$

In this picture, null configurational entropy $S_c(f_{eq}(T_k)) = 0$ at T_k leads to the equivalence between $S_{vib}(T_k)$ and $S_{tot}(T_k)$. This equivalence is the realization of the Kauzmann entropy crisis at the temperature we just called T_k. Indeed it means that the liquid's entropy is equal to the entropy of a single basin of the potential energy as it is in the crystal case.

The application of this clean and easy picture to finite dimensional systems is not straightforward. Indeed, the finite dimensionality does not allow to use the saddle-point in the thermodynamical limit. Some thermodynamic methods have been successfully developed to solve this problem and to analytically treat the liquid in an approximated scheme [27–29]. In this case the assumption of the partitioning of the phase space in metastable states is the starting point of the theoretical speculation. These theories analytically find the entropy crisis in liquid models. However the solidity of this result has been questioned pointing out that the assumption of the phase space partition is an implicit introduction in the model of the mean field approximation. For this reason, it is matter of debate whether or not they show the evidence of a thermodynamic transition at T_k.

We need a phenomenological analysis to understand if the partitioning of the phase space in states is reasonable. In real liquids, the only reference landscape is provided by the potential energy. However, the correspondence between minima of the free-energy and of the potential energy does not strictly holds. Indeed the structure of minima in the potential energy landscape includes large minima with high barriers and other minima (usually nested in the formers) with much smaller barriers. For each temperature not all of these minima can give rise to thermodynamically significant states. The structure of the very small ones turns out to be irrelevant to the physics of the system.

In Goldstein's picture, the distinction of the dynamically relevant minima, and thus the partition in states of the phase space, finds its roots in the emergence of two different time scales. The small time scale during which the system vibrates within a single energy minimum. And the large time scale for the activated passage between two different minima. If these two scales are well separated, it is possible to define (and also compute or measure) the vibrational entropy S_{vib} within each minimum. Thus the free-energy of the single minimum is

$$f = E - TS_{vib} \,, \tag{2.42}$$

where E is the energy density of the bottom of the basin.

We already met the problem of the crossover between activated and non activated dynamics. Decreasing the temperature, the dynamics becomes activated for the presence of trapping minima. Indeed, though not all the basins of the potential energy landscape are states, many of them are deep enough to be responsible of the crossover to the activated mechanism for the phase space exploration. Hence at low temperature trapping minima do exist. However at the crossover all the barriers between stationary points of the potential energy landscape are small. In this case identifying well-defined states is not conceivable. For this reason, a partition of the phase space in states is only possible at low enough temperature.

In the low temperature regime where activation dominates the dynamics, we can apply the mean field argument. For each free energy level f, an exponential number of metastable states is present. In particular the configurational entropy of the typical equilibrium state at temperature T operatively follows from

$$S_c(f_{eq}(T)) = S_{tot}(T) - S_{vib}(T) \,, \tag{2.43}$$

where $S_{vib}(T)$ depends on the temperature and also on the stiffness of the equilibrium states.

According to a more theoretical reasoning, the different single state free energy at equilibrium comes from the optimization of $f - TS_c(f)$. The states with f_{eq}, such that the free energy minus the configurational entropy contribution is minimum, dominates the partition function. Thus when $S_c(f_{eq}) \neq 0$, the total free energy of the system is extensively larger than f_{eq}. Moreover, $f_{eq}(T)$ decreases upon lowering the temperature for the smaller weight of the entropic term $TS_c(f_{eq}(T))$. Till the entropy crisis occurs.

We saw that the potential energy barriers in finite dimensions are finite. This is the reason why in real liquids activation can take place. The *tout-court* application

of the mean field picture fails: in finite dimensions the low temperature dynamics does not remain indefinitely trapped in basins with infinite barriers. On the contrary, the dynamics will evolve via activated events and this typically involves small numbers of neighboring particles (Goldstein picture). We can thus say that, not global, but local rearrangements in real space mark the difference between two states in the phase space. Along these lines, the careful transposition of the mean field concepts to the finite dimensional systems is at the origin of a real space theory centered on local rearrangements: the Mosaic theory.

2.5 The Mosaic theory

The Mosaic theory was firstly formulated by Kirkpatrick and Wolynes in 1987 in a paper [30] centered on the possible connection between the mean-field solution of the Potts model and structural glasses. The key ingredient of the Mosaic picture is the presence of a large number of deep basins of the supercooled liquid potential energy. This statement is suggested by the configurational entropy S_c of the mean-field analysis and it is supported by the highly complex potential energy landscape of liquids models.

The claim of Kirkpatrick and Wolynes is that out of the mean field approximation the large number of states implies the existence of different portions of the system arranged in different states. The configurational entropy that influences the mean field thermodynamics is in finite dimensions the entropic drive for a fragmentation of the real liquid configuration. In the following we will see how can this happen. Before, we remark that the very assumption of spatial portions in different metastable states involves the existence of interfaces among them. Since the states are amorphous and they all look the same, their existence is coupled to the free energy mismatch at their interfaces. The assumption of different portions in the systems carries the introduction of the interface energy cost of their contacts.

This quantity is the second key element of the Mosaic theory. It has its traditional definition in every coexistence problem and in the physics of first order phase transitions [31]. In these cases, the interface cost is quantified using the surface tension σ, i.e. the free energy cost per unit area to create an interface. Indeed such free energy cost is assumed to scale like the interface of the droplet: $F_s = \sigma L^{d-1}$ with L the linear droplet's size. On the other hand, in the case of disordered systems like supercooled liquids, a safer definition of the interface cost implies the introduction of a more general scaling:

$$F_s = Y L^{\theta} \,, \tag{2.44}$$

where Y is called generalized surface tension. The expectation on this exponent is

$$\theta \leq d - 1 \tag{2.45}$$

since the effect of disorder is at most to reduce the value of θ with respect to the ordered case. Moreover in general θ depends on the order parameter. A smaller θ is usually due to a softer order parameter. In our case the order parameter is not

clearly defined, thus it is hard to guess the value of θ. We will see that the value of the exponent θ plays a central role in the theory.

The inspiration for the Mosaic description of supercooled liquids equilibrium mechanism comes from nucleation theory of classical first order phase transitions. In the second section of this chapter we introduced this theory. In the nucleation picture only two states compete. A droplet of the stable phase become thermodynamically favored to grow if its size l is such that the bulk free energy gain $\delta f l^d$ balances the interface cost σl^{d-1}.

In the Mosaic theory the thermal dynamics at equilibrium is ruled by an exponential number $\mathcal{N}$ of states with the same free energy density, i.e. $\mathcal{N} \sim \exp(NS_c)$ and $\delta f = 0$. In this case, the free energy gain is null. However, each single basin gives an exponentially low contribution to the equilibrium. It is unstable. In this case, the drive to escape from the initial state is given by the large number of possible target states, i.e. the configurational entropy.

The full thermal equilibrium picture reads as follows. On the scale ξ, thermal fluctuations could induce the reorganization of the particles into other states. The states with larger free energy are not thermodynamically favored. Those with smaller free energy are exponentially less frequent. Finally the ones with the same bulk free energy are the most frequent without any free energy price. Their formation is the chance of the system to leave its initial configuration thus earning the purely entropic gain given by the configurational entropy $-TS_c(T)\xi^d$. On the other hand, this local reorganization also produces interfaces with finite free energy cost $Y(T)\xi^\theta$. When the droplet is too small, this cost induces the droplet to shrink back. On the other hand, for large ξ the entropic gain dominates and the initial configuration once left cannot be recovered. An intermediate size of the excitations should provide the right balance between these two terms.

A direct connection with the nucleation theory scenario would imply for this size an equation correspondent to (1.15):

$$\xi_{max} = \left(\frac{\theta}{d} \frac{Y(T)}{TS_c(T)} \right)^{\frac{1}{d-\theta}} . \tag{2.46}$$

However, in the passage to disordered systems, some considerations are required. Classical nucleation theory indicates the critical size of the droplet as the smallest size for which the droplet is thermodynamically favored to grow. The size at which $\Delta G(l)$ (in (1.14)),

$$\Delta G(l) = \sigma l^{d-1} - \delta l^d , \tag{1.14}$$

is maximum. In the nucleation case we can indeed figure the growth of the droplet as the reorganization at the interface of more and more particles in the stable phase. When the maximum of ΔG is reached, the growth, not the shrink, induces a free-energy decrease. This very mechanism in disordered systems is not as clear as it looks in first order transition. Indeed, in the Mosaic case, where the volume gain $TS_c\xi^d$ only comes from configurational entropy, we cannot justify the droplet growth. On the contrary we can just figure the formation of regions in different states as result of thermal fluctuations.

A second relevant value of the droplet size is l_c, the size at which $\Delta G(l_c) = 0$. It is related to l_{max} by a trivial factor depending on the dimensionality. Actually in nucleation theory l_c is not conceptually as important as l_{max} which corresponds to the maximum of ΔG and influences the activation time scale, τ_N. However, we mention it here because in the Mosaic picture of disordered systems the main role is played by the length scale ξ_c correspondent to the length l_c of the nucleation theory.

We are going to introduce ξ_c in liquids mentioning the reformulation of the Mosaic mechanism proposed in [32] by Bouchaud and Biroli. A *gedanken* experiment on a system with N particles is at the basis of this reformulation. The idea is to focus on the thermodynamics of n particles in a spherical region of linear size $R \propto n^{1/d}$ surrounded by a frozen environment. The environment is given by the remaining $N - n$ particles fixed in the positions of a typical equilibrium configuration α. The frozen environment acts as a pinning field on the n particles of the sphere. This gives a perfect match if the sphere configuration is in the α configuration while it represents a random field for all the other state $\beta \neq \alpha$. The thermodynamics of the sphere pinned in this way is given by the following approximated partition function:

$$\begin{aligned} Z(R,T) &= Z_{in}(R,T) + Z_{out}(R,T) \\ &\approx \exp\left[-R^d \frac{f_\alpha}{k_B T}\right] + \sum_{\beta\neq\alpha} \exp\left[-R^d \frac{f_\beta}{k_B T} - R^\theta \frac{Y}{k_B T}\right] \\ &\approx \exp\left[-R^d \frac{f_\alpha}{k_B T}\right] + \int_0^\infty df \exp\left[\frac{-f + TS_c}{k_B T} R^d - R^\theta \frac{Y}{k_B T}\right] . \end{aligned} \tag{2.47}$$

In equation (2.47) the two terms are respectively proportional to the probability $p_{in} = Z_{in}/Z$ to remain in the initial state and to the probability $p_{out} = Z_{out}/Z$ to be rearranged in other states. The mismatch at the boundaries is given by the generalized surface tension YR^θ of equation (2.44). Moreover the summation over all the possible target states β has been replaced by the integral over f with the exponential degeneracy $\mathcal{N}(f,R) \sim \exp(R^d S_c/k_B)$. At equilibrium, the integral is dominated by the free energy level, f^*, such that $dS_c/df^* = 1/T$. Also the initial α configuration belongs to an equilibrium state, thus we have $f_\alpha = f^*$. Finally, we can write

$$Z(R,T) \approx \exp\left[-\frac{f^* R^d + YR^\theta}{k_B T}\right] \left(\exp\left[R^\theta \frac{Y}{k_B T}\right] + \exp\left[R^d \frac{TS_c(f^*)}{k_B T}\right]\right) . \tag{2.48}$$

In this way, it is clear how the thermodynamics of the sphere can be governed by the interplay between the frozen boundary and the configurational entropy. Since $\theta < d$, the equation (2.48) reads as follows. In a very small sphere the interface cost will dominate with respect to the second term. The probability to remain in the initial state α,

$$p_{in}(R) = \frac{Z_{in}(R,T)}{Z(R,T)} = \frac{\exp\left[R^\theta \frac{Y}{k_B T}\right]}{\exp\left[R^\theta \frac{Y}{k_B T}\right] + \left[R^d \frac{TS_c(f^*)}{k_B T}\right]} , \tag{2.49}$$

is thus high. On contrary the probability p_{out} to reorganize the sphere in a different state β,

$$p_{out}(R) = \frac{Z_{out}(R,T)}{Z(R,T)} = \frac{\exp\left[R^d \frac{TS_c(f^*)}{k_B T}\right]}{\exp\left[R^\theta \frac{Y}{k_B T}\right] + \left[R^d \frac{TS_c(f^*)}{k_B T}\right]} , \tag{2.50}$$

is very small. Large spheres, on the contrary, will have $TS_cR^d > YR^\theta$. Thus the first term, which weights the probability to remain in the state α, becomes negligible. The thermodynamics is dominated by the other exponentially numerous states despite the cost of the mismatch at the interface, and therefore we have $p_{in} \ll p_{out}$.

The critical size in this picture is given by the length $R = \xi_c$ that provides the balance of the two probabilities and then of the two terms TS_cR^d and YR^θ. Therefore, we have

$$\xi_c = \left(\frac{Y}{TS_c(f^*)}\right)^{\frac{1}{d-\theta}} . \tag{2.51}$$

This is the the Mosaic length scale which corresponds to l_c in nucleation theory.

What do we expect for the equilibrium configuration in this picture? The small size excitations are exponentially suppressed by the presence of the interface cost. On the other hand, regions of size R such that the entropic gain compensates the surface cost ($R \sim \xi_c$) are able to rearrange independently from the boundary. Hence, the system can be arranged in patches of different states of size equal or larger than ξ_c. Actually regions much larger than ξ_c in a single state need very large time to form (their formation requires the cooperation of much more particles). Moreover they are very short-lived because new droplets of size ξ_c will rapidly form in the space they occupy. Thus the equilibrium configuration is an ensemble of patches in different states whose typical size is the critical length scale ξ_c.

Differently from the first order transition mechanism, the Mosaic provides a stationary picture of the system at equilibrium. In first order transition, nuclei of stable phase with $l > l_{max}$ develop during the transient in which the metastable phase disappears. They enlarge and cover the entire system, because in this regime the free energy gain monotonically grows with l. The configurational entropy of Mosaic is a very different kind of drive. It only exists thanks to the large number of states. Thus it would not lead to a final single state picture, but to a fragmented system in which many states coexist in different spatial regions. The continuous formation of new states is the stationary mechanism for the phase space exploration at equilibrium.

This picture shares some key concepts with the AGD theory, although it seems to provide a clearer explanation of the physical results. First, both the theories provides a connection between length scale and configurational entropy. Second, the cooperative rearranging regions of the AGD theory are conceptually similar to the Mosaic tiles. A CRR was defined as the smallest portion of the system that can be arranged independently from its surrounding. Moreover, the interactions between the CRRs are explicitly neglected in the theory. The Mosaic tiles, similarly,

are the portions of the system large enough to be arranged in different configurations despite the interface cost which in this case represents the interaction between tiles. This new interface term influences the final dependence of the critical size on the configurational entropy. Thus, equation (2.12) of AGD theory becomes in the Mosaic picture equation (2.51) where the larger exponent $1/(d-\theta)$ governs the correlation length growth with decreasing configurational entropy. From the theoretical point of view, the Mosaic theory goes deeper inside the reason why the static correlation length exists. The interface cost between different states prevents the fragmentation till the entropic drive is large enough. This also explains why AGD can describe the liquids dynamics assuming the existence of independent portions like the CRRs.

2.5.1 Relaxation time *vs.* correlation length

Since its first formulation by KTW, the Mosaic theory provided an explanation for the slowing down of the dynamics. The recovering of a growing time scale from ξ_c follows the lines first proposed by AGD. Within the activation picture valid at low temperature, the dependence of the relaxation time scales on the energy barriers, Δ, is $\tau \sim \exp(\Delta/T)$. Moreover, if the dynamics is local it proceeds through the rearrangement of ξ^d particles at a time. Thus the barriers are non-extensive and have to scale with ξ. Equation (2.9), which we rewrite here, follows

$$\tau \sim \exp\left(\frac{\xi^\psi}{k_B T}\right) \qquad \Delta = \xi^\psi \,. \tag{2.9}$$

where the exponents ψ rules the scaling of Δ with ξ. In the Mosaic case ξ is the critical ξ_c thus

$$\tau = \tau_0 \exp\left[\frac{A}{T}\left(\frac{Y}{TS_c}\right)^{\frac{\psi}{d-\theta}}\right] \,, \tag{2.52}$$

and then, near T_k,

$$\tau = \tau_0 \exp\left[\left(\frac{A'}{T-T_k}\right)^{\frac{\psi}{d-\theta}}\right] \,. \tag{2.53}$$

In AGD picture the independence of the CRRs can be rephrased as a null interface energy, i.e. an exponent $\theta = 0$. They thus obtained the VFT relation choosing $\psi = d$ in (2.53). However, the very concept of cooperativity on scale ξ_c leads to the more sensible conclusion that the rearrangement of ξ_c^d particles should involve a barrier scaling with an exponent $\psi < d$. In nucleation theory, for instance, the barrier is given by $\Delta G(l_{max})$ and it scales with l_{max} as $\Delta G \sim l_{max}^{d-1}$, thus the result is $\psi = d-1$. KTW entirely followed the nucleation paradigm obtaining in this way that the barrier to 'nucleate' new states is $\Delta \sim \xi_c^\theta$ and then the time scale is

$$\tau = \tau_0 \exp\left[\left(\frac{A'}{T-T_k}\right)^{\frac{\theta}{d-\theta}}\right] \,. \tag{2.54}$$

Hence, they also recovered the VFT law. Moreover they fixed with a renormalization group argument the value of the exponent θ to $\theta = d/2$ and they had in (2.54) $\theta/(d-\theta) = 1$.

We already saw that the nucleation picture cannot entirely explain liquids physics, especially in the issue of the droplet formation. In particular, we explained why in the Mosaic picture it is preferable to refer to the length scale ξ_c at which the entropic term TS_cR^d and the interface cost term YR^θ balance. In the nucleation paradigm, the length scale ξ_c corresponds to the droplet size l_c at which ΔG becomes zero ($\Delta G(l_c) = 0$) and not to the maximum of ΔG. Therefore the assumption $\Delta = \Delta G(l_{max}) \sim l_{max}^{d-1}$ is not applicable to disordered system.

For this reason, in their reformulation of Mosaic, Bouchaud and Biroli did not accept entirely the KTW picture and did not give any indication on the exponent ψ. We note that in this way the new free parameter ψ loosen the Mosaic theory predictions. Nevertheless we also assume this more careful point of view.

2.5.2 Empirical discovery of a static correlation length

The main ingredients of the Mosaic theory are the configurational entropy S_c and the interface cost Y. The prediction of a static correlation length ξ_c growing with decreasing temperature represents its main result.

Several numerical and theoretical studies have been devoted to the study of the configurational entropy also in finite dimensional models with liquid like interactions [27–29, 33]. Moreover, a new evidence in favor of the Mosaic theory has recently come from the measure of a growing static correlation length R_c [34, 35].

Concerning the interface cost, many interesting studies on spin disordered systems with quenched disorder, like the Edward Anderson model, have been developed [36]. However the inspection of this quantity in models of liquids with deterministic pairwise potential was lacking till now. This is the original part of the present Ph.D. thesis.

Before directly dealing with the amorphous interface cost we want to report some details of the measure of the static correlation length in [35]. This issue indeed shares many elements with the problem of the interface detection. As we will see the result of this measure also indicates some precise features of the surface tension.

The *gedanken* experiment proposed by Bouchaud and Biroli (BB) rephrased the Mosaic theory and also suggested the guidelines for a measure of a static correlation length. Static quantities in supercooled liquids traditionally do not present any remarkable new features. In particular no fast growing correlation length can be extracted from the $G(r)$. On the other hand, theories like the Mosaic picture requires the existence of such a growing length scale.

The Mosaic picture seems conceptually quite clear but we do not have any proper tool to distinguish different amorphous orders which should be present in the Mosaic tiles. Without the right order parameter the Mosaic tiles and their interfaces are completely hidden. We will face the same problem dealing with the measure of the interface energy.

The idea of BB is to use the traditional tool of the boundary condition to favor only one of the possible amorphous states. The pinning field they suggested is just one of the equilibrium configurations of the liquid. They proposed this set-up for a theoretical speculation but the method was subsequently developed and applied to a numerical experiment by Cavagna, Grigera, and Verrocchio [34,35]. In practice this is the idea: after a thermalization at low temperature, all the particles in a system are stopped in their position except those within a sphere of fixed radius R. This is the numerical reproduction of the BB environment frozen in state α. If the Mosaic picture is the right one, for small R the formation of any other state $\beta \neq \alpha$ is prevented by the interface cost. At large R the configurational entropy dominates and the sphere asymptotically explores different states. The different results with the R variation are more evident observing only the thermodynamics of the center of the sphere (this has been cheked for first order transitions in CTLS, i.e. coupled two level system, model in [37]). The size R_c which correspond to a transition between these two different behaviours should represent the critical length scale ξ_c. Moreover in the Mosaic picture, the transition is expected to be sharp and R_c is expected to increase with lowering temperature.

A specific observable is required to detect the asymptotic behaviour of the sphere. Once again the problem of detecting amorphous order is managed comparing different configurations of the sphere during its time evolution, with a reference initial configuration. The typical order parameter to do this is the overlap: this quantity ranges between 0 and 1. It is high if the configurations we compare are similar and small for different configurations. In this case the natural reference configuration to compare with is α. Thus for a sphere of radius R in presence of a quenched environment α we can define $q_\alpha(R)$ and average it over different α: $\langle q_\alpha(R)\rangle_\alpha = q(R)$. The trapping of the sphere in the initial state would correspond to high overlap. On the contrary, the change of state should be revealed by a low overlap.

The result of this numerical test is very interesting [35]. Despite a sharp transition at a specific value of R has not been found, the overlap $q(R)$ does indicate a major decorrelation of the sphere as R is larger. Moreover upon lowering the temperature the decorrelation process with increasing R is slower and slower. This indicates that the effect of the amorphous boundary condition is the more long-ranged the lower the temperature. Finally the temperature decrease influences also the functional form of $q(R)$. Indeed, a simple exponential decay is revealed at high temperature, but at low temperature only a compressed exponential,

$$q(R) \sim \exp(-(R/\xi)^\alpha) \tag{2.55}$$

with $\alpha > 1$, can fit the data. We report in Fig.2.1 the results of the overlap at the center of the sphere obtained in [35]. The fit in Fig.2.1 are compressed exponentials as equation (2.55) with α ranging from 1 (at the highest temperature) to ~ 4 (at the lowest temperature).

Even at low temperature, the decay of $q(R)$ is still far from the sharp transition expected by the Mosaic picture. However, the exponent $\alpha > 1$ is the signature that some qualitative differences between the high and low temperature liquids is

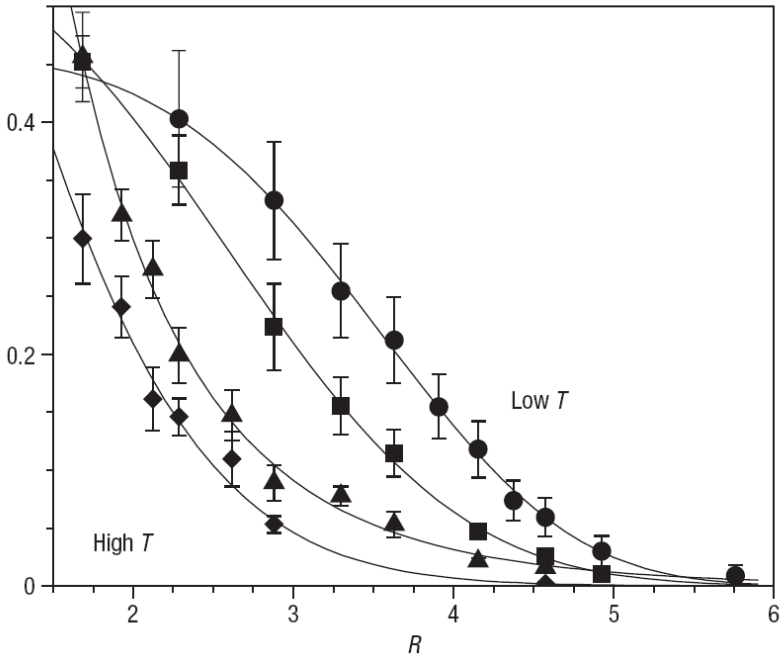

Figure 2.1. Overlap at the centre of the sphere $(q(R) - q_0)$ *vs* the radius R, for temperatures $T = 2.13T_c$ (diamonds), $T = 1.55T_c$ (triangles), $T = 1.09T_c$ (squares), $T = 0.89T_c$ (circles). Lines are fits to compressed exponentials. (Figure from [35]).

emerging. In particular, upon further cooling a larger and larger exponent would mean the recovering of the Mosaic sharp drop of $q(R)$. This sensible intuition is developed in [35], where, a precise explanation of the $q(R)$ decay is given within an extended version of the Mosaic Theory.

2.5.3 The Mosaic with fluctuating surface tension

The first assumption of the Mosaic theory is the existence of a large number of equilibrium states with the same free energy density f^*. This is the conceptual origin of the configurational entropy term. On the other hand, a unique value of the surface tension Y has been introduced for every interface between different states in the system. A more sensible assumption is instead that such a variety of amorphous states gives rise to many different Y with a unique typical value but probably with a non negligible variance. We thus in general should refer not to a single surface tension value Y but to a distribution $P(Y)$. This simple consideration leads to some interesting consequences on the Mosaic mechanism.

In the classic Mosaic the probability for a region to rearrange in different states despite its surrounding is

$$p_{out}(R) = \frac{\exp[R^d S_c]}{\exp[R^d S_c] + \exp[R^\theta Y/T]} \sim \Theta(R - R_c) \, . \tag{2.56}$$

Indeed, due to the sudden increase from 0 to 1 around $R_c = (Y/(TS_c))^{1/(d-\theta)}$, equation (2.56) can be approximated by a Θ-function. The transition is sharp and the larger is Y the larger is the critical size, since only at the size such that $YR_c^\theta < TS_cR_c^d$ the sphere decorrelates. On the other hand, we now consider the presence of target states α with different interfacial cost Y_α. In this case, for each size R the region can decorrelate towards all the target states such that

$$Y_\alpha R^\theta < TS_cR^d \; . \tag{2.57}$$

Hence for each size R the region can decorrelate provided the final generalized surface tension is

$$Y_\alpha < TS_cR^{d-\theta} \; . \tag{2.58}$$

For these states the Θ in (2.56) is nonzero. They are not all the target states, but they may represent a finite fraction of them. Then, the probability to escape from the initial state becomes

$$p_{out}(R) = \int_0^{TS_cR^{d-\theta}} dy \; P(y) \; . \tag{2.59}$$

In the extended version of Mosaic, the transient between small spheres pinned by the boundary in the initial state and large spheres able to decorrelate is smooth. The broader is $P(R)$, the smoother is the transition of p_{out} from 0 to 1.

The classic Mosaic is recovered in the limit $P(y) = \delta(y - Y)$. On the contrary, for large distributions, the slow change in p_{out} and $p_{in} = 1 - p_{out}$ affects the slow transient in the observables like the overlap. Indeed under the assumption that q_1 is the overlap within the single state α and q_0 the overlap between α and $\beta \neq \alpha$, we can in general write

$$q(R) = q_1p_{in} + q_0p_{out} = (q_1 - q_0)(1 - p_{out}) + q_0 \; . \tag{2.60}$$

In the case of the extended Mosaic (2.60) becomes

$$q(R) - q_0 = (q_1 - q_0) \int_{TS_cR^{d-\theta}}^{\infty} dyP(y) \; . \tag{2.61}$$

The measure of the growing static correlation length $\xi_c(T)$ in [35] is undoubtedly the signature that the thermodynamics of the system is changing at low temperature. Despite the numerical method is inspired by the Mosaic theory, the result does not completely agree with the original theory and the introduction of a distribution in the surface tension is required. This new picture, still requires the existence of a surface tension between amorphous states. Moreover it also needs the existence of a distribution of this quantity. These two issues are going to be investigated in the next chapter.

Chapter 3

The surface tension

The core of the first part of the thesis is the study of the surface tension between amorphous phases, which is not quite the same surface tension as that present in first order transitions. In the case of the liquid-crystal transition, for instance, the surface tension is the free-energy cost for unit surface to build the interface between the two phases. It is present in systems at coexistence or during the transient of first order transition. The two phases have different bulk free energies and the order parameter is a well-defined quantity.

In a multi-state scenario, the hint for the existence of surface tension in disordered systems comes from the presence of a large number of different amorphous states. In real space, different portions of the space should be arranged in different states. In this case the states have the same bulk free energy density and there is no obvius order parameter able to distinguish different amorphous phases. The surface tension at the interface between two portions is the landmark of a multi-state scenario. This quantity is at any time present in the low temperature equilibrium energy since at any time the configuration is a collection of tiles in different states.

3.1 Surface tension and low temperature dynamics

As we suggested in the introduction the surface tension is the landmark of the existence of different states. These states are equally amorphous. Their definition is thus at least due to an energy price at the interfaces. This energy price indeed would be the only measurable consequence of the existence of more than one state. Hence, in the Mosaic theory, where the key-point is the existence of a large number of states, the interface cost is as much a fundamental ingredient as the configurational entropy. Moreover, we already saw the problem of the application of the mean field paradigm to finite dimensional models. Metastable states are not sharply defined in real liquids. The difficulty in partitioning the phase space may cast some concerns on the results of [27–29]. Indeed, the assumption of many states in these papers has been read by some [38] as the consequence of a non realistic mean field picture if there are no other independent indications. The surface tension would provide a certification of the distinction between states and also an indication for the applicability of the mean field paradigm. However, this quantity

has never been computed or measured in liquid models. Its scaling with the size of the excitations has never been studied.

Beside these fundamental questions, the study of the surface tension could also shed light on the validity of the extended Mosaic theory presented in the previous section. Indeed, if the distribution of the surface tension $P(Y)$ could be obtained, it should be compared with the overlap $q(R)$ measured in [35]. This check would directly indicate whether the distribution in the surface tension does influence the smooth decay of $q(R)$. On the contrary, a non-compatible $P(Y)$ would exclude a Mosaic origin of a growing ξ_c.

This chapter is devoted to the measurement of the surface tension in a glass-former model. Among the results, we anticipate:

- the individuation of a finite surface tension value dependent on the temperature [39]
- the discovery of a spinodal point for the interface cost and thus also for the multi-state scenario [39]
- the measurement of the surface tension distribution as to directly confirm the Mosaic extended theory [39]
- an estimate of the exponent θ (the exponent of the interface cost $\Delta E = Y R^{\theta}$) and ψ (the exponent of the barriers for low temperature activation $\Delta \sim R^{\psi}$) as to recover the VFT law [40].

3.2 Detecting the interface

Detecting amorphous excitation is not an easy task, as we lack the right order parameter able to distinguish immediately the presence of droplets of different phases. We met the same problem about the different tiles of the Mosaic theory. For this very reason we need a protocol to artificially build amorphous excitations in the system. After an appropriate construction, we exactly know the position and more or less the shape of the excitation thus its interface energy cost follows. Indeed the difference between the energy of the system in presence of excitations and the energy of the system without excitations fixes the interface energy cost, i.e. the excess energy of the excitation. We thus follow the process of relaxation of artificially produced excitations, rather than detect the spontaneous formation of excitations.

The core of our idea to mimic the formation of amorphous excitations is the following: we pick up pairs of independently thermalized configurations, $\mathcal{C}_\alpha$ and $\mathcal{C}_\beta$, and from these we create a mixed configuration via a simple *exchange*: all particles within a sphere of fixed radius R of $\mathcal{C}_\alpha$ are moved to a spherical cavity of the same shape and size in the configuration $\mathcal{C}_\beta$; conversely, the particles within the sphere of $\mathcal{C}_\beta$ are moved in the spherical cavity of $\mathcal{C}_\alpha$ as it is shown in figure 3.1. In this way two new configurations arise, $\mathcal{C}_{\alpha+\beta}$ and $\mathcal{C}_{\beta+\alpha}$. In each initial configuration the cavity is chosen in order to preserve the concentration of the two species

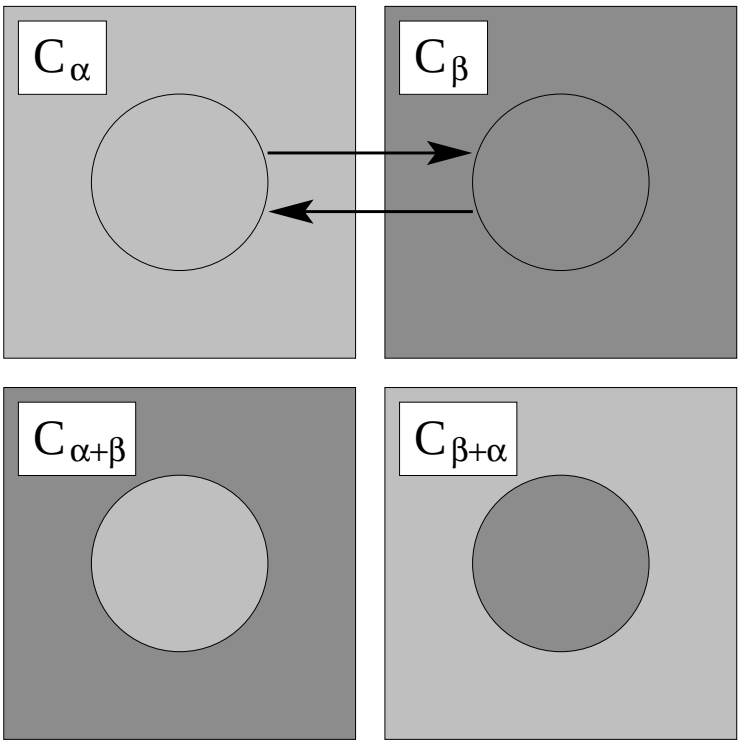

Figure 3.1. Construction of the mixed configurations $\mathcal{C}_{\alpha+\beta}$ and $\mathcal{C}_{\beta+\alpha}$ using configurations $\mathcal{C}_\alpha$ and $\mathcal{C}_\beta$.

of particles in the mixed configuration $\mathcal{C}_{\alpha+\beta}$. We can then study both the energetic and geometric evolution in time of these excitations in configurations $\mathcal{C}_{\alpha\beta}(t)$ at the same temperature as we used to obtain the initial configurations.

We choose a round shape to mimic localized cooperativity. We are aware that there may also be string like cooperative sets of particles. However, a recent study [41] indicates that if both kinds of cooperativity rule the relaxation of the system, the activated relaxation is in particular due to the formation of compact excitations. In the following we will see the emerging in the final configurations of roughening of the interface we created in the initial configurations. This confirms that with the used protocol the geometry of the final configuration is not trivially determined by the initial one we built.

As sketched at the beginning of this section, by using this protocol, we know exactly two very important things: 1. where the excitation is; 2. what is its geometry, and hence what is the co-ordinate orthogonal to the interface between the two phases (in our case the radial one). Such knowledge is the only reason why we are able to compute and say something about these excitations. For spontaneous excitations, of course, we lack both pieces of information.

In particular, we can measure the excess energy $\Delta E_{\alpha\beta}$ of the excitation, due to the interface between α and β. Let E_α^{in} be the energy of the particles within the sphere when the whole system is in configuration $\mathcal{C}_\alpha$, E_β^{out} be the energy of the particles out of the sphere when the whole system is in configuration $\mathcal{C}_\beta$, and $E_{\alpha\beta}$

be the energy of the configuration $\mathcal{C}_{\alpha\beta}$. At each time, the excess energy can then be defined as,

$$\Delta E_{\alpha\beta} = E_{\alpha\beta} - E^{in}_{\alpha} - E^{out}_{\beta} \ , \tag{3.1}$$

where in detail (the origin of the axes is at the center of the sphere)

$$E^{out}_{in} = \sum_{i,j:|\mathbf{r}_i| \gtrless R} V_{ij}(\mathbf{r}_i - \mathbf{r}_j) \ , \tag{3.2}$$

and $V_{ij}(\mathbf{r}_i - \mathbf{r}_j)$ is the pairwise potential of the liquid model. Averaging over all the pairs of initial configurations we have (about 15), we obtain an estimate of the average excess energy cost $\Delta E = \langle \Delta E_{\alpha\beta} \rangle_{\alpha\beta}$. This approach measures energy rather than free energy, so we expect our results to apply quantitatively only at quite low temperatures.

We now observe how the excess energy $\Delta E(t)$ of the excitation relaxes with time. However, in addition to the problem of finding excitations in space, another difficulty in the detection of the interface cost is their finite lifetime. Excitations are constantly forming and relaxing: this is the relaxation mechanism of the Mosaic picture, through which the whole liquid state is slowly explored. Hence the excess energy of our excitations asymptotically will completely relax. Thus the problem is to single out the interface cost of excitations before their full relaxation. For an initial study of surface tension we choose to avoid such complications and focus on inherent structures (ISs), i.e. the local minima of the potential energy [42]. In the second part we will come back to the interface cost in temperature as defined in (3.1).

The study of glass-forming liquids has taken great advantage from the approach based on the ISs study. The ISs are the local minima of the potential energy of the system. They can be traced in every off-lattice model defined by an Hamiltonian. Indeed, in these cases each configuration of the system corresponds to a point on the potential energy landscape. A simple gradient descent on the energy manifold from any initial point α in the phase space leads to the individuation of the corresponding inherent structure α_{IS}. Many initial configurations, belonging to the same basin of the potential energy, makes reference to the same IS, i.e. the configuration of the bottom of the basin.

As we saw in section 2.3, the study of the landscape is very fruitful for the comprehension of the low temperature behaviour of glass-forming liquids. In particular the study of the ISs has first shown the signature of two qualitatively different dynamical regimes [43]. An high temperature regime where the equilibrium configurations are associated to ISs belonging to the same density free-energy level roughly independent from the temperature. A low temperature regime where the lower is the temperature of the initial equilibrium configuration, the lower is the density energy of the corresponding IS. The distinction between these two regimes is not possible using the energy of the thermal configurations since it simply slowly decreases with the temperature. The ISs, differently from the equilibrium configuration, are free from any thermal contribution although they still depend on the temperature. Hence they provide an interesting but more sharp description of the physics of complex systems.

The search of the ISs is not an easy task. Due to the large number of variables of the problem (i.e. proportional to the number of the particles in the system) the gradient descent of the potential energy requires large numerical efforts and optimized algorithms. A warning is that the ISs may depend on the algorithm used for the search, however their mean energy level is a quite sound result. In this work, the search of the ISs from the instantaneous configurations and from the mixed configurations has been performed with the LBFGS algorithm [44], i.e. an optimized conjugate gradient method suitable for large scale minimization problems (we consider systems up to 16384 particles).

In the IS framework, in place of the initial equilibrium configurations, we use the configurations, $\mathcal{C}_{\alpha_{IS}}$ and $\mathcal{C}_{\beta_{IS}}$, of the ISs α_{IS} and β_{IS} corresponding to the initial thermalized α and β. Then we perform the same exchange procedure as the one described for the equilibrium configurations to build the mixed configuration $\mathcal{C}_{\alpha_{IS}+\beta_{IS}}$. We finally consider the IS $\mathcal{C}^{IS}_{\alpha_{IS}\beta_{IS}}$ obtained from $\mathcal{C}_{\alpha_{IS}+\beta_{IS}}$ by means of a further minimization procedure.

The mixed configuration $\mathcal{C}_{\alpha_{IS}+\beta_{IS}}$ is not an IS. On the contrary, its energy is very high. Indeed after exchanging the particles of the sphere, some pairs of particles end up at very short distances, giving very high energies. We observed that directly applying the minimizer algorithm to these configurations we obtained some unphysical results in the minimization procedure. The very high gradients due to the presence of pairs of particles arbitrarily close one to each other caused uncontrolled large displacements of the particles during the first minimization steps. A solution to this problem was found in using a combination of 100 standard Metropolis Monte Carlo steps at $T = 0$ plus the minimizer LBFGS. In this way, the initial local stress is readily smoothed by the zero temperature Metropolis which is a local algorithm. Then the LBFGS efficiently find the nearest IS: $\mathcal{C}^{IS}_{\alpha_{IS}\beta_{IS}}$.

The excess energy $\Delta E_{\alpha_{IS}\beta_{IS}}$ of the frozen interface obtained in such a way can be retrieved subtracting the energy contribution of the parent ISs α_{IS} and β_{IS} from the energy of $\mathcal{C}^{IS}_{\alpha_{IS}\beta_{IS}}$, $E^{IS}_{\alpha_{IS}\beta_{IS}}$:

$$\Delta E_{\alpha_{IS}\beta_{IS}} = E^{IS}_{\alpha_{IS}\beta_{IS}} - E^{in}_{\alpha_{IS}} - E^{out}_{\beta_{IS}} \, . \tag{3.3}$$

In (3.3), E^{out}_{in} is again given by the (3.2) now computed in the ISs configurations. The estimate of the mean excess energy cost ΔE_{IS} follows from averaging over all the pairs of initial configurations: $\Delta E_{IS} = \langle \Delta E_{\alpha_{IS}\beta_{IS}} \rangle_{\alpha_{IS}\beta_{IS}}$.

Using the ISs, we lie in the sharp framework of the potential energy landscape where no thermal relaxation is present. Indeed we will speak about the zero temperature surface tension. In this case, the interface we build in $\mathcal{C}_{\alpha_{IS}+\beta_{IS}}$ has to relax only during the subsequent minimization, after this minimization process it does not change anymore. Thus on the one hand, the interface energy does not completely vanish. On the other hand, during the minimization procedure the initial stress we artificially put in can relax in many ways. In particular

- the system can keep memory of the initial surface showing a finally interface cost proportional to R^2.

- Otherwise it can rearrange all the particles within a finite distance from the interface to gain a larger amount of energy. In this case the resulting interface cost can depend on R in a different way.

We note here that after the first 100 MC steps we found an interface cost proportional to R^2. In this case only the particles chancely very near one to each other have been significantly moved. Therefore the resulting interface energy is trivially scaling as a surface. This is the first case we listed. On the contrary we expect that during the remaining minimization procedure something similar to what described in the second case happens. Hence the final interface cost in $C^{IS}_{\alpha_{IS}\beta_{IS}}$ has not to be trivial at all. For this reason we are interested in what remains of the initial stress in $\mathcal{C}^{IS}_{\alpha_{IS}\beta_{IS}}$.

3.2.1 The soft sphere model

The system we consider is a binary mixture of soft particles. This model has been introduced in mid-eighties by Bernu, Hiwatari, and Hansen [45] as a model for metallic alloys which very easily bypass crystallization. Indeed, the presence of two kinds of particles in the system strongly inhibits the crystallization and allows the observation of the deeply supercooled phase. It is thus suitable for the low temperature study of liquids dynamics. It is an handy glass-former. This model showed two relaxation time-scales in the mean-square displacement, i.e. the signature of cage effects. In the time range numerically reproducible, the low temperature growth of the relaxation time (obtained via the observation of the diffusion coefficient) cannot be studied in a large enough temperature window. It exhibits [46] a power law increase of the relaxation time scale compatible with the Mode Coupling theory description. However, the power law behaviour breaks down at the lowest temperatures observed. The activated diffusion was analyzed in detail as to reveal at low temperature the existence of correlated jump motions of several grouped atoms, i.e. non-homogeneous dynamics [47,48]. The conjecture of Kirkpatrick Thirumalay and Wolynes (the basis of the Mosaic theory) that equilibrium properties of glassy systems belong to the same universality class of systems like p-spin model has found a support in [49] using the soft sphere model. In this paper, the non-equilibrium dynamics of the soft sphere model is analyzed and it has been found an agreement between the results and the predictions of one step replica symmetry breaking. Further analytical [28] and numerical [33] results on this model have found it compatible with a thermodynamic glass transition due to the configurational entropy vanishing at finite temperature. The soft sphere model has thus revealed to be a fragile glass-former.

In this model system, particles are of unit mass and they belong to one of the two species $\gamma = 1, 2$, present in equal amounts and interacting via a potential:

$$\mathcal{V} = \sum_{i<j}^{N} V_{ij}(|\mathbf{r}_i - \mathbf{r}_j|) = \sum_{i<j}^{N} \left[\frac{\sigma_{\gamma(i)} + \sigma_{\gamma(j)}}{|\mathbf{r}_i - \mathbf{r}_j|} \right]^{12}. \tag{3.4}$$

The radii σ_γ are fixed by $\sigma_2/\sigma_1 = 1.2$ and setting the effective diameter to unity, that is $(2\sigma_1)^3 + 2(\sigma_1 + \sigma_2)^3 + (2\sigma_2)^3 = 4l_0^3$, where l_0 is the unit of length. The

density is $\rho = N/V$ in units of l_0 , and we set Boltzmann's constant $k_B = 1$. A long-range cut-off at $r_c = \sqrt{3}$ is imposed. The thermodynamic quantities of this system depend only on $\Gamma = \rho/T^{1/4}$, with T the temperature of the system [50]. Here $\rho = 1$ in units of l_0^{-3} thus the thermodynamic parameter Γ is $\Gamma = T^{-1/4}$.

An estimate of the Mode Coupling transition temperature T_c has been given in [48]. In this article the dynamical results for the soft sphere model with the same ratio $\sigma_2/\sigma_1 = 1.2$ are reported. Analyzing the self-Van Hove autocorrelation function it is found a different behaviour below and above $\Gamma = 1.45$: below, the main peak of the Van Hove function moves with the time increase towards the gaussian hydrodynamic limit. Above, the main peak does not change position but its area decreases while a secondary peak develops and grows at about an interparticle distance. This result indicates that the free diffusion of the particles is arrested at $\Gamma = 1.45$ and the activation is responsible of the remaining relaxation of the system. This is also evident in the self-intermediate scattering function which shows a change in its behaviour from an ergodic to a non-ergodic behaviour at $\Gamma = 1.45$. Also in this case the ergodicity is restored via activation as the time grows. Both these results indicates that the non activated channels are interrupted at $\Gamma = 1.45$ hence it is the Mode Coupling transition mark:

$$\Gamma_c = 1.45 \; . \tag{3.5}$$

We chose $\rho = 1$, hence we have $T_c = \Gamma_c^{-4} = 0.226$

In this work we study thermalized configurations of a system with $N = 16384$ particles confined in a periodic box. The temperatures considered, corresponding to $\Gamma = 1.49$, 1.47, 1.44, 1.42, and 1.35, are two below and three above the Mode Coupling temperature T_c: $T \simeq 0.89T_c$, $0.95T_c$, $1.03T_c$, $1.09T_c$, $1.33T_c$. For each temperature we created mixed configurations as explained in the previous section from a collection of about 10 or 15 independent equilibrium configurations, using spheres of sizes between 1.5 and 8.5 (in units of l_0). The upper limit of the size of the considered excitations is due to the emergence of boundary condition effects for larger droplets in the already numerically challenging system with $N = 16384$ particles.

The effects of boundary conditions are directly visible if we consider the exchange of the two initial configurations in a different geometry. We take a system in a configuration α and we move all the particles within a slice of thickness d in a region of the same shape and size of a second configuration β. We sketch the final mixed configuration in figure 3.2, left panel. If we perform the minimization procedure of this configuration (100 MC steps plus LBFGS) we obtain the IS which corresponds to this new geometry. The excess energy density of the final ISs with respect to the initial configurations is plotted in terms of d in figure 3.2, right panel. As we can see, for large enough d, the excess energy does not depend on d. On the contrary, for very thin slices (d very small) the excess energy is small and decreases with d decreasing. The initial trend is due to the existence of two well separated interfaces. The excess energy does not change with d as long as the separation between the interfaces is large enough so they do not interact. The decrease in the

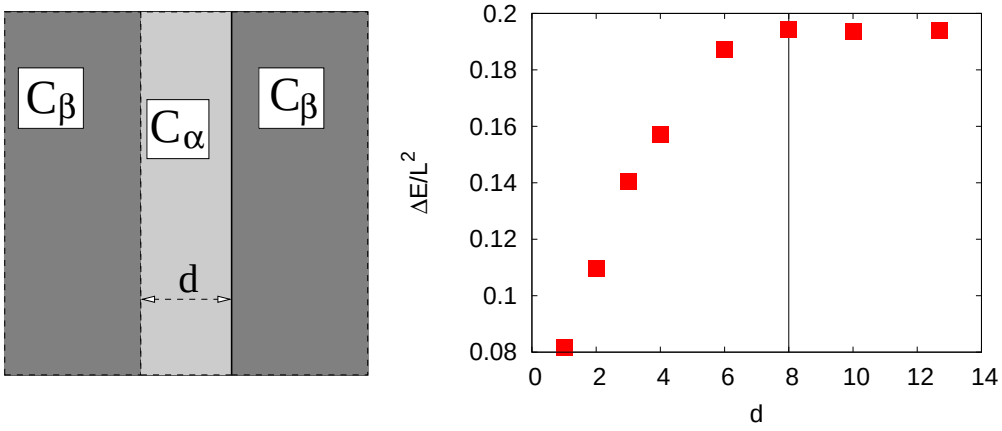

Figure 3.2. Left panel: construction of the mixed configurations $\mathcal{C}_{\alpha_{IS}+\beta_{IS}}$ using configurations $\mathcal{C}_{\alpha_{IS}}$ and $\mathcal{C}_{\beta_{IS}}$ in the slice geometry. Right panel: trend of the density excess energy in terms of the thickness of the slice d.

excess energy indicates that the two interfaces are merging. In this way we desume the minimal distance between two non-interacting surfaces. It is 8 in unit of l_0.

Let us come back to the shperical geometry. Due to the periodic boundary condition we impose, we can roughly say that each sphere interact with its mirror image if the distance between them is smaller than 8. In a system with $N = 16384$ particles and with $\rho = 1$ the side of the box L is about $L \sim 25.4$. Hence the largest sphere which is not influenced by the boundary conditions has radius 8.7.

3.2.2 The Swap Monte Carlo algorithm

We listed in the previous section the values of temperature we considered for the study of the surface tension. We considered also temperatures below the Mode Coupling temperature. For each temperature the protocol for the measure of the amorphous surface tension requires several equilibrium configurations. The equilibration at the smallest temperature values is not an easy task. At these temperatures the relaxation time is very high and any standard numerical algorithm cannot reach the equilibrium with a reasonable numerical effort.

A very important advance in this field has been achieved by T.S. Grigera and G. Parisi in [33]. They proposed a fast Monte Carlo algorithm, the Swap Monte Carlo (SW), able to numerically equilibrate systems faster than other algorithms. SW combines Monte Carlo moves of the particles in the system with non local moves which will be called "swaps" of particles. The factor $p_s \in [0, 1]$ is the probability to choose the swap of two particles in place of the simple local motion.

This algorithm was fist applied in the soft sphere binary mixture model we also study. The SW is indeed built for system with two or more different types of particles.

The elementary steps of the algorithm is the following

- Draw 8 random numbers r_k (with $k \in [1, 8]$) uniformly distributed in $[0, 1]$

- Pick a particle i in the system
- If $r_1 < 1 - p_s$
  - Perform a standard MC trial move shifting the particles by $\Delta\mathbf{r} = (2r_2 - 1, 2r_3 - 1, 2r_4 - 1)\Delta r$

  If $r_1 > 1 - p_s$
  - Choose another random particle j of a different type from the particle i
  - Swap the two particles positions
  - Shift the particles by the two following random displacements: $\Delta\mathbf{r_i} = (2r_2 - 1, 2r_3 - 1, 2r_4 - 1)\Delta r$ and $\Delta\mathbf{r_j} = (2r_5 - 1, 2r_6 - 1, 2r_7 - 1)\Delta r$
- Accept the motion if $r_8 < \exp[-\beta(\Delta e)]$, with Δe the energy difference between the system in the initial state and the system in the final state, according to the Metropolis rule.

A combination of the two parameters Δr and p_s tunes the final acceptance of the algorithm.

As we saw, the cage effect is one of the reasons for the slowing down the dynamics at low temperature. The non-locality of the SW algorithm partially avoid this problem. Hence the disorder equilibrium configurations can be quickly obtained.

3.2.3 The overlap

Provided that we know the position of the excitations in the final configuration $\mathcal{C}^{IS}_{\alpha_{IS}\beta_{IS}}$, a useful tool to detect the changes occurred during the minimization is the overlap. We can compute the overlap between the initial mixed configuration $\mathcal{C}_{\alpha_{IS}+\beta_{IS}}$ and the final IS $\mathcal{C}^{IS}_{\alpha_{IS}\beta_{IS}}$ using the initial configuration as reference. $\mathcal{C}_{\alpha_{IS}+\beta_{IS}}$ indeed encodes the initial partition of the system in regions of different configurations $\mathcal{C}_{\alpha_{IS}}$ and $\mathcal{C}_{\beta_{IS}}$.

The definition of the overlap in an off-lattice model with N particles is not simple. Differently from the lattice systems, the particles can occupy each position in space. Moreover the particles are point-like thus an infinitesimal displacement for each of them from the reference configuration means overlap zero. A solution to this problem can be obtained partitioning the space in M small boxes. In each box it is possible to define the occupation number $n(x_i, y_i, z_i)$ which is the number of the particles that the box contain. x_i, y_i, z_i is the position of the i-th box. The overlap between two configurations α and β can be defined as follows

$$q_{\alpha\beta} = \frac{1}{N}\sum_{i=1}^{M} q_{\alpha\beta}(x_i, y_i, z_i) \qquad q_{\alpha\beta}(x_i, y_i, z_i) = n_\alpha(x_i, y_i, z_i) n_\beta(x_i, y_i, z_i)\,. \tag{3.6}$$

The non-zero terms of the sum are given by the boxes which contain a particle in both the configurations. If all the particles have not changed box N terms are non

zero and the overlap is 1. The number of boxes M has not to be too much high otherwise small displacements of the particles (for instance the displacements due to trivial thermal vibrations) cause rapid diminution in the final result. On the other hand too much high large boxes can give large overlap even if important changes in the system has occurred. In the case of large boxes another problem emerges. It can happens that a box contains more than one particle in one of the configurations and at least one in the other configuration. This may lead to an unphysical overlap result larger than one. If, in place of $n(x_i, y_i, z_i)$, we used a number $m(x_i, y_i, z_i)$ which only indicates whether the box contains at least one particle $m(x_i, y_i, z_i) = 1$ or not $m(x_i, y_i, z_i) = 0$ we did not distinguish in the multiple occupation cases if the number of particles in a box is changed.

In an equilibrium configuration where the particles are not oddly close one to the other, it is possible to choose the optimal number of the boxes M so to avoid all these problems. See [34, 35] for an application of this definition. In our case, in the configuration $\mathcal{C}_{\alpha_{IS}+\beta_{IS}}$ a very odd disposition of the particles occurs at the interface. We already saw the consequence of this fact at an energetic level. Hence we need to define the overlap in a more careful way [39,40]. We divide the system in $M = 64^3$ small cubic boxes with side $L/64$ and, having two configurations α and β, we compute the quantity

$$q_{\alpha\beta}(x, y, z) = m_\alpha(x, y, z)m_\beta(x, y, z) \,, \tag{3.7}$$

where $m_\alpha(x, y, z)$ is 1 when the box with center at coordinates x, y, z contains at least one particle and it is 0 when the same box is empty. To each box we assign the weight

$$w_{\alpha\beta}(x, y, z) = \frac{m_\alpha(x, y, z) + m_\beta(x, y, z)}{2} \,. \tag{3.8}$$

The global overlap $q_{\alpha\beta}$ between these two configurations α and β is given by

$$q_{\alpha\beta} = \frac{\sum_i q_{\alpha\beta}(x_i, y_i, z_i)w_{\alpha\beta}(x_i, y_i, z_i)}{\sum_i w_{\alpha\beta}(x_i, y_i, z_i)} \,. \tag{3.9}$$

where i runs over all boxes in the system.

With this choice of the overlap we avoid the problem of an overlap larger than one and we distinguish whether in a multi-occupation case the number of particles in a box has changed: if the box i contains two particles in both configurations and j contains zero particles $q_i = 1$ and $w_i = 1$, and $q_j = 0$ and $w_j = 0$. But if i contains two particle and j zero in the first configuration and both contain a particle in the second configuration, $q_i = 1$ and $w_i = 1$, and $q_j = 0$ and $w_j = 1/2$. Hence summing up, in the first case the overlap on the two boxes is higher in the first case than in the second.

We are also interested in the local value of the overlap $q_{\alpha\beta}(r)$ at distance r from the center of the sphere. The definition of the local overlap $q_{\alpha\beta}(r)$ for a spherical corona between $r - dr$ and $r + dr$ is given by considering in (3.9) only the sum of boxes belonging to this region.

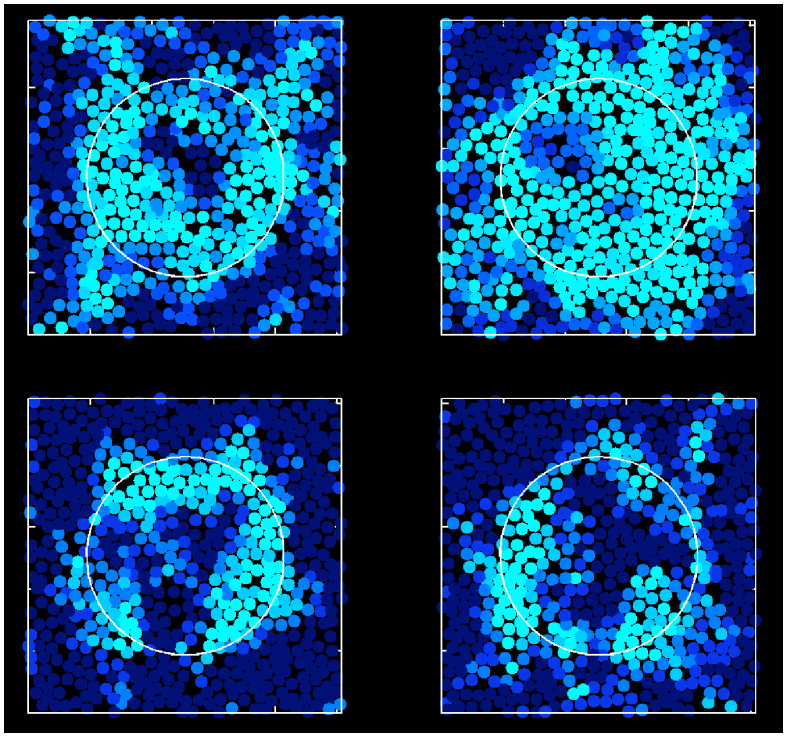

Figure 3.3. Overlap, i.e. similarity, between the configuration right after the exchange of the spheres , $\mathcal{C}_{\alpha_{IS}+\beta_{IS}}$, and the hybrid inherent structure after minimization, $\mathcal{C}^{IS}_{\alpha_{IS}\beta_{IS}}$. The off-lattice local overlap in our system is defined in section 3.2.3. Upper panel: two configurations at high temperature $T = 1.33\,T_c$. Lower panel: two configurations at low temperature $T = 0.89\,T_c$. far from the boundary of the sphere (white circle). The regions inward and outward the sphere in $\mathcal{C}^{IS}_{\alpha_{IS}\beta_{IS}}$ resemble the parent minima far from the surface of the sphere but rearrange close to it.

3.3 Inherent structures surface tension

3.3.1 The interface

Using the local overlap defined in section 3.2.3, we can observe the change in configurations during the minimization. This is shown in Fig.3.3 which report the local overlap between chosen pairs of $\mathcal{C}_{\alpha_{IS}+\beta_{IS}}$ and $\mathcal{C}^{IS}_{\alpha_{IS}\beta_{IS}}$ [39]. A thin slice located at half height of the whole three dimensional system is shown. Each particle is colored according to how much it moved after the artificial excitation was created (dark blue: small displacement, high overlap; light blue: large displacement, small overlap). In the figure is clear that the hybrid minimum bears memory (high overlap, dark blue) of the parent ISs: far from the interfaces it has high local overlap with the initial mixed configuration. On the other hand, the memory is lower (low overlap, light blue) along the interface, where particles have been moved the most by the minimization procedure. Although at lower temperature the interface is sharper, it is in general quite rough. The hybrid configuration is also a typical IS of the system: the only reason why we can visualize the interface is that we know

a priori the shape and position of the excitation. We indeed used the mixed configurations $\mathcal{C}_{\alpha_{IS}+\beta_{IS}}$ as reference to calculate the overlap. Without this information, it would be impossible to distinguish the hybrid inherent structure from any other one.

3.3.2 Scaling of the interface cost

Fig.3.4 shows the sample-averaged surface energy ΔE_{IS} *vs.* R for several temperatures [39]. What we suddenly note is that there is a well defined relationship between surface energy and size, regulated by the temperature: at fixed R, ΔE_{IS} increases by decreasing T. This relationship does not correspond to a simple

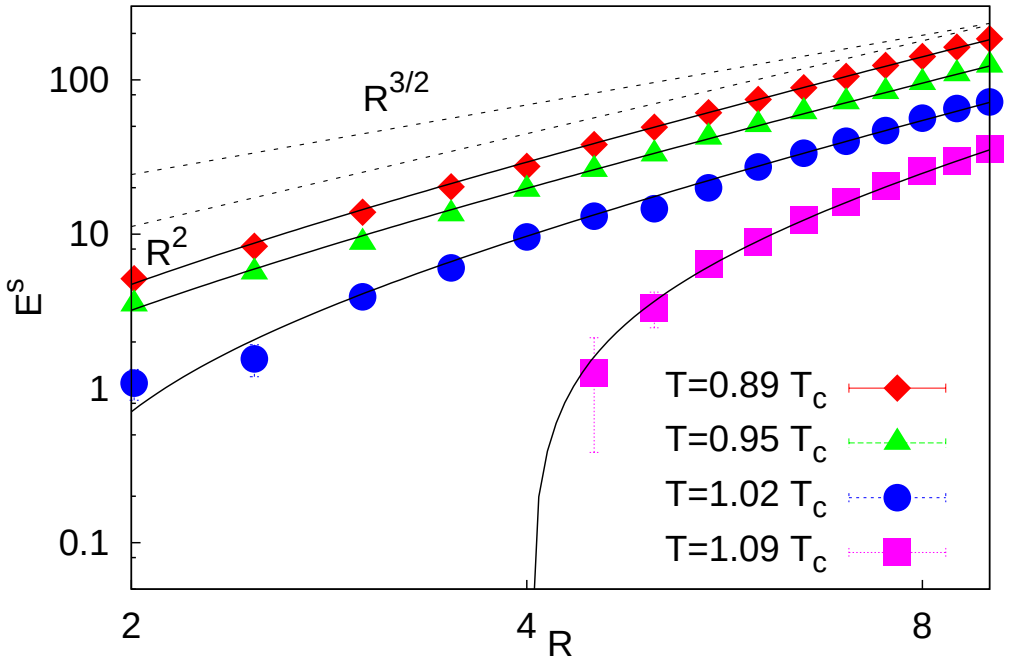

Figure 3.4. The sample-averaged interface cost in configurations $\mathcal{C}_{\alpha_{IS}+\beta_{IS}}$ as a function of R at various temperatures.

power-law behaviour. Indeed, the data seem to deviate from the large R trend as it is present a small size correction.

A quite natural form for the interface cost in disordered system is

$$\Delta E_{IS} = Y_\infty R^\theta - \delta R^\omega \,, \tag{3.10}$$

where Y_∞ is the asymptotic surface tension and $\omega < \theta$.

The sub-leading correction, δR^ω, may arise from bulk contributions: in the random field Ising model [51] it represents the neat contribution of the random field to the stability of ferromagnetic droplets. Indeed, in this model, a local field h_i randomly extracted with zero mean and variance h^2, at enough low temperature,

promotes the fragmentation of the ferromagnetic phase in positive and negative droplets. On scale l, the variance of the global energy term due to the interaction with the random field is $h^2 l^d$. Thus droplet of linear size l can form at the price $\Delta E = Y l^2 - h l^{d/2}$. This is the case in which $\omega = d/2$.

A decrease of the interface cost may also come from the roughening of the interface that lowers the surface energy, as in the random bond Ising model [52]. This is an Ising spin model where the nearest neighbors bonds are random, albeit typically positive. In such a system the position of a domain wall strongly depends on the disorder, since the weak bonds are more likely to be broken. On the one hand, a smooth domain wall is preferable, as it would break the smallest number of bonds. On the other hand, some suitable deviation from smoothness could induce the breaking of weaker bonds and hence a lower energy cost. Hence, a rough interface is the result of a complicated optimization problem: the cost of a large number of broken bonds is balanced by the gain due to the presence of very weak bonds among them. As a result, in disordered systems a rough interface can be energetically favored with respect to a smooth interface, so that a correction like δR^ω may arises.

Finally the term δR^ω is also present in liquids without any connection to the disorder. In this case the curvature of the droplets leads to (3.10) with $\omega = 1$ [53]. In our case where the smallest sphere has radius 1.5, this term could be quite important. However, the prefactor δ of this kind of correction is found to depend on the symmetry under the exchange of two phases [54]. In disordered liquids, we have many states. We can imagine that two of them would not be symmetric under exchange. Nevertheless we can suppose that on average the correction due to this asymmetry should be zero.

A meaningful fit of the $\Delta E_{IS}(R)$ results requires to choose the exponents in (3.10) with some criterion, because the non-linear fit with four parameters is marginally stable, and many sets of parameters give good fits. Our data strongly suggest the conservative choice $\theta = 2$ [39] (see figure 3.4), which seems to describe the large R behaviour better than the alternative $\theta = 3/2$ predicted by a wetting argument [55,56]. The value $\theta = 2$ is also found in Kac spin models [57].

Our estimate of ω relies on the physical hypothesis that the prefactor δ in the correction term of (3.10) (unlike Y_∞) has large fluctuations even for $R \to \infty$. This behaviour is rather in disordered media [51, 52, 58] and finds a confirmation here by the departure from the central limit theorem prediction shown by the variance of the surface tension at large R (see inset in Fig.3.11 later on).

To fix ω, we take (3.10) as valid for the whole population of surface energies, $\Delta E_{\alpha_{IS}\beta_{IS}}$, (instead of just the average ΔE_{IS}), and ascribe all fluctuations of $\Delta E_{\alpha_{IS}\beta_{IS}}$ to the quantity

$$\delta_{\alpha\beta} = \frac{Y_\infty R^2 - \Delta E_{\alpha_{IS}\beta_{IS}}}{R^\omega} \,. \tag{3.11}$$

We then require that the variance $\mathrm{Var}[\delta(\omega)]$ of $\delta_{\alpha\beta}$ be independent of R, which is the typical behaviour of random systems [52,58]. We thus fix ω with the following self-consistent procedure: for a running value of the exponent, $\tilde{\omega}$, we fit the average

of ΔE via (3.10) to obtain $Y_\infty(\tilde{\omega})$ and a population of $\delta_{\alpha\beta}$ with variance $\mathrm{Var}[\delta(\tilde{\omega})]$. At large R

$$\mathrm{Var}[\Delta E] \sim \mathrm{Var}[\delta(\tilde{\omega})] R^{2\tilde{\omega}} \,, \tag{3.12}$$

where $\mathrm{Var}[\delta(\tilde{\omega})]$ will in general depend on R. A similar formula holds for $\tilde{\omega} = \omega$, but with R-independent variance (i.e. $\mathrm{Var}[\delta(\tilde{\omega})]$ have not to change with the R variation), so that

$$\log \mathrm{Var}[\delta(\tilde{\omega})] = \log \mathrm{Var}[\delta(\omega)] + 2(\omega - \tilde{\omega}) \log R \,. \tag{3.13}$$

The procedure is to fit $\log \mathrm{Var}[\delta]$ *vs.* $\log R$ at large R for several values of $\tilde{\omega}$ to obtain the slope $a(\tilde{\omega})$. In Fig.3.5, the trend of $a(\tilde{\omega})$ *vs.* ω for the lowest temperature $T =$

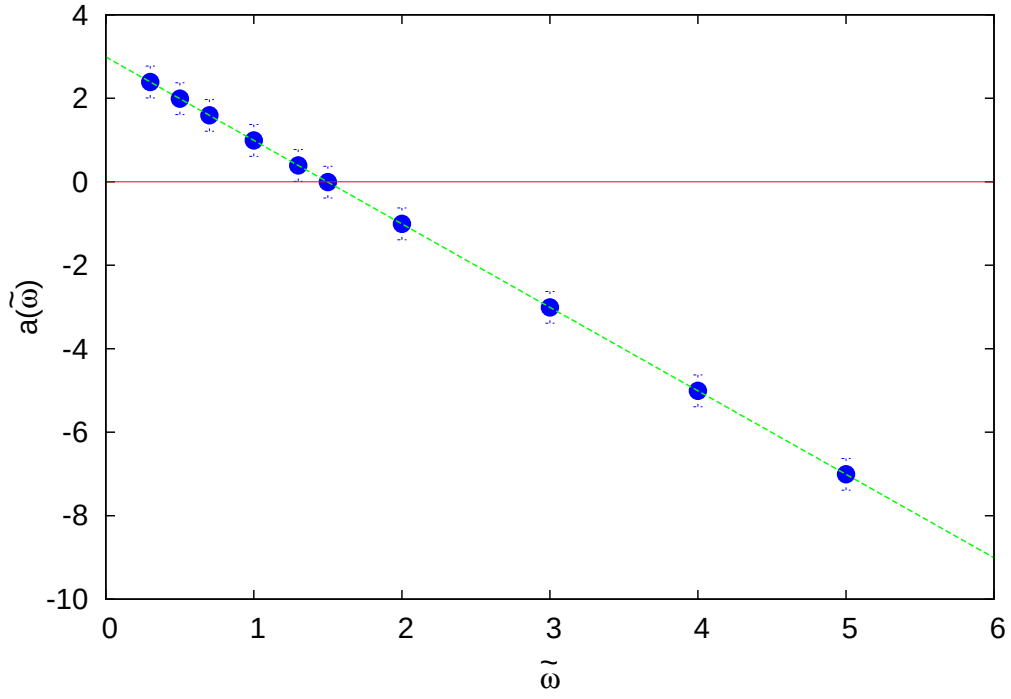

Figure 3.5. Trend of $a(\tilde{\omega})$ *vs.* $\tilde{\omega}$ for the lowest temperature $T = 0.89\,T_c$. The full thin line indicates the zero level. The broken line is the linear fit of the data. The two lines cross at $\tilde{\omega} = 1.5$.

$0.89\,T_c$ is shown. This trend is finally fitted to $a(\tilde{\omega}) = 2(\omega - \tilde{\omega})$ to obtain ω. We do this for different values of the temperature T but we do not find any trend of ω with the temperature. Thus, to get rid of unwanted thermal noise in the determination of this exponent we use the lowest T to fix its value. This procedure gives $\omega = 1.5(2)$ [39], which is very much within the range of values provided by nonlinear fit of the data surface energy with all four parameters free.

The result $\theta = 2$ is somewhat sensible and not particularly exciting: it is basically telling us that disorder in a supercooled liquid is not strong enough to change in any exotic way the leading term of the surface energy cost: surfaces remain surfaces, albeit a correction term arises at small R. We already discussed the typical

origin of this correction term but we have to further analyze this issue: a more detailed analysis allows a direct interpretation of this term within the theory of rough surface in disorder media.

3.3.3 The interface roughening

The signature of roughening is the fact that the interface thickness w grows with the linear size R of the interface itself,

$$w \sim R^{\gamma}, \tag{3.14}$$

where γ is the so-called roughening exponent.

We already saw how the roughening of the interfaces in random media (like random bond Ising model) can lead to a decrease of the interface energy cost. The interesting point is that in the context of elastic manifolds in random media [59, 60], a precise relation exists between the energy gain term and the roughening exponent γ. The energy gain by roughening appears as a negative correction to the ground state energy of the manifold,

$$E_s = AR^{\theta} - BR^{2\gamma}\,, \qquad d = 3\,. \tag{3.15}$$

Equation (3.15) is similar to (3.10). Thus, our hypothesis is that the interface energy $\Delta E_{\alpha_{IS}\beta_{IS}}$ of the amorphous excitations can be described as in (3.15) by a leading term (due to the generalized surface tension Y_{∞}) plus the sub-leading correction δR^{ω}, where $\omega = 2\gamma$, due to roughening.

In random manifolds $\theta = d - 1$. Also in our case the asymptotic trend of the interface cost data seem to indicate such a value for the leading exponent ($\theta = 2$). Still we now try to find θ again via a determination of the interface roughening in the $\mathcal{C}_{\alpha_{IS}\beta_{IS}}$ configurations.

To study the roughening properties of the excitations, we focus on ISs obtained by equilibrium configurations at the lowest available temperature, $T = 0.89T_c$. Indeed the roughening mechanism is ruled by the a zero temperature fixed point. For this reason, working with the ISs is a good approach. The lower is the temperature the smaller is the disturbing effect of thermal fluctuations also in the initial configurations, and hence we consider the temperature $T = 0.89T_c$.

In order to define the thickness w of the excitation we can look at the overlap between the just-switched configuration $\mathcal{C}_{\alpha_{IS}+\beta_{IS}}$ and its relative minimum $\mathcal{C}^{IS}_{\alpha_{IS}\beta_{IS}}$ (the definition we used for the off-lattice local overlap is in section 3.2.3). The overlap is small close to the interface, where particles have moved most, while it gets close to one away from it. Hence, we can define w as the thickness of the region for which the local radial overlap of the excitation is smaller than an arbitrary threshold value q_{th}. In figure 3.6 [40], the local overlap is plotted as a function of the distance r from the center of the sphere. The increase of the overlap for a sphere of radius $R = 8$ is not completely asymmetric since the size of the sphere is large enough. On the contrary, in very small spheres the overlap has no room to reach high values in the inside. For the smallest spheres, $q(r)$ inside the sphere

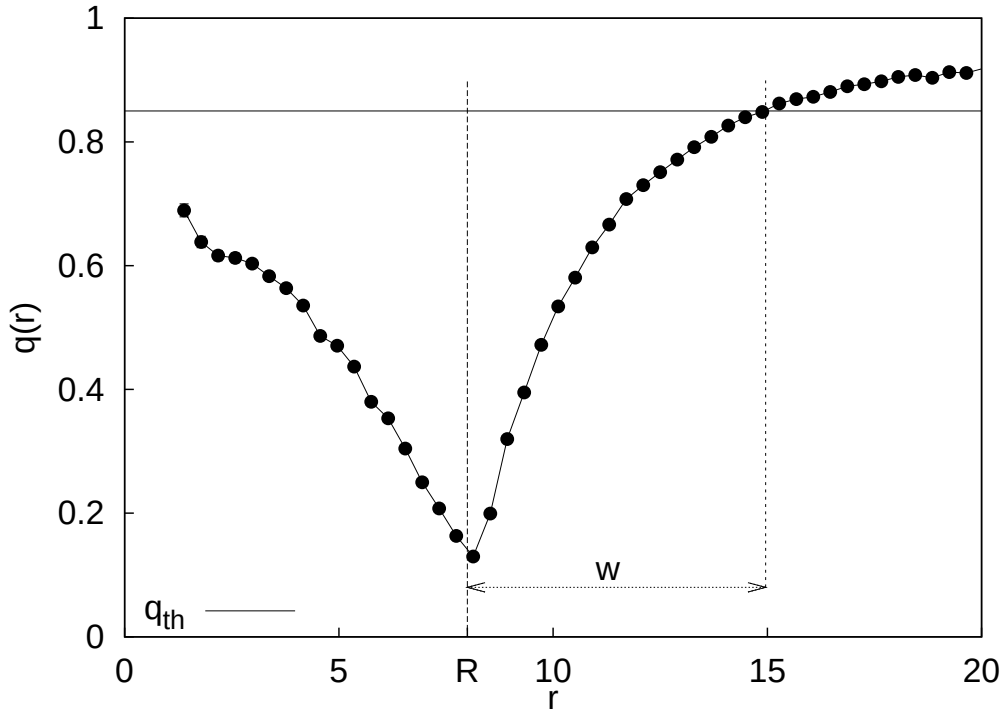

Figure 3.6. Radial local overlap of a sphere of radius $R = 8$. For the estimate of w we look only at the outer part of the interface. This side is not affected by finite size effects in small spheres.

remains smaller than 0.2. It is moreover quite noisy since the corona at small r have poor statistics. To define a unique protocol for the measure of w for all the R values, we consider only the increase of the radial overlap outside the sphere. This is sketched in figure 3.6. Given the radial overlap $q(r)$, the interfacial thickness w is defined as the distance between R and the value $\hat{r}$ at which $q(\hat{r}) = q_{th}$, where q_{th} is a threshold value. In figure 3.7, we report w as a function of the radius R of the excitation in a log-log plot. We conclude that the excitations' interfaces roughen according to relation (3.14), with

$$\gamma = 0.62 \pm 0.01. \tag{3.16}$$

A roughening exponent smaller than one implies that the ratio w/R between width and linear scale of the surface decreases for larger spheres. Thus large excitations have *relatively* thin interfaces. This is clearly shown in figure 3.8 [40], where two excitations with different radius ($R = 4$ *vs.* $R = 8$) are compared in a coordinate system where all lengths are rescaled by R, so that both rescaled spheres have virtual radius unity. The rescaling emphasizes the thick interface of the smaller excitation compared to the sharper interface of the larger excitation.

A fit of $\Delta E_{\alpha_{IS}\beta_{IS}}$ at the lowest temperature $T = 0.89 T_c$ with the functional form (3.15) where θ is free and the value of γ is the one found in (3.16), $\gamma = 0.62$, gives [40]

$$\theta = 2.08 \pm 0.04\ . \tag{3.17}$$

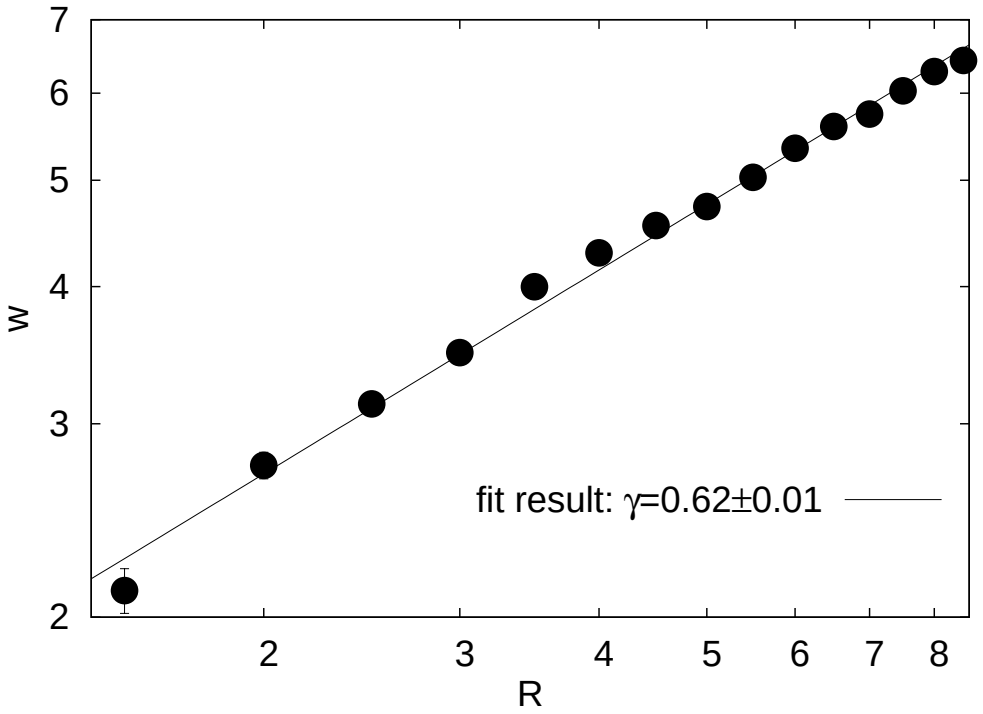

Figure 3.7. Scaling of the interface thickness w with the size R of the sphere.

In this way, we recover the value $\theta = 2$ we had obtained simply observing the large R trend of $\Delta E_{\alpha_{IS}\beta_{IS}}$.

Finally summing up, a roughening of the interfaces in $\mathcal{C}_{\alpha_{IS}\beta_{IS}}$ has been effectively found. In this context, result (3.17) confirms that the roughening explanation of the small size correction to the interface energy is perfectly compatible with our numerical data.

3.3.4 A new spinodal point

With θ and ω fixed, equation (3.10) fits the $\Delta E_{IS}(R)$ data very well (Fig.3.4). We thus obtain the asymptotic surface tension Y_∞ as a function of the temperature T. This is shown in Fig.3.9 [39] top. We find that Y_∞ decreases for higher T, and becomes quite small above T_c.

In the same figure (lower panel), we present the mean inherent structure energy, $E_{IS} = \langle E_{\alpha_{IS}} \rangle_{\alpha_{IS}}$, as function of the quenching temperature. A comparison of the two curves clearly shows that they are correlated. The high temperature regime is the regime where the dynamics is weakly influenced by the potential energy landscape. Correspondingly, the distinction between different states is softer and the surface tension Y_∞ at interfaces smaller. On the contrary, as the temperature is lowered, the system explores an highly complex landscape at a lower energy level. In this regime the sharp distinction between minimum and minimum corresponds to an high surface tension value. This finding is perfect agreement with

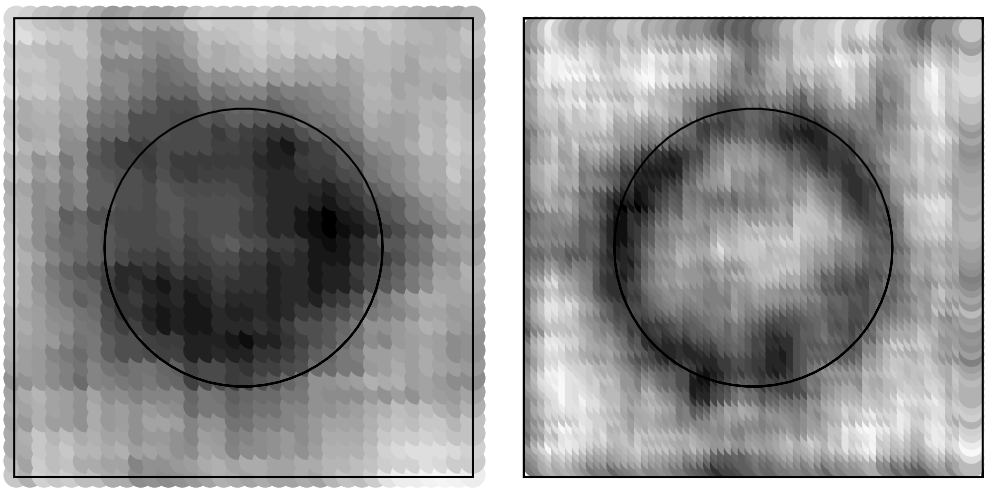

Figure 3.8. Local overlap $q_{\alpha\beta}(r)$ between $\mathcal{C}^{IS}_{\alpha_{IS}\beta_{IS}}$ and $\mathcal{C}_{\alpha_{IS}+\beta_{IS}}$ for configurations with interface placed at $R = 4$ (left) and $R = 8$ (right). Plots are rescaled so that both spheres appear as having the same size. Low overlap (dark grey) at interfaces indicate major rearrangements of particles, while far from interfaces the overlap with initial configurations is high (light grey). Clearly the larger sphere (right) has a relatively thinner, or smoother, interface.

the idea that in finite dimension the surface tension is the fingerprint of multi-state scenario.

We can thus use the interface cost to fix a limit of validity to the existence of many states. This limit is represented by a spinodal point, since classically the spinodal does mark the limit of existence of a metastable state (it can indeed be defined in systems which present first order phase transition). The spinodal would indicate the passage from the multi-state scenario (and the Mosaic picture) to the single liquid state in which the dynamics does not require activation. However the decrease in Fig.3.9 is rather smooth, so that it is hard to define a spinodal temperature. On the other hand, the plot of the average IS energy, E_{IS}, *vs.* T (Fig.3.9, bottom) suggests using the *energy* as a control parameter.

The Y_∞ *vs.* $E_{IS}(T)$ curve is nearly linear (Fig.3.10, left), indicating that Y_∞ vanishes quite sharply at a well-defined energy E_{th}. Interestingly enough, E_{th} is very close to the *threshold*, i.e. the energy below which minima start to dominate the energy landscape [24, 26]. As discussed in section 2.3, the threshold E_{th} is defined as the point where the instability index of saddles vanishes (Fig.3.10, right). The stationary points above this energy level are typically saddles. Below, they are minima. Crossing this saddle-minima transition, the non activated channels for the relaxation of the systems becomes subdominant and only activation rules the dynamics. What we now observe is that the surface tension estimated via the ISs study starts to be different from zero below the same saddle-minima transi-

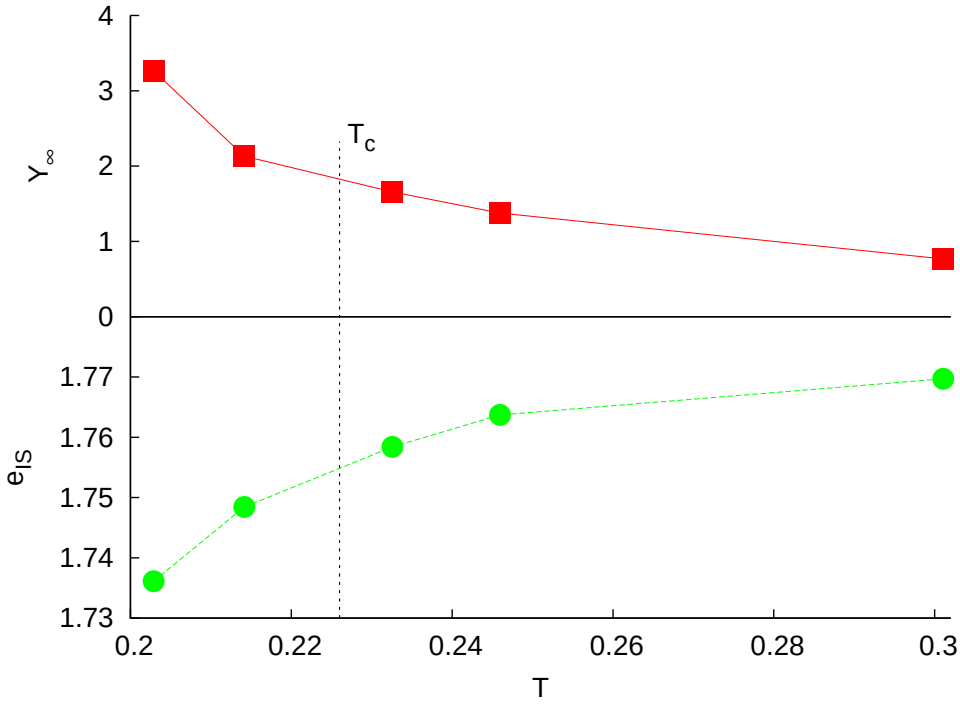

Figure 3.9. Upper panel: Y_∞ as a function of the quenching temperature of the inherent structures. The vertical dotted line marks the mode coupling temperature. Lower panel: inherent structure energy as a function of the quenching temperature.

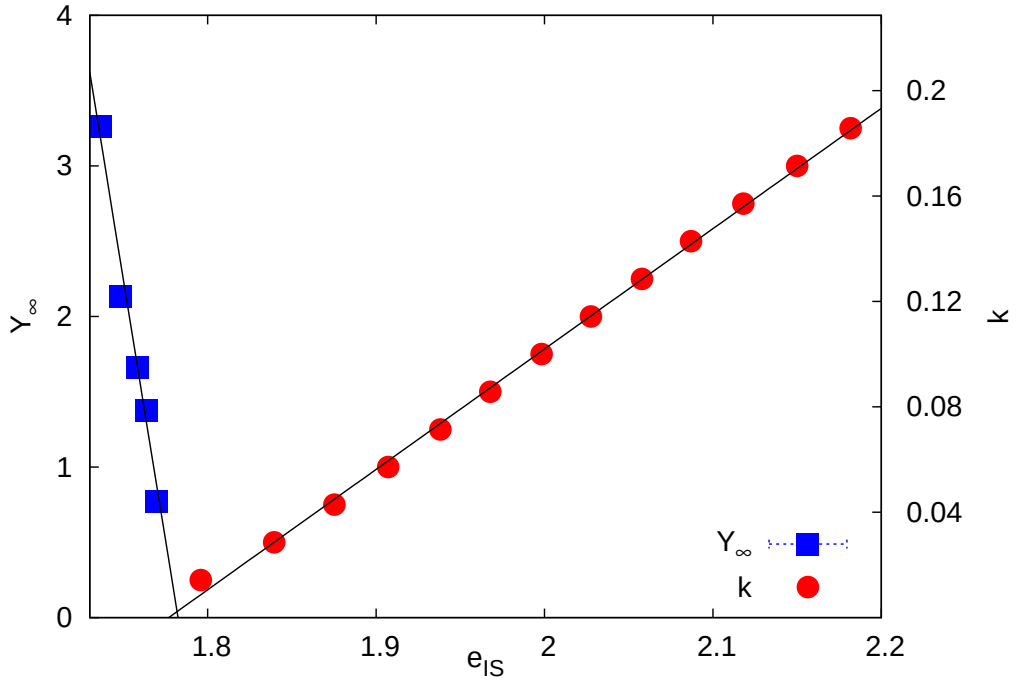

Figure 3.10. Left: Y_∞ (squares) *vs.* IS energy. Right: intensive saddle instability index k (circles) *vs.* IS energy. Lines are linear fits to the data. Both the surface tension and the instability index seem to vanish at a similar energy, the threshold E_{th}, which is therefore the spinodal point. Instability index data are from [24].

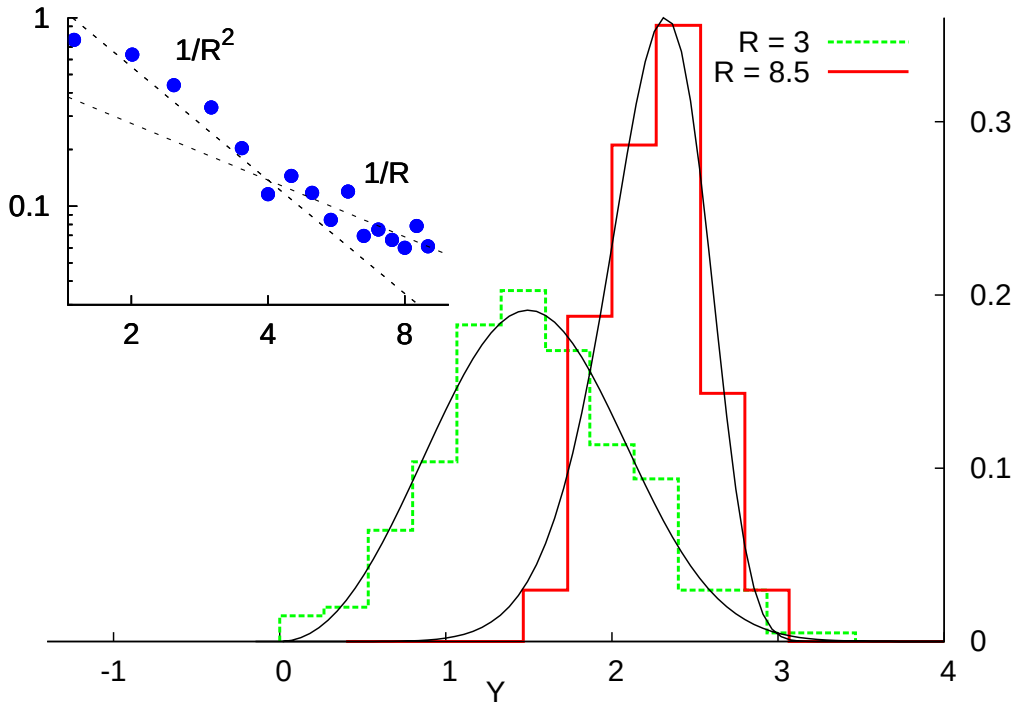

Figure 3.11. Normalized histograms of the surface tension for $T = 0.89T_c$ at two values of R. Solid lines correspond to fits with the Weibull distribution $P(Y) = -d/dY \exp[-(Y/y_c)^{\hat{\zeta}}]$ (see Ref. [35]). Inset: variance of $Y_{\alpha\beta}$ vs. R.

tion point. Below this point the equilibrium dynamics typically refers to stationary points which pays a well-defined surface tension when they are in contact one to each other. For this reason they cannot be considered different configurations of a unique phase, the liquid one, but they represent well-distinct amorphous minima, metastable amorphous states. E_{th} is thus the true spinodal point of amorphous order. It fixes the upper limit of stability of the Mosaic mechanism. It moreover indicates when the partition of the phase space in states can be applied in a finite dimensional system, like the soft sphere model, without implicating an implicit mean field approximation.

3.3.5 Surface tension fluctuations

As introduced in the previous chapter, we expect the surface tension to fluctuate when considering different pairs of IS. We thus compute the distribution of the single-sample surface tension,

$$Y_{\alpha\beta} \equiv \frac{\Delta E_{\alpha_{IS}\beta_{IS}}}{R^2}. \tag{3.18}$$

The distribution $P(Y, R, T)$ for two values of R is shown in Fig.3.11 [39]. This distribution does not depend on the exponent ω and its average tends to $Y_\infty(T)$ for $R \to \infty$.

The first thing we notice is that the distribution is quite broad. This means that the original version of the Mosaic, which assumed a sharp value of Y, cannot hold strictly. Briefly summarizing, if there is a single surface tension, a region smaller than ξ_c cannot rearrange, so that a nonfluctuating surface tension implies a sharp drop of the point-to-set correlation $q(R)$ at $R \sim \xi_c$. With a fluctuating surface tension, on the other hand, any region can decorrelate, as long as there are target states with surface tension $Y < T\Sigma R^{d-\theta}$. Our finding is thus qualitatively consistent with the smooth decay of the correlation observed numerically [34,35]. Also a quantitatively agreement will be revealed in what follows.

The second important result [39] is that the distribution narrows as R grows. The variance of $Y_{\alpha\beta}$ (inset of Fig.3.11) is monotonically decreasing. In particular for small R this quantity seems to decay as $1/R^2$, but at larger R it is larger than that. This result is further evidence of the presence of a small size correction term δR^ω. Usually in disordered media the variance of such a term grows like $\mathrm{Var}[\delta R^\omega] \sim R^{2\omega}$, since $\mathrm{Var}[\delta]$ remains constant. On the other hand the term $Y_\infty R^2$ obeys the central limit theorem giving $\mathrm{Var}[Y_\infty R^2] \sim R^2$. Using the approximation $\mathrm{Var}[\Delta E_{IS}] \sim \mathrm{Var}[Y_\infty R^2] + \mathrm{Var}[\delta R^\omega]$, we can thus write

$$\mathrm{Var}[Y_{\alpha\beta}] \sim R^{-2} + R^{2\omega-4} \; . \tag{3.19}$$

Equation (3.19) accounts for the crossover between two different decreasing trends, the faster at small R like R^{-2} which is visible in Fig.3.11, and the slower at large R. Moreover, in Fig.3.11, the large R decrease of $\mathrm{Var}[Y_{\alpha\beta}]$ is compatible with an R^{-1} decay, consistent with $\omega \sim 3/2$. This is the result ($\omega = 1.5$) we already obtained using a more quantitative approach previously reported. In Fig.3.11 the deviation of the numerical data from the R^{-2} decay thus confirms our physical hypothesis that the large R fluctuations of $Y_{\alpha\beta}$ are dominated by the correction term δR^ω.

To physically interpret the variance decrease, we have to note that $P(Y)$ depends on T both directly through the quench temperature of the IS and indirectly through R. Since the only relevant length-scale is $\xi_c(T)$, the typical size of the rearranging regions, we can define

$$P(Y,T) \equiv P(Y, R = \xi_c(T), T), \tag{3.20}$$

where $\xi_c(T)$ is taken from simulations [35]. When T decreases, $\xi_c(T)$ grows, $P(Y,T)$ narrows, and the decay of $q(R,T) - q_0$ sharpens. This is indeed the numerical finding of [35], where the decay is well described by a compressed exponential,

$$q(R,T) - q_0 = (q_1 - q_0) \exp\left[-(R/\xi_c)^\zeta\right], \tag{3.21}$$

where the anomaly ζ grows from 1 at high temperature up to ~ 4 at low T. Note that higher ζ means sharper decay.

The link between $P(Y,T)$ and the sharpness of decay can be made more quantitative [39]. The overlap $q(R)$ is given, as anticipated in (2.61), by [35]

$$q(R,T) - q_0 = (q_1 - q_0) \int_{TS_cR^{d-\theta}}^{\infty} P(Y,T)\, dY \; . \tag{3.22}$$

Using the approximation (3.20) we now have an estimate of $P(Y,T)$. A problem is that we cannot integrate it between the two extremes $TS_cR^{d-\theta}$ and ∞ as in (3.22). This would require a guess for the value of the configurational entropy S_c. However its estimate is always very tricky [28]. To avoid this problem we choose to work with a variable that implicitly include S_c and thus we define a variable with the dimensions of the surface tension: $y = T\Sigma R^{d-\theta}$. In terms of this new variable we can integrate our numerical data in the following way

$$I(y,T) = \int_y^\infty P(Y,T)\, dY \ . \tag{3.23}$$

If the distribution $P(Y,T)$ provides a good estimate of the real surface tension distribution, the correspondence

$$I(y,T) = \frac{\hat{q}(y,T) - q_0}{q_1 - q_0} \tag{3.24}$$

holds, where $\hat{q}(y,T) = \hat{q}(TS_cR^{d-\theta},T) = q(R,T)$. In this way we theoretically fixed the equivalence between the result of [35] and our numerical result.

To perform a direct comparison of our numerical result, encoded in $I(y,T)$, with the $q(R,T)$ of [35], in general we still need to know S_c. However in the particular case of the functional form (3.21), the change of variables turns out to be crucial. Given $y(R) = TS_cR^{d-\theta}$, we have

$$I(y(R),T) = \frac{\hat{q}(y(R),T) - q_0}{q_1 - q_0} = \frac{q(R,T) - q_0}{q_1 - q_0} = \exp\left[-(R/\xi_c)^\zeta\right] \ . \tag{3.25}$$

Defining $Y_c = TS_c\,\xi_c^{d-\theta}$, we can write

$$\left(\frac{R}{\xi_c}\right)^\zeta = \left(\frac{TS_cR^{d-\theta}}{TS_c\,\xi_c^{d-\theta}}\right)^{\frac{\zeta}{d-\theta}} = \left(\frac{y}{Y_c}\right)^{\frac{\zeta}{d-\theta}} \ . \tag{3.26}$$

Hence we have

$$I(y,T) = \exp\left[-(y/Y_c)^{\hat{\zeta}}\right] \tag{3.27}$$

with $\hat{\zeta} = \zeta/(d-\theta)$ and $Y_c = TS_c\,\xi_c^{d-\theta}$.

In [35] a fit of $q(R,T)$ has been performed using the functional form (3.21) with three free parameters: $q_1 - q_0$, ξ_c and ζ. The first interesting result was the growth with lowering temperature of the exponent ζ. Beside an increase in the parameter ξ_c has been found. This second result is perhaps more fundamental than the first: irrespective of the Mosaic picture the $q(R)$ has turned out as the first static function which indicates a growing correlation length.

We want to compare these results with our findings about the surface tension. We computed $I(y,T)$ at the lowest temperature, $T = 0.89\,T_c$, where the difference between energy and free energy should be less harmful. $I(y,T)$ is shown in Fig.3.12, in the inset we report the distribution $P(y, T = 0.89\,T_c, R = 4)$ from which we computed this result. The integration significantly cleans the noise of the numerical data. We fitted $I(y,T)$ with the function (3.27) with two free parameters:

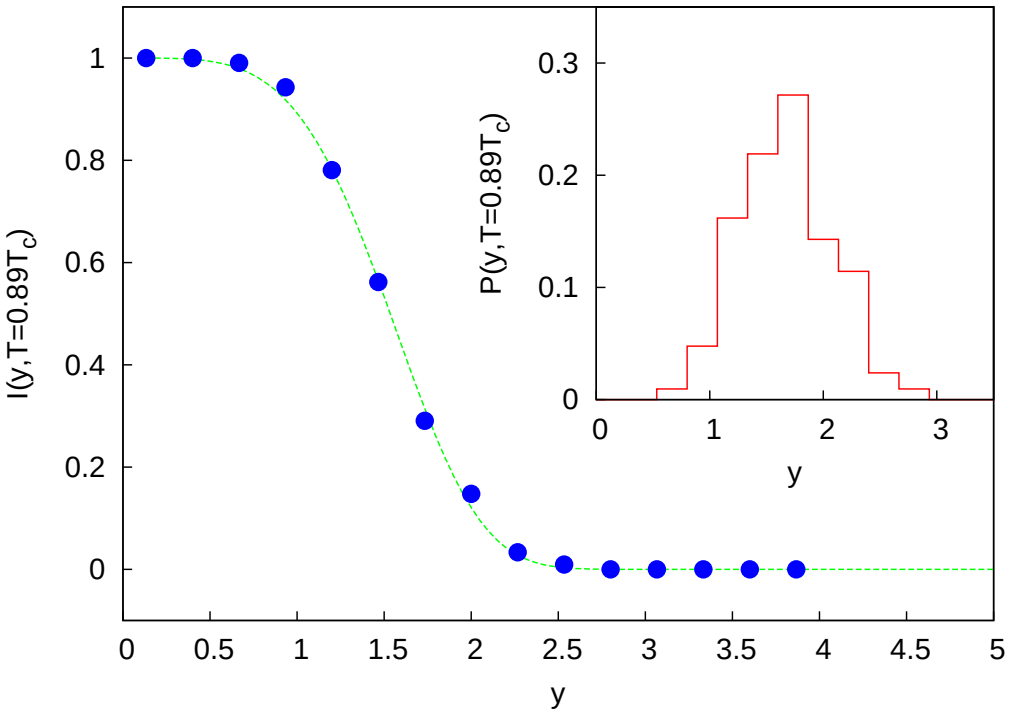

Figure 3.12. Integral between y and ∞ of the distribution of the surface tension we numerically find. The temperature is the lowest one ($T = 0.89\,T_c$) and the size of excitation is the nearest one to the size that, according to [35], corresponds to the chosen tenperature ($\xi_c(T = 0.89\,T_c)$): $R = 4$. The distribution is shown in the inset.

Y_c and $\hat{\zeta}$. The broken line in Fig.3.12 is the best fitting compressed exponential we found. The comparison of results for the exponents does not imply any knowledge of the configurational entropy. From what we explained above, we expect $\hat{\zeta} = \zeta/(d-\theta)$. Thus, since $d = 3$ and $\theta = 2$, it should be $\hat{\zeta} = \zeta$. The result for the exponent $\hat{\zeta}$ is [39]

$$\hat{\zeta} = \zeta = 4.2 \pm 0.1\ . \tag{3.28}$$

This result is encouragingly close to the value $\zeta = 4.0(6)$ of [35].

The agreement on the values of ζ found with two completely different protocols puts the extended version of the Mosaic on a firmer basis.

The result for Y_c is

$$Y_c = 1.67 \pm 0.01\ . \tag{3.29}$$

To compare this result with the finding of [35] $\xi_c = 3.8(1)$ we should know the configurational entropy. We can do the inverse procedure and, assuming the consistence between the two independent results, we can estimate the configurational entropy. Since $Y_c = TS_c\xi_c$ we have

$$S_c = \frac{Y_c}{T\xi_c} = 2.16 \pm 0.07\ . \tag{3.30}$$

However, we want to compare this result with the configurational entropy in [28], which is $\mathcal{S}_c = \log \mathcal{N}/N$ and N is the number of the particles. Since in our case the

number of the particles in the excitation of size ξ_c is $N_{sphere} = 4/3\pi\xi_c^3$, we have to compute

$$\mathcal{S}_c = \frac{3}{4\pi} S_c \, . \tag{3.31}$$

The result we find is

$$\frac{3}{4\pi} \, S_c = 0.52 \pm 0.02 \, . \tag{3.32}$$

This result is not too far from the one in [28] which is $\mathcal{S}_c = 0.7 \pm 0.1$.

We conclude this section noting that $P(Y,T)$ broadens and clusters around $Y \sim 0$ for $T \gtrsim T_c$, indeed Y_∞ goes to zero for $E \geq E_{th}$. The crossover from many states to one state through a spinodal mechanism is smooth: instead of disappearing abruptly at T_c (as in mean-field [20]) metastable states slowly "fade out", because states are slowly merging with each other, as indicated by the broadening of $P(Y,T)$ which means that many pairs of states have near-zero surface tension.

3.4 The finite temperature analysis

Till now we have studied the surface tension only focusing on the ISs. The results of the previous section are indeed zero temperature results. The surface tension has been obtained only from estimates of the energy cost of interfaces, not dealing with the true free-energy cost. These results are indeed applicable only at low enough temperature.

In this section we instead deal with the full dynamics of the system. On the one hand we will study the scaling with R of the energy part of the real surface tension. On the other hand the relaxation of the excitations, we will observe, will indicate what happens in the real dynamics.

The data of this section are obtained studying thermalized configurations of the soft sphere system. For each temperature we created mixed configurations, as explained in section 3.2, from a collection of about 10 independent equilibrium configurations, using spheres of sizes between 3 and 8 (in units of l_0).

We now observe how the excess energy $\Delta E(t;R)$ of the excitations, defined in 3.1, relaxes with time. We can look at the trend of these data either depending on R having t fixed, or depending on t with R fixed. The first analysis will account for an estimate of the exponent θ at finite temperature. The second will allow to find the exponent ψ of the barriers scaling with R.

3.4.1 Interface cost at finite temperature

To estimate θ we must measure how the excess energy ΔE defined in (3.1) scales with R. This is shown in figure 3.13 [40] for different temperatures and times. As it is natural, the excitations decay with time, and therefore for long times the dependence of ΔE on R becomes rather hazy. However, for intermediate times and for all analyzed temperatures it is clear that a power law R^2 seems to reproduce the data rather satisfyingly. From these data we therefore conclude [40]

$$\theta = 2 \, . \tag{3.33}$$

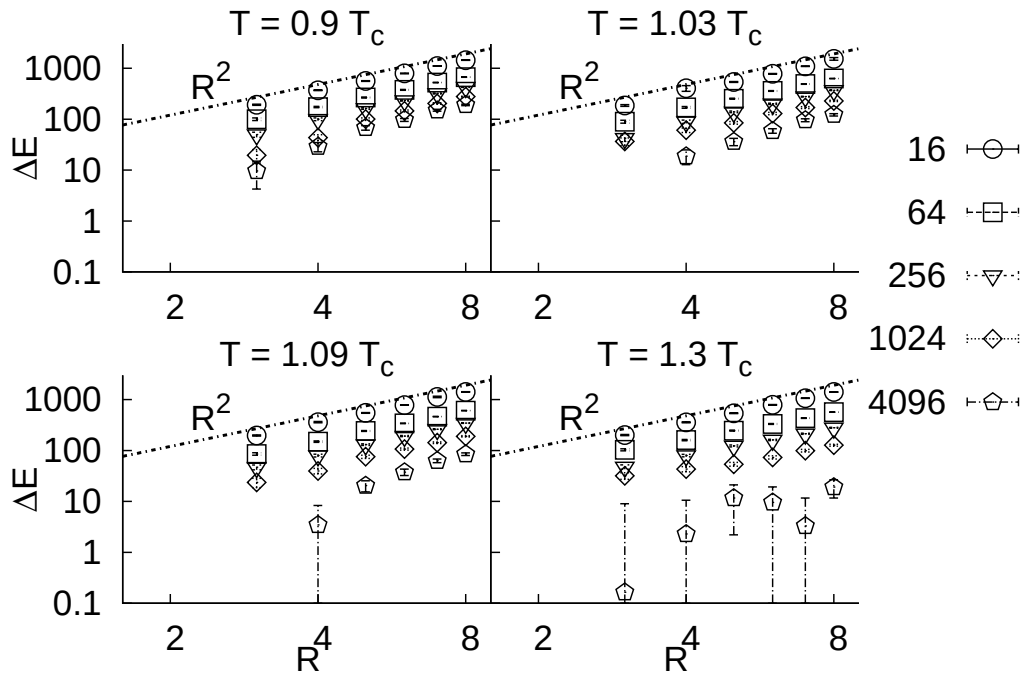

Figure 3.13. Time dependence of the excess energy $\Delta E(t)$ *vs.* R at four different temperatures. From left to right and top to bottom: $T = 0.89T_c, 1.03T_c, 1.09T_c, 1.33T_c$. Time is measured in MonteCarlo steps.

The same value of θ was found in section 3.3.4 using inherent structures. However, we remark that the present data are obtained at *finite* temperature, using equilibrium configurations rather than potential energy minima. Hence, the value $\theta = 2$ seems to be quite robust. Moreover, the data also show that a nonzero surface tension Y survives for quite some time after the formation of the droplet, especially at the lowest temperature.

3.4.2 The activation barriers scaling

As discussed in section 2.3, the relaxation in deeply supercooled liquids proceeds through the activated rearrangement of clusters of correlated particles. As a result, the relaxation time scales exponentially with the size of these regions, see equation (2.9). In this framework we expect that the timescales involved in the formation and in the relaxation of the cooperative regions are in fact the same: each excitation relaxes through the cooperative rearrangement of new excitations. This means that we can follow the process of relaxation of an artificially produced excitation, rather than detect the spontaneous formation of an excitation.

Fixing R, we look at the decay of $\Delta E(t)$. Figure 3.14 [40] (obtained at $T = 0.89T_c$) clearly shows that the rate of relaxation of the excitations changes with their size R: bigger spheres relax over larger time scales.

The artificial construction of the excitations affects the excess energy only for

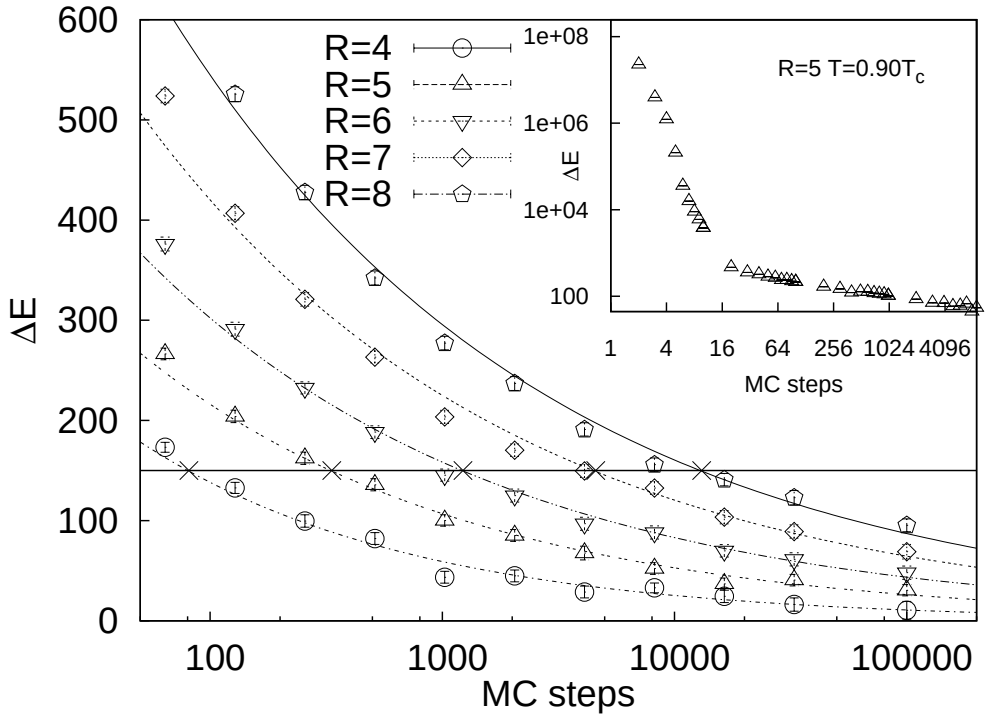

Figure 3.14. $\langle \Delta E(R,t) \rangle$ *vs.* t for R ranging from 4 to 8, left to right. Points are numerical data, curves are power law $\langle \Delta E(t,R) \rangle \sim t^{-\gamma(R)}$ fits. The fits are used to give an estimate of $\tau(R)$, represented by crosses on the threshold line in figure. The values of γ are within the range $0.2 < \gamma(R) < 0.4$.

the first few MC steps (see inset of Fig.3.14). This initial fast decrease of the energy is due to the relaxation of the unphysical stress due to pars of particles arbitrarily close one to each other at the spherical interface in the initial mixed configurations $\mathcal{C}_{\alpha+\beta}$. We met the same problem when we study the ISs. In that case 100 MC steps at $T = 0$ allowed the system to relax the initial stress before minimizing the energy with a non-local more efficient algorithm. In this case the dynamics is ever local, thus we have only to wait for the emergence of the true physical relaxation. The abrupt change in the relaxing energy before 16 MC steps marks a crossover between the initial regime and a slower decrease of the energy. The crossover indicates a sort of discontinuity between the two regimes. The artificial contributions to the energy of the initial transient seems not to influence the following slower relaxation.

We analyze the relaxation of the excitations from 16 MC step. Simply by fixing a threshold value for $\Delta E(t)$, and measuring the time needed to drop below this value, we obtain an estimate of the time τ needed to relax an excitation of size R. The interpolation is obtained fitting the data with a power law in the range $t > 100$ MC steps. We perform the same procedure at different sizes R of the sphere thus obtaining a function $\tau(R)$. We have checked that the exponent in $\tau(R)$ curve below is insensitive to changes in the threshold from $\Delta E_{th} = 100$ to $\Delta E_{th} = 175$.

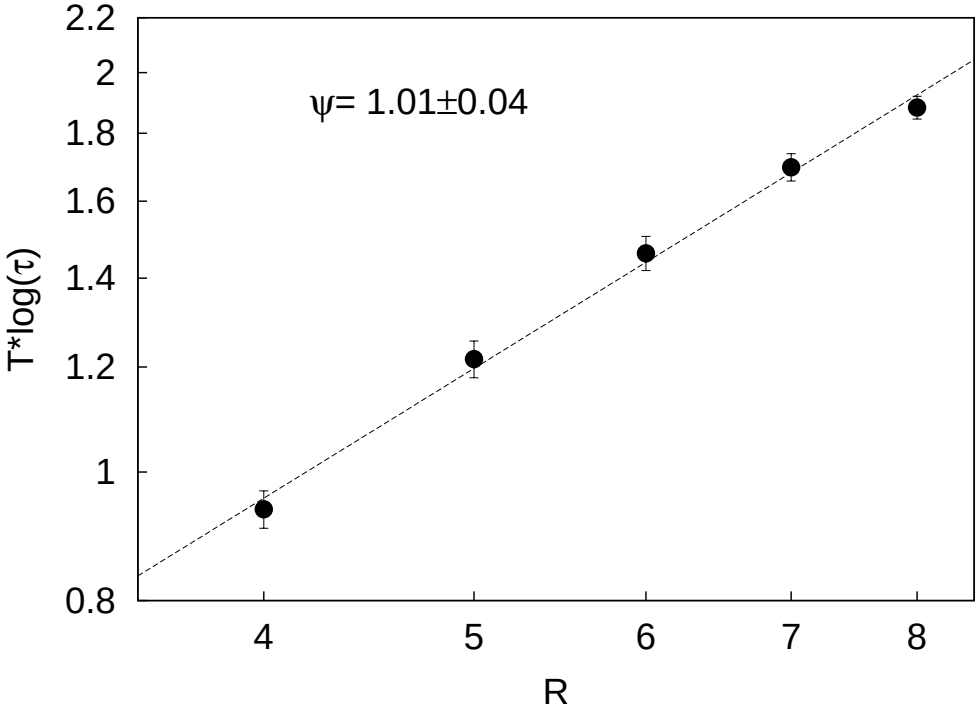

Figure 3.15. $T\log(\tau)$ *vs.* R for $T = 0.89T_c$; errors are evaluated using the bootstrap method. The linear behaviour on log-log plot allows for a scaling ansatz $\tau(R) \sim \exp(R/T)$.

According to (2.9), $T\log(\tau)$ has to scale as R^{ψ}. In the log-log plot in Fig.3.15 [40] we report $T\log(\tau)$ *vs.* R for our lowest temperature. The data lie with good approximation on a straight line, thus confirming that the process of relaxation of the excitations indeed follows the Arrhenius law. A fit of the exponent gives $\psi = 1.01 \pm 0.04$ [40], and hence we conclude,

$$\psi = 1\ . \tag{3.34}$$

The value $\psi = 1$ we find implies that the barrier for the rearrangement of a correlated region scales linearly with its size,

$$\Delta \sim \xi. \tag{3.35}$$

The proposal of AG, $\Delta \sim \xi^d$, has always seemed a bit exaggerated, since one can imagine several ways for the system to pay less than the entire volume to rearrange a region. One of this ways, and not the most pedestrian, is suggested by the fact that the greatest part of the energy necessary to create the excitation is stored in the interface. Hence, one may expect that the barrier scales with the same exponent as the surface energy cost, i.e. θ. This is, basically, the idea of original Mosaic theory deeply rooted in the theory of nucleation and reported in section 2.5.1.

This result, however, is at variance with what we find here, relation (3.35): in fact, whatever one thinks about our numerical result for θ, a value of θ as small as 1 seems rather unlikely. In any case, it is important to emphasize that $\psi = \theta$ is

a natural choice only if one accepts the nucleation paradigm. It has been noted, however, that nucleation is perhaps not a fully correct paradigm to describe the formation of amorphous excitations within a deeply supercooled liquid [32]. The essence of the Mosaic, namely the competition between a surface energetic term and a bulk entropic term, keeps its deepest value even if we do not cast it within the strict boundaries of nucleation theory. The value of the correlation length may come from the point where the two contributions balance, ξ_c, rather than from the Mosaic correspondent to l_{max} of nucleation theory, and (for obvious dimensional reasons) one gets the same expression for ξ_c (up to an irrelevant constant), while ψ remains undetermined. The reference to the nucleation picture indeed fixed $\psi = \theta$: the Gibbs free-energy barrier at l_{max} grows as l_{max}^{θ}. Focusing on the balance of the two competing contributions as it is in the Mosaic picture, the length scale ξ_c does not single out any barrier. However a natural thinking is that the barriers depend on the cooperative length of the Mosaic tiles via an unknown exponents ψ. Only a further analytical effort can explain in more detail the activation mechanism and give a theoretical indication for this exponent ψ.

Up to now the prediction of the Mosaic theory are loosened by the introduction of a new parameter, the unknown exponent ψ. In this more free theory our results perfectly fit. In this section on the finite temperature dynamics, we have determined numerically (in $d = 3$) the exponents linking the size of rearranging regions to barrier height (ψ) and to surface energy cost (θ). This is to our knowledge the first direct measure of these exponents. We find

$$\psi = 1 \,, \qquad \theta = 2 \,. \tag{3.36}$$

Both values are in disagreement with those assumed by the AG and Mosaic schemes. However, if we stick to equation (2.53), we still obtain for the relaxation time the VFT relation (1.22) [40]. It seems that, albeit lying in none of the preexisting theories which propose a numerical value of ψ, we managed to get back the most used fitting relation in the physics of glass-forming systems. There is no particular reason to stick to such VFT. In fact a generalized VFT with an extra fitting exponent ν, such that $\log \tau \sim (T - T_k)^{-\nu}$, would do an even better job in fitting the data. Yet, to get back VFT as the product of the independent numerical determination of two rather different exponents, remains a rewarding result to some extent.

The disagreement between our exponents and those proposed in the original Mosaic do not imply as harsh a blow to RFOT as it might seem at first. RFOT can be cast in a form [32] that retains its most essential aspect, namely the competition between a surface energy cost and a bulk energy gain, without using nucleation theory. If one does this, the exponents ψ and θ remain unrelated and compatible with our findings. Within this context, our result $\psi = 1$ seems to be an indication that Mosaic is a better theory if one does not push the nucleation analogy too hard.

We must note at this point that it exists an argument by Fisher and Huse [36] which fixes the relation $\psi > \theta$, in disagreement with our result. The argument says that if the droplet formation is an activated mechanism, the barrier has to scale at least as the final interface cost, $\Delta E \sim R^{\theta}$. Indeed slower scaling would mean that for an enough large droplet the barrier is smaller than the final interface

cost. It has to hold $\psi > \theta$. We think that this result is not straight applicable to the low temperature liquid case where a large number of states influence the dynamics. Indeed the argument only account for the energy part of the barriers, while in supercooled liquids the large number of states plays a central role. The number of the possible target states is exponential with the volume of the droplet. Similarly the paths in the phase space can be large enough to significantly decrease the time scale of the excitation formation. Thus if the time to change the excitation α in an other specific state β scales like $\exp(\Delta/T)$, the time to nucleate any other different state should be much smaller. As a matter of fact our result for θ comes from an energy measure, whereas the exponent ψ has been estimated by observing the relaxation time, i.e. the possibility to rearrange the region in any other state. In this more complicated picture, the final relation between the surface exponent and the barriers' exponent is not clear. However the restriction imposed by Fisher and Huse should not necessary hold.

3.4.3 The thermal surface tension

One of the aims of the study at finite temperature is the confirmation of some of the results of the inherent structure analysis. A direct comparison of the ISs results and the full-thermal analysis can be accomplished as follows. During the Monte

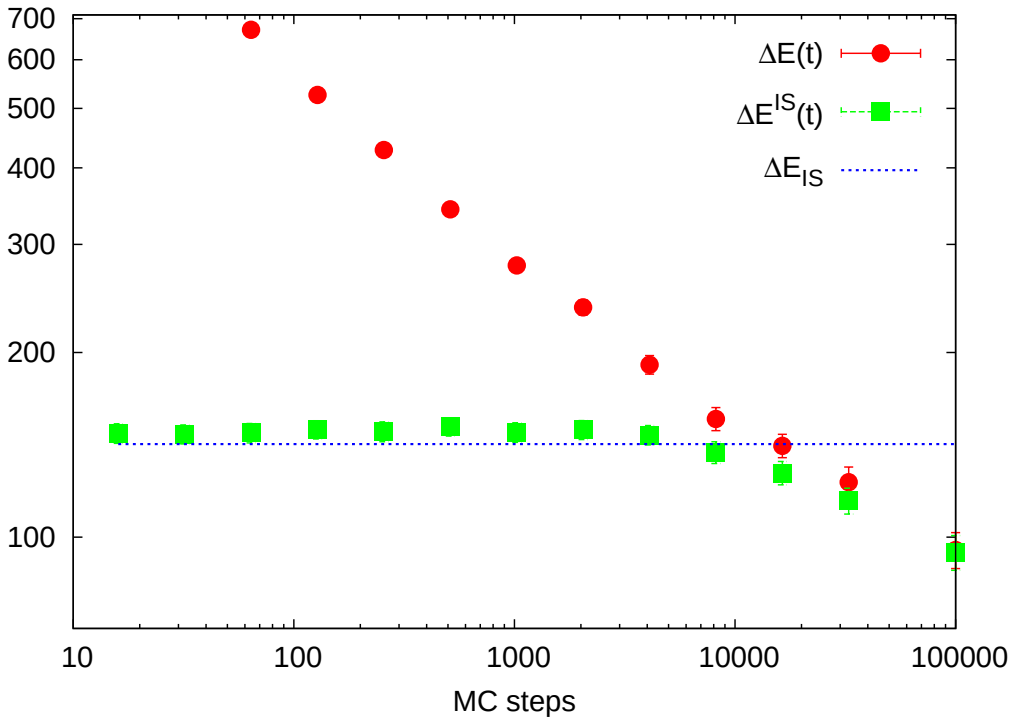

Figure 3.16. The thermal excess energy decrease with temperature increasing (the circles) compared to the istantaneous IS excess energy (the squares) and to the IS excess energy obtained with the direct minimization.

Carlo dynamics at finite temperature, the istantaneous configuration $\mathcal{C}_{\alpha\beta}(t)$ can be

used as the initial configuration for a minimization of the energy. In this way each istantaneous configuration can be associated to an istantaneous inherent structure that we will call $\mathcal{C}^{IS}_{\alpha\beta}(t)$ (which is different from the ISs we defined in the zero temperature study, $\mathcal{C}^{IS}_{\alpha_{IS}\beta_{IS}}$). This procedure gives information about the IS within which the system lies during the relaxation.

We expect that the thermal relaxation does not immediately push the system out of its initial IS. An initial part of the relaxation should indeed concern the extra energy contribution due to our artificial construction (see figure 3.14). This extra energy term was eliminated also in the minimization procedure that from $\mathcal{C}_{\alpha_{IS}+\beta_{IS}}$ led to $\mathcal{C}^{IS}_{\alpha_{IS}\beta_{IS}}$. Hence this initial IS should be the one we studied thoroughly in the zero temperature section. On longer time scales, however, the activated relaxation of the excitation let the system leave the initial IS and decorrelate as required by the complete ergodicity restoration.

This is exactly what is shown in Fig.3.16. We computed the excess energy $\Delta E(t)$ of the istantaneous thermal configurations subtracting from their energy the energy of the initial configurations $\mathcal{C}_\alpha$ and $\mathcal{C}_\beta$. Moreover we evaluate the excess energy of the istantaneous ISs $\Delta E^{IS}(t)$. In this case we subtract from the energy of the istantaneous ISs the energy of the initial ISs $\mathcal{C}_{\alpha_{IS}}$ and $\mathcal{C}_{\beta_{IS}}$. In figure 3.16 we report $\Delta E(t)$ *vs.* time with circles and $\Delta E^{IS}(t)$ *vs.* time with squares for a single size of the excitations: $R = 8$ and at the lowest temperature available $T = 0.89\,T_c$. The corresponding $\Delta E_{IS}(R = 8)$ is drawn with a dashed line.

The decrease of $\Delta E(t)$ hides the crossover between two different regimes: the relaxation of the extra energy due to the artificial interface creation and the subsequent activated relaxation. This is put in evidence by $\Delta E^{IS}(t)$. What we remark here is that the thermal interface cost $\Delta E(t)$ approaches $\Delta E^{IS}(t)$ just when it deviates from ΔE_{IS}, i.e. when the activation pushes the system out of the initial IS. Thus we conclude that the surface tension we obtained using ISs (ΔE_{IS}) can be considered a quite good estimate of the thermal surface tension energy part.

The thermal analysis thus confirms that the interface energy grows with the size of the excitations as a power law with exponent 2, as we saw previously in this section. Moreover it signals that the amount of the energy part of the zero temperature surface tension is a good estimate of the real one.

Part II

Non-equilibrium dynamics and aging

Chapter 4

Aging

4.1 Aging phenomenology

As we saw in chapter 1, glass-forming systems are characterized by the impressive growth of their relaxation time. The non-equilibrium dynamics of glass-forming liquids at low temperature is in fact the most easily observed piece of phenomenology. Out of equilibrium, a certain degree of universality emerges in the so called *aging* regime provided that the full relaxation time scale of the system τ_{eq} is much larger than the microscopic time scale τ_0, $\tau_{eq} \gg \tau_0$.

Aging means that the phenomenology of the system presents a kind of covariance. The equations which describes the out of equilibrium dynamics of the system do not change if each time variable they involve is rescaled by a factor t_w, i.e. the age of the system.

The aging phenomenology is very rich. It reflects not only the complex energy landscape feature (see the experiments described later on) but also the hierarchical structure of nested valleys (for instance in the rejuvenation-memory experiments [61, 62]) suggested by the theoretical description of low temperature equilibrium [63]. In the following we will focus only on the more direct and classical experiments revealing aging.

The dependence of non-equilibrium dynamics on t_w has been observed in measurements of susceptibility. In these experiments, the sample has been quenched from high temperatures to $T < T_g$ at time $t = 0$. An oscillating field with frequency ω has been applied. After the elapsed time t, the measure of the susceptibility $\chi(\omega, t_w)$ depends on ω and t_w. In particular $\chi(\omega, t_w)$ can be parametrized as the sum of a stationary part, χ_{ST}, and an aging contribution

$$\chi(\omega, t_w) = \chi_{ST}(\omega) + A(\omega t_w)^{-b} \,. \tag{4.1}$$

In the aging contribution, the dependence on the rescaled variable ωt_w (see Fig.4.1) means that the effective relaxation time of the aging sample is of the order of its age t_w. This is because the susceptibility of a system with single relaxation time τ is a function of $\tau\omega$.

The same phenomenon emerges in the so-called thermo remanent magnetization experiment. In this case the system is quenched at $t = 0$ in presence of a small

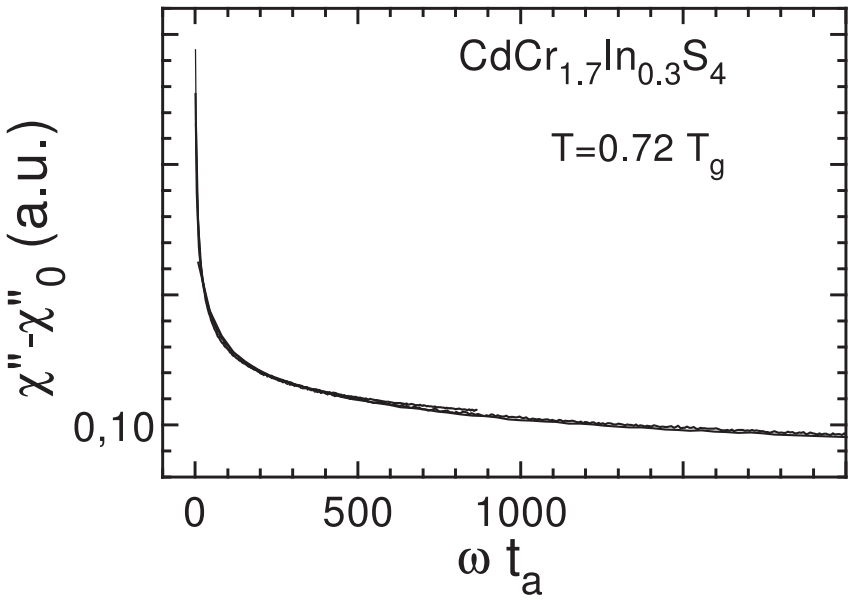

Figure 4.1. Out of phase part of susceptibility $\chi(\omega, t_w) - \chi_{ST}$ (i. e. $\chi'' - \chi''_{ST}$) *vs.* ωt_w for the insulating $CdCr_{1.7}In_{0.3}S_4$ sample (figure from [64]). To account for the various stationary values of χ''_{ST}, the curves have been vertically shifted by different frequencies $\chi''_{ST} = \chi_0$, $t_a = t_w$ in our notation. Four curves ($\omega = 0.01, 0.03, 0.1, 1Hz$) collapse.

magnetic field h to small temperatures ($T_f < T_g$). The field is kept on till $t = t_w$ than it is suddenly switched off. The relaxation of the magnetization $M(t_w + t, t_w)$ of the system can be described by the sum of two parts

$$M(t_w + t, t_w) = M_{ST}(t) + M_{AG}(t_w + t, t_w) \, , \tag{4.2}$$

where M_{ST} is the stationary part of the relaxation and M_{AG} is the aging part. Only the aging part depends on the age of the system: it is generally a function of the unique rescaled variable $t/(t+t_w)$. This again suggests that the effective relaxation time of the system scales as its age t_w.

Actually both these pieces of phenomenology reflect the emergence of aging in the response function $R(\tau, \tau')$. In the linear approximation we have

$$M(t_w + t, t_w) = h \int_0^{t_w} d\tau' R(t_w + t, \tau') \tag{4.3}$$

and

$$\chi(\omega, t_w) = \int_0^{t_w} d\tau' R(t_w, \tau') \exp(i\omega(\tau' - t_w)) \, . \tag{4.4}$$

Thus thermo-remanent magnetization relaxation and susceptibility are connected by a Fourier transform.

A different information is contained in the correlation function. In the off-equilibrium dynamics the connection between response and correlation function

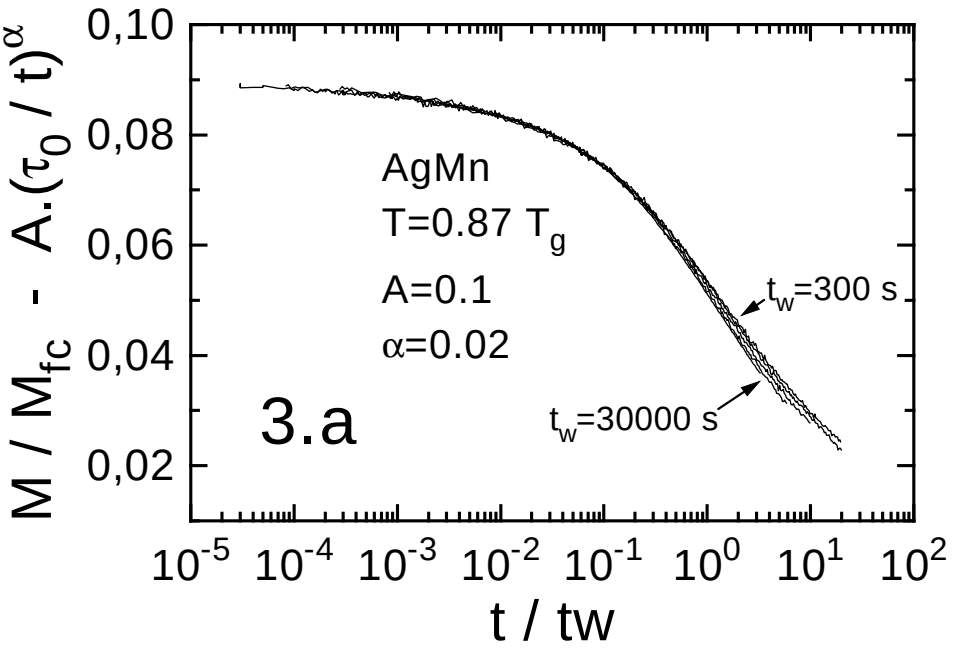

Figure 4.2. Aging part of the (4.2) (figure from [64]). The estimated stationary contribution has been subtracted from the measured value. A quite good collapse of the curves is obtained rescaling the time variable by the t_w factor.

provided by the fluctuation dissipation theorem breaks down. However also correlation functions show aging. This quantity (see (1.24) for a general definition) is very easy to compute in numerical systems. For instance, in a spin system, it is defined as

$$C(t_w + t, t_w) = \frac{1}{N} \sum_i^N \langle \sigma_i(t_w + t) \sigma_i(t_w) \rangle \ . \tag{4.5}$$

At low temperature, $C(t_w + t, t_w)$ reveals aging in a similar way to $M(t_w + t, t_w)$:

$$C(t_w + t, t_w) = C_{ST}(t) + C_{AG}(t_w + t, t_w) \ . \tag{4.6}$$

Off-equilibrium means that configurations are not visited according to the Gibbs-Boltzmann probability. Yet, the aging phenomena do not emerge simply because there are metastable states. In such case, the system remains trapped in a long-lived metastable state. However, the relaxation within this state requires a very fast transient. This case also belongs to the non-equilibrium picture, even though the long and the short time scales are so different that the system experiences the metastable equilibrium in between. On the contrary, during aging things happen along every time scales depending on the t_w considered. The larger is t_w, the longer the system remains in the configuration it has reached

$$\lim_{t \to \infty} \lim_{t_w \to \infty} C(t_w + t, t_w) \neq 0 \ . \tag{4.7}$$

On the other hand, for finite waiting times the system completely decorrelates:

$$\lim_{t_w\to\infty}\lim_{t\to\infty} C(t_w+t,t_w)=0\ . \tag{4.8}$$

This is the so-called weak-ergodicity breaking.

4.2 Theories of aging

A large variety of theories have been developed to explain the aging phenomenon [65–73]. These theoretical efforts have shed light on experimental and numerical results. Yet, contradictions among different theories and the not complete matching between theories and experiments signal that the aging problem is still open.

On the one hand, aging phenomenology is found in mean field models. Exact solutions of Langevin equations in p-spin models lead to the emergence of weak ergodicity breaking and then to aging phenomena [20,71–73]. Aging phenomenology is also present in ordered systems, as it is in the case of domain growth in the Ising model after a quench of a the high temperature disordered phase below its Curie point. In both these cases, the dynamics in phase space can be pictured as a continuous decay trough flatter and flatter regions.

On the other hand, aging may arise when the dynamics is ruled by activation. It could seem a completely opposite point of view. However at low temperature, the non activated escaping directions become fewer and fewer, the dynamics slows down and the system ages. A possible connection of this phenomenon with the activated picture is that, with increasing time, entropic barriers are responsible of the aging mechanism. The number of trapping directions is large with respect to the paths along which the energy only decreases. This represents an entropic obstacle to the system relaxation. In this picture, despite the different origin of the barriers, the aging could be viewed as the consequence of an activated mechanism. In real system it is reasonable to expect that both energy and entropy barriers contribute to non-equilibrium dynamics.

4.3 The REM-like trap model

The trap model belongs to the class of phase-space models of aging with activated dynamics. It is a phenomenological model. The dynamics of the system is represented as the motion of a single point in the configuration phase space (see section 2.3 for details on the limits of the potential energy landscape description for finite dimensional systems). The presence of many basins and sub-basins in a complex landscape can be described in a coarse grained picture as a collection of M states between which the system wanders. Generally, the dynamics can be summed up in the following master equation: the probability to find the system in state α instead of any other state β is

$$\frac{\partial P_\alpha}{\partial t}=-\sum_\beta^M W_{\alpha\to\beta}P_\alpha+\sum_\beta^M W_{\beta\to\alpha}P_\beta\ . \tag{4.9}$$

The statistics of the barriers heights and the geometry of the phase space are encoded in the choice of the hopping rate.

A simple but useful approximation is that the hopping rates only depend on the starting state: $W_{\alpha\to\beta} = (M\tau_\alpha)^{-1}$, where τ_α is the mean trapping time of state α. In this approximation the process starts anew at each jump.

The trapping times depend on the depth of the states. If ϵ_α is the height of the barriers surrounding the single state α, we have that

$$\tau_\alpha = \tau_0 \exp(\frac{\epsilon_\alpha}{T}) \,. \tag{4.10}$$

In this description the equilibrium measure, P_α^{eq}, of each state is proportional to τ_α. Moreover the Boltzmann equilibrium is reproduced if ϵ_α is minus the free energy $\widetilde{f}_\alpha$ of the state α. Note that this connection is not in general obvious [74] but for all practical purposes this assumption seems to be the correct one. We also assume an exponential distribution of the barriers with rate r independent from T. Writing $r = x(T)/T$ to introduce the key parameter x, the exponential distribution reads

$$\rho(\epsilon) = \frac{x}{T} \exp(-\frac{x\epsilon}{T}) \,. \tag{4.11}$$

In (4.11), the rate r does not depend on the temperature The distribution (4.11) follows from the extreme value statistics [75] of systems with energy levels distributed as

$$P(E) \sim \frac{A}{|E|^\gamma} \exp(-B|E|^\delta) \quad B, \delta > 0 \quad E \to -\infty \,. \tag{4.12}$$

In what follows we will describe the extreme statistics of random variables distributed according to (4.12). In this brief digression, we will see how equation (4.23) and hence (4.11) can be obtained from the extreme value statistics of random variable with distribution (4.12).

The statistics of the lowest energy state $E^* = \min\{E_1, \ldots, E_n\}$ for large n is described by

$$P_n(E^*) = nP_<(E^*)[1 - \mathcal{P}_<(E^*)]^{n-1} = -\frac{d}{dE^*}[1 - \mathcal{P}_<(E^*)]^n \,, \tag{4.13}$$

where

$$\mathcal{P}_<(E^*) = \int_{-\infty}^{E^*} dE \; P(E) \tag{4.14}$$

is the repartition function of E. In (4.13), $P_n(E^*)$ is the probability that, on n drawn random variables with distribution (4.12), the lowest is E^* and $[1-\mathcal{P}_<(E^*)]^n$ is the cumulative distribution function of the minimum E^*.

For large n, E^* will be negative and large so that we have

$$\begin{aligned} [1 - \mathcal{P}_<(E^*)]^n \simeq [1 - \int_{-\infty}^{E^*} dE \; \exp(-B|E|^\delta)]^n \simeq \\ \simeq [1 - \exp(-B|E^*|^\delta)]^n \simeq 1 - n\exp(-B|E^*|^\delta) \end{aligned} \tag{4.15}$$

and

$$\exp[-n\mathcal{P}_<(E^*)] \simeq \exp[-n\exp(-B|E^*|^\delta)] \simeq 1 - n\exp(-B|E^*|^\delta) \,. \tag{4.16}$$

In other words

$$[1 - \mathcal{P}_<(E^*)]^n \simeq \exp[-n\mathcal{P}_<(E^*)] \tag{4.17}$$

thus the repartition function is very small if $E^* < E_c(n)$ with $E_c(n)$ such that

$$n\mathcal{P}_<(E_c) = 1 \, . \tag{4.18}$$

This means that

$$E_c(n) = -\left(\frac{\log n}{B}\right)^{\frac{1}{\delta}} \, . \tag{4.19}$$

As n increases, the typical value of E^* is $E_c(n)$. Coming back to (4.17), and using (4.16), the cumulative distribution function of the minimum E^* reads

$$[1 - \mathcal{P}_<(E^*)]^n \simeq \exp\left[-n\exp\left(-B|E^*|^\delta\right)\right] \simeq \tag{4.20}$$

$$\simeq \exp\left[-\exp\left(-B|E^*|^\delta + \log(n)\right)\right] \simeq \exp\left[-\exp\left(-\delta\varepsilon|E_c|^{\delta-1}\right)\right] \tag{4.21}$$

with $E^* = E_c + \varepsilon$ and E_c as in (4.19) We can define a rescaled variable $u = \varepsilon\delta|E_c|^{\delta-1}$. Using this variable, equation (4.20) becomes

$$[1 - \mathcal{P}_<(E^*)]^n \simeq \exp(-\exp(-u)) \, , \tag{4.22}$$

with $u = (E^* - E_c)/(\delta^{-1}|E_c|^{1-\delta})$. The associated probability distribution function is the universal Gumbel distribution

$$p(u) = \exp(-u - \exp(-u)) \tag{4.23}$$

which for $u \to -\infty$ vanishes exponentially: $p(u) \sim \exp(-u)$. In other words the low-lying energies, in a system where the energy levels are distributed like (4.12), are random variable exponentially distributed (see (4.11)).

Coming back to our problem, if the free-energy f is distributed according to (4.12), the extremes of $-f$, $-\widetilde{f}$, are random variables with distribution (4.11). We will call these random variable ϵ. Using (4.11), we are fixing our attention on the deepest traps, the ones which dominate the low temperature dynamics.

We can obtain the distribution of the corresponding trapping times: from equations (4.11), (4.10), and

$$\rho(\tau)d\tau = \rho(\epsilon)df \, , \tag{4.24}$$

$\rho(\tau)$ is

$$\rho(\tau) =_{\tau \gg \tau_0} \frac{x\tau_0^x}{\tau^{x+1}} \, . \tag{4.25}$$

In (4.25) the importance of the parameter x is clear: for $0 < x < 1$ the mean value $\langle\tau\rangle$ is infinite and the aging phenomenon emerges.

The trap model reflects the extreme value statistics of the Random Energy Model (REM) [76] when $x = T_{REM}/T$ where T_{REM} is the temperature below which the REM is frozen in its ground state. In this case, $x < 1$ means $T < T_{REM}$. For this reason we will also use the name REM-like trap model to indicate the Bouchaud's trap model. Yet, in general the value of T_{REM} is not important. In our simulations of the trap model, we will use in (4.11) $x = 1/T$.

In this system, we focus our attention on the quantity $\Pi(t_w, t)$ defined as the probability that the process has not jumped between t_w and $t_w + t$. This quantity is connected to the spin-spin correlation function $C(t_w + t, t_w) = \langle \sigma(t + t_w)\sigma(t_w)\rangle$. Given the overlap between different states $q_0 = 0$ and the self-overlap q_1, the correlation function reads

$$C(t_w + t, t_w) = q_1 \Pi(t_w, t) \; . \tag{4.26}$$

It is convenient to work with the Laplace transform: we define

$$\widehat{\Pi}(E, t) = \int_0^\infty dt_w \; E \exp(-E t_w) \Pi(t_w, t) \; . \tag{4.27}$$

The amount of the time that the system spends in each state is a random variable exponentially distributed with rate $1/\tau$ and the Laplace transform assures quite simple calculations under this condition.

The probability that at a time $\hat{t}_w$, drawn from an exponential distribution of rate E, the system is found in a trap α with hopping rate $1/\tau_\alpha$ is $p(E, \tau_\alpha)$. This is the the probability to remain in α till $\hat{t}_w$ if the initial state is α plus the probability to go to α if the initial state is $\beta \neq \alpha$. The probability p^{in} to not escape from a state with trapping time τ before $\hat{t}_w$ is

$$p^{in} = \int_0^\infty d\hat{t}_w E \exp(-E\hat{t}_w) \int_0^{\hat{t}_w} dt \, \tau^{-1} \exp(-t/\tau) = \frac{E}{E + \tau^{-1}} \tag{4.28}$$

and the probability to escape from a state with trapping time τ before $\widehat{t}_w$ is

$$p^{out} = 1 - \frac{E}{E + \tau^{-1}} = \frac{\tau^{-1}}{E + \tau^{-1}} \; . \tag{4.29}$$

Thus the probability to stay in a state with hopping rate $1/\tau_\alpha$ can be summarized as

$$p(E, \tau_\alpha) = \frac{1}{M} \frac{E\tau_\alpha}{E\tau_\alpha + 1} + \frac{1}{M} \sum_\beta^M \frac{1}{E\tau_\beta + 1} p(E, \tau_\alpha) \; , \tag{4.30}$$

where $p(E, \tau_\alpha)$ in the sum over β does not depend on β. During the dynamics, the final trap reached at each step does not depend on the initial trap. Thus after the system has escaped from β, the probability to go in α does not depend on β. At each step the dynamics starts anew.

In this way, we have

$$p(E, \tau_\alpha) = \frac{\dfrac{E\tau_\alpha}{E\tau_\alpha + 1}}{\sum_\beta^M \dfrac{E\tau_\beta}{E\tau_\beta + 1}} \; . \tag{4.31}$$

In the large M limit, the denominator becomes

$$\sum_\beta^M \frac{E\tau_\beta}{E\tau_\beta + 1} = M \langle \frac{E\tau}{E\tau + 1} \rangle_\tau \tag{4.32}$$

where

$$\langle \frac{E\tau}{E\tau+1} \rangle_\tau = \int_{\tau_0}^{\infty} d\tau \, \frac{x\tau_0^x}{\tau^{x+1}} \frac{E\tau}{E\tau+1} = x\tau_0^x E^x \int_{E\tau_0}^{\infty} dw \, \frac{w^{-x}}{w+1} \, . \tag{4.33}$$

In the regime where $E\tau_0 \ll 1$ (equivalent to $t_w \gg \tau_0$), we have

$$\langle \frac{E\tau}{E\tau+1} \rangle_\tau \simeq x\tau_0^x E^x \Gamma(x)\Gamma(1-x) \tag{4.34}$$

since the integral in (4.33) is

$$\begin{aligned} \int_0^{\infty} dw \, \frac{w^{-x}}{w+1} &= \int_0^{\infty} dw \, w^{-x} \int_0^{\infty} d\nu \, \frac{\exp(-\nu)}{w+1} \\ &= \int_0^{\infty} dw \, w^{-x} \int_0^{\infty} dt \, \exp(-(w+1)t) \\ &= \int_0^{\infty} dt \, \exp(-t) \, t^{x-1} \int_0^{\infty} du \, \exp(-u) \, u^{-x} \\ &= \Gamma(x)\Gamma(1-x) \, , \end{aligned} \tag{4.35}$$

where we used

$$\int_0^{\infty} d\nu \, \exp(-\nu) = 1 \, , \tag{4.36}$$

$\nu = (w+1)t$, and $u = wt$. In this way $p(E, \tau_\alpha)$ has become

$$p(E, \tau_\alpha) = \frac{\sin(\pi x)}{\pi \, x \, \tau_0^x E^x} \frac{E\tau_\alpha}{E\tau_\alpha + 1} \, , \tag{4.37}$$

since $\Gamma(x)\Gamma(1-x) = \pi / \sin(\pi x)$.

After an initial waiting time t_w, the probability that during the time interval $[t_w, t_w + t]$ the system has not changed the state where it was at t_w is

$$\widehat{\Pi}(E,t) = \langle \sum_\beta^M p(E, \tau_\beta) \exp(-t/\tau_\beta) \rangle = \frac{\sin(\pi x)}{\pi \, E^x} \int_{\tau_0}^{\infty} d\tau \, \tau^{-x-1} \frac{E\tau}{E\tau+1} \exp(-t/\tau) \, . \tag{4.38}$$

This result has to be carefully handled with an appropriate change of variables:

$$\begin{aligned} \frac{1}{E^x} \int_{\tau_0}^{\infty} d\tau \, \tau^{-x-1} \frac{E\tau}{E\tau+1} \exp(-t/\tau) &= \int_{\tau_0 E}^{\infty} dy \, \frac{y^{-x}}{y+1} \exp(-tE/y) \\ &\simeq \int_0^{\infty} dw \, \frac{w^{x-1}}{t^x} \frac{t}{w+t} \int_0^{\infty} dt_w \, E \exp(-t_w E) \, \theta(t_w - w) \\ &= \int_0^{\infty} dt_w \, E \exp(-t_w E) \int_{\frac{t}{t_w+t}}^1 du \, (1-u)^{x-1} u^{-x} \, , \end{aligned} \tag{4.39}$$

where we used $y = \tau E$ in the limit $(\tau_0 E) \to 0$, $w = t/y$,

$$\exp(-wE) = \int_0^{\infty} dv \, E \exp(-vE) \, \theta(v-w) \, , \tag{4.40}$$

and $u = t/(w-t)$. Therefore we have

$$\widehat{\Pi}(E,t) = \frac{\sin(\pi x)}{\pi} \int_0^{\infty} dt_w \, E \exp(-t_w E) \int_{\frac{t}{t_w+t}}^1 du \, (1-u)^{x-1} u^{-x} \, . \tag{4.41}$$

Recalling equation (4.27), we can write

$$\Pi(t_w,t)=\frac{\sin(\pi x)}{\pi}\int_{\frac{t}{t_w+t}}^{1}du\,(1-u)^{x-1}u^{-x}\,. \tag{4.42}$$

From the last equation, it is clear that in this model the correlation function only depends on the rescaled time $t/(t+t_w)$: the larger is t_w the longer the system will be trapped in the same state. In particular on the time-scale t_w the hopping rate of the typical state is $1/t_w$ and the process will jump away only after $t\gtrsim t_w$.

The (4.42) has two interesting asymptotic regimes: if $t\ll t_w$, we can write

$$\int_{\frac{t}{t_w+t}}^{1}du\,(1-u)^{x-1}u^{-x}=\int_0^1 du\,(1-u)^{x-1}u^{-x}-\int_0^{\frac{t}{t_w+t}}du\,(1-u)^{x-1}u^{-x}\,, \tag{4.43}$$

where the first term is $\pi/\sin(\pi x)$ and the second term can be approximated at the first order expansion in the small parameter $\varepsilon=t/(t_w+t)$ using

$$\int_0^{\varepsilon}du\,u^{a-1}(1-u)^{b-1}=\varepsilon^a\sum_{n=0}^{\infty}\frac{\prod_{i=0}^{n}(1-ib)}{n!(a+n)}\varepsilon^n \tag{4.44}$$

with $a=1-x$ and $b=x$. In this way we obtain

$$\Pi(t_w,t)\sim_{t\ll t_w}1-\frac{\sin(\pi x)}{\pi(1-x)}\left(\frac{t}{t+t_w}\right)^{1-x}\,. \tag{4.45}$$

On the other hand, in the opposite limit $t\gg t_w$, we use $w=1/u$ in (4.42) and we obtain

$$\Pi(t_w,t)=\frac{\sin(\pi x)}{\pi}\int_0^{\frac{t_w}{t_w+t}}dw\,w^{x-1}(1-w)^{-x} \tag{4.46}$$

which is the (4.44) with $a=x$, $b=1-x$, and $\varepsilon=t_w/(t+t_w)$. Thus we have

$$\Pi(t_w,t)\sim_{t\gg t_w}\frac{\sin(\pi x)}{\pi x}\left(\frac{t_w}{t+t_w}\right)^{x}\,. \tag{4.47}$$

This means that for all finite t the correlation function does not decay provided that an infinite waiting time has spent. Hence, the Bouchaud's trap model recovers the weak ergodicity breaking.

4.4 Universality of the trap model

Recent works [77–82] by Ben Arous, Bovier, Černý, and Gayrard (BBCG) have mathematically proved that the trap model paradigm of aging is at work in the REM model and in p-spin models under specific conditions.

The feeling is that the trap model should not be recovered in mean field models which are typical examples of models where the dynamics is activated. They are usually studied in the thermodynamic limit where the barriers among states are infinite. However, we will now consider models with large but finite number of spins and we will use a time variable rescaled by the exponential of the size of the

system. We are going to look at the activation in mean field models on rescaled time scale. We recall here the main results of BBCG on these models.

BBCG review the trap model of Bouchaud (the REM-like trap model) with M traps. Recall that the waiting time in each trap α is exponentially distributed with mean value given by (4.10). In (4.10) ϵ is also an exponential random variable with rate one (see equation (4.11) with $T_{REM} = 1$). The following jump is equally probable towards one of the other $M - 1$ states: the transition rates are

$$p_M \propto (M-1)^{-1} \exp(-\epsilon/T) \,, \tag{4.48}$$

as it follows from (4.10).

Given

$$H_x(w) \equiv \frac{\sin(\pi x)}{\pi} \int_w^\infty dt \, \frac{1}{(1+t)t^x} \,, \tag{4.49}$$

the Bouchaud and Dean result in [69,70] can be re-written as

$$\lim_{t,t_w \to \infty} \lim_{M \to \infty} \frac{\Pi(t_w, t)}{H_x(t/t_w)} = 1 \,, \tag{4.50}$$

where $x = 1/T$ and $\Pi(t_w, t)$ is the probability that during a time interval $[t_w, t_w + t]$ the process do not jump. The result in (4.49), which is known as the arcsine law, follows from (4.42) by means of the simple change of variables $t = u/(1-u)$.

In [78–80] this result is extended by Ben Arous, Bovier, Černý, and Gayrard to the Derrida's REM model. The REM is a simple but interesting model introduced by Derrida [76]. In this model with N spins, the energy levels E_σ, corresponding to $M = 2^N$ configurations σ, are independent random variable with Gaussian distribution, with zero mean and variance $s^2 = N$ (the distribution is in fact the (4.12) with $B \propto N^{-1}$ and $\delta = 2$). The BBCG result has been obtained assuming a particular dynamics in which the transition rates of each jump only depend on the energy dept of the initial trap. The final trap is simply randomly drawn from a uniform distribution among the N configurations connected to the initial one by a single spin flip:

$$p_N(\sigma, \sigma') = N^{-1} \exp(\beta E_\sigma) \,, \tag{4.51}$$

where $\beta = 1/T$.

The result of [78–80] is that for every $0 < \rho < 1$, if $\beta_\rho \equiv \beta/\sqrt{\rho} > \beta_c \equiv \sqrt{2\log(2)}$, and $\gamma = \beta\beta_c\sqrt{\rho}$ the non-equilibrium dynamics on conveniently rescaled time scales is dominated by the trap model aging process:

$$\lim_{N \to \infty} \Pi\left(t_w e^{\gamma N}, t e^{\gamma N}\right) = H_x(t/t_w) \tag{4.52}$$

with $x = \beta_c/\beta_\rho$.

In this result we find two new parameters: ρ and γ. They account for the progressive exploration of the configuration space. The trap-model-like scaling (4.49) is valid in different time regions ($e^{\gamma M}$ with $\gamma = \beta\beta_c\sqrt{\rho}$) for different β_ρ provided that $\beta_\rho > \beta_c$. In a smaller time window the system explores a fraction of the configuration space. It has not found the lowest minimum thus the trapping time it

is experiencing is still not the longest available. Hence, the effective temperature, which the system feels, is larger than the real temperature ($T_{eff} = 1/\beta_\rho < T$). The smaller is the time region we observe the higher is the effective temperature of the system. However, there is a limit. The aging regime holds if its effective temperature is not larger than the critical one. This means that the aging is observable if the time region is at least large enough that the process has already spent all but a negligible part of its time in the lowest state it has reached.

These new issues arise in the REM and not in the REM-like trap model since the latter is a coarse grained version of the former. In the trap model the traps are exponentially distributed as the lowest lying traps of the REM. One step in the Bouchaud's trap model corresponds to $n = 2^{\rho N}$ steps in the REM, i.e. to the complete exploration of a system where the number of spins is ρN. The reason is that the energy distribution in REM is equivalent to the (4.12) with $B \propto 1/N$ and $\delta = 2$. In this case, the typical lowest energy level among n traps is given by (4.19). The mean trapping time of this configuration is proportional to

$$\exp(\beta|E_c|) = \exp(\beta N\sqrt{2\rho\log(2)}) = e^{\gamma N} \ . \tag{4.53}$$

Thus, aging in the Bouchaud's model on scale t, is recovered in REM on the time scale $te^{\gamma N}$.

The same aging result has been found in the p-spin SK model. It is defined on the same N spin system as the REM model but in this case the energy of each configuration is given by the following Hamiltonian:

$$H_N(\sigma) \equiv -\frac{\sqrt{p!}}{N^{(p-1)/2}} \sum_{i<j<k} J_{ijk}\sigma_i\sigma_j\sigma_k \tag{4.54}$$

where the J_{ijk} are Gaussian random variables with variance 1. It is well known that in the limit $p \to \infty$ the p-spin and the REM coincide [76]. The dynamics for which the aging result is mathematically proven also in the p-spin model is the one in (4.51) with $E_\sigma = H_N(\sigma)$.

In the case of p-spin model valleys in the free energy landscape contain more than one configuration. Hence, the two-point function $\Pi^\varepsilon_N(t_w, t)$, which should age, needs a reformulation. In particular, we have to measure the similarity between two configurations. As usual, this similarity can be measured by the normalized overlap

$$q_N(\sigma, \sigma') = N^{-1}\sum_{i=1}^{N} \sigma_i\sigma'_i \ . \tag{4.55}$$

Identical configurations have $q_N = 1$, completely different configurations have $q_N = 0$. We can thus introduce the $\Pi^\varepsilon_N(t_w, t)$. This quantity is defined as the probability that the configuration at $\sigma(t_w)$ and at $\sigma(t)$ have overlap larger than $1 - \varepsilon$:

$$\Pi^\varepsilon_N(t_w, t) = \Pr\{q_N(\sigma(t_w e^{\gamma N}), \sigma((t_w + t)e^{\gamma N})) \geq 1 - \varepsilon\} \ , \tag{4.56}$$

The two point function $\Pi^\epsilon_N(t_w, t)$ in p-spin model shows a similar aging result as the $\Pi(t_w, t)$ in REM. If $p \geq 3$, it exists a p-dependent constant ρ_p such that for

$\rho < \rho_p$ and $\beta_\rho > \beta_c$ then, for any $\varepsilon \in (0,1)$, and for any $t_w > 0$ and $t > 0$,

$$\lim_{N\to\infty} \Pi_N^\varepsilon(t_w, t) = H_x(t/t_w) \tag{4.57}$$

with $x = \beta_c/\beta_\rho$. The ρ_p function is such that $\rho_{p=3} \simeq 0.763$ and

$$\lim_{p\to\infty} \rho_p = 1 \ , \tag{4.58}$$

hence the aging result for the REM is recovered.

The difference between p-spin model and REM is in the correlation of the energies. This requires the reformulation of the two-point function $\Pi_N^\epsilon(t_w, t)$ and also the restriction of the range of parameter ρ. Indeed, this restriction essentially ensures that the process does not have time to get so close to a point visited before that it feels the energy correlation.

The dynamics (4.48) of the REM-like trap model is quite different from the REM dynamics and the p-spin dynamics (4.51). In the REM-like trap model, at each step, any configuration can be reached from any other configuration. On the other hand, in the dynamics of REM and p-spin, the single step requires that initial and final configurations are related by a single spin flip. The latter kind of dynamics is more localized in the phase space: the number of spin flip that are needed to obtain a configuration β from a configuration α acts as a distance between the two configurations. This difference could influence the aging mechanism.

In the dynamics we described, the jumping rate does not depend on the final configuration of each step but only on the initial one. Thanks to this choice, the random walk trajectory does not depend on the random environment defined by the Hamiltinian. This element is crucial for the mathematical proof in [78, 79, 81]. On a mathematical point of view, it is not clear how to deal with a different, and more usual, dynamics like Metropolis. This is indeed one of the great challenge of the field. Our aim is to implement numerical simulations of the models like the ones above described. Initially, we will analyze the non-standard dynamics in (4.48) and (4.51). We want to re-obtain the analytical results using numerical simulations. Then we will study the REM-like model with the more usual Metropolis dynamics which cannot still be handled on the analytical level.

Chapter 5

Numerical study of aging

5.1 Aging in REM-like trap model with non-standard dynamics

The first step is to check the arcsine law in the simplest model where it was mathematically found for the first time. We implemented the numerical simulation of the REM-like trap model described by

$$\tau_\alpha = \tau_0 \exp(\frac{\epsilon_\alpha}{T}) \,, \tag{4.10}$$

$$\rho(\epsilon) = \frac{x}{T} \exp(-\frac{x\epsilon}{T}) \,, \tag{4.11}$$

$$p_M \propto (M-1)^{-1} \exp(-\epsilon/T) \,. \tag{4.48}$$

We computed in these systems the probability $\Pi(t_w, t)$ to do not jump during the time interval $[t_w, t_w + t]$. We observed 1000 dynamics on each of 100 realization of the disorder. The sizes are $M = 2^i$ with i ranging from 4 to about 25. In detail, we looked at larger and larger systems up to those such that the uncertainty on the results of $\Pi(t_w, t)$ is higher than the difference $|\Pi_{M=2^{i-1}}(t_w, t) - \Pi_{M=2^i}(t_w, t)|$.

In Fig.5.1 the large t_w limit, for t/t_w fixed, is shown for three different sizes of the system and for $\beta = 2$. The boxes represent the result for $t/t_w = 0.5$, the circles for $t/t_w = 1$, and the triangles for $t/t_w = 2$. The red color indicates small system ($M = 2^5$), the green is for $M = 2^{10}$, and the large systems ($M = 2^{15}$) results are the ones in blue. For small sizes, $\Pi(t_w, t)$ decays for large t_w with t/t_w fixed. On the other hand, increasing the sizes of the system, a plateau forms. The large time limit is a well defined value different from zero. The ergodicity of the system is weakly broken.

A fit with a constant of the large t_w data for large M gives the results reported in Fig.5.2. In Fig.5.2 there are also the results obtained following the same procedure for two other values of β: $\beta = 3$ and 4. The lines do correspond to the function $H_x(t/t_w)$ defined in (4.49). The agreement between numerical and analytical results is striking.

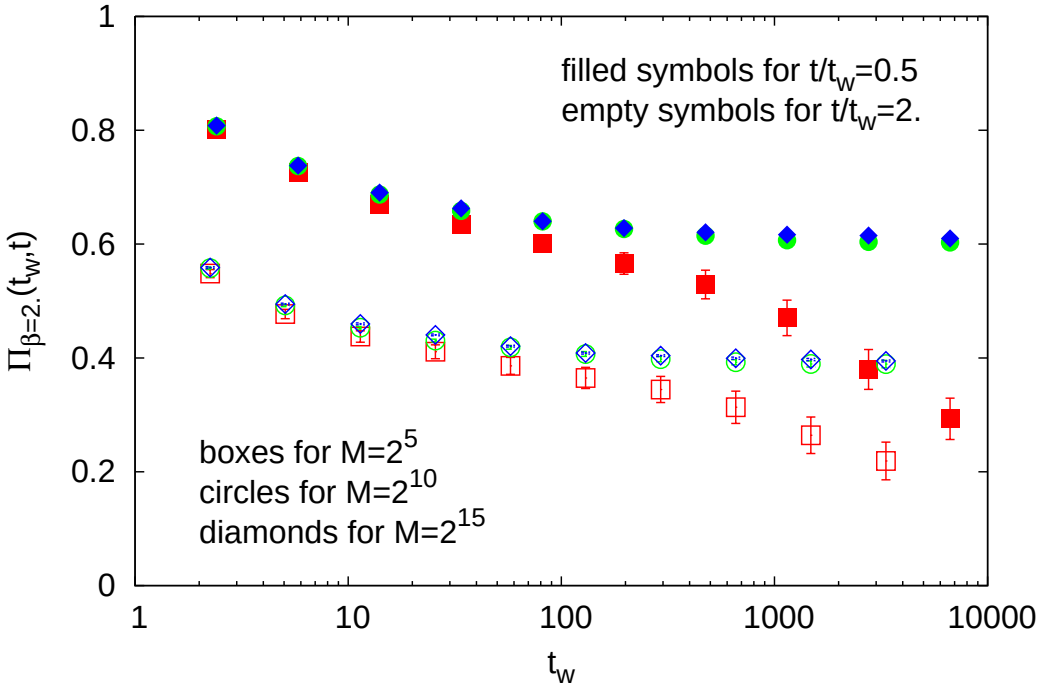

Figure 5.1. $\Pi(t_w, t)$ *vs.* t_w for t/t_w fixed.

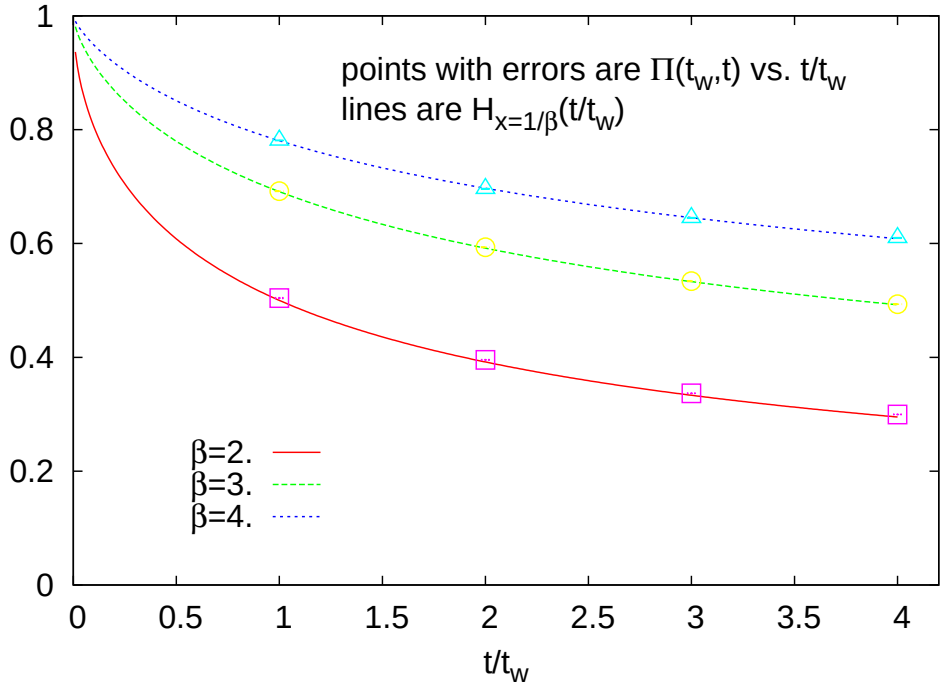

Figure 5.2. $\Pi(t_w, t)$ *vs.* t/t_w for large M and large t_w.

5.2 Aging in p-spin model with non-standard dynamics

We simulated the p-spin model with Ising spins defined in (4.54) with J_{ijk} Gaussian random variables with variance 1 and with $p = 3$. The dynamics is the one in

(4.51) with $\epsilon_\sigma = H_N(\sigma)$. In this system, the equilibrium overlap distribution $P(q)$ at low temperature is a bimodal distribution with two peaks. The first peak is at overlap zero and the second is at $q = 1$. The higher value of the overlap which corresponds to a peak is the Edward Anderson parameter, q_{EA}, i.e. the value of the self-overlap of the low temperature states. The function $\Pi(t_w, t)$ in the p-spin

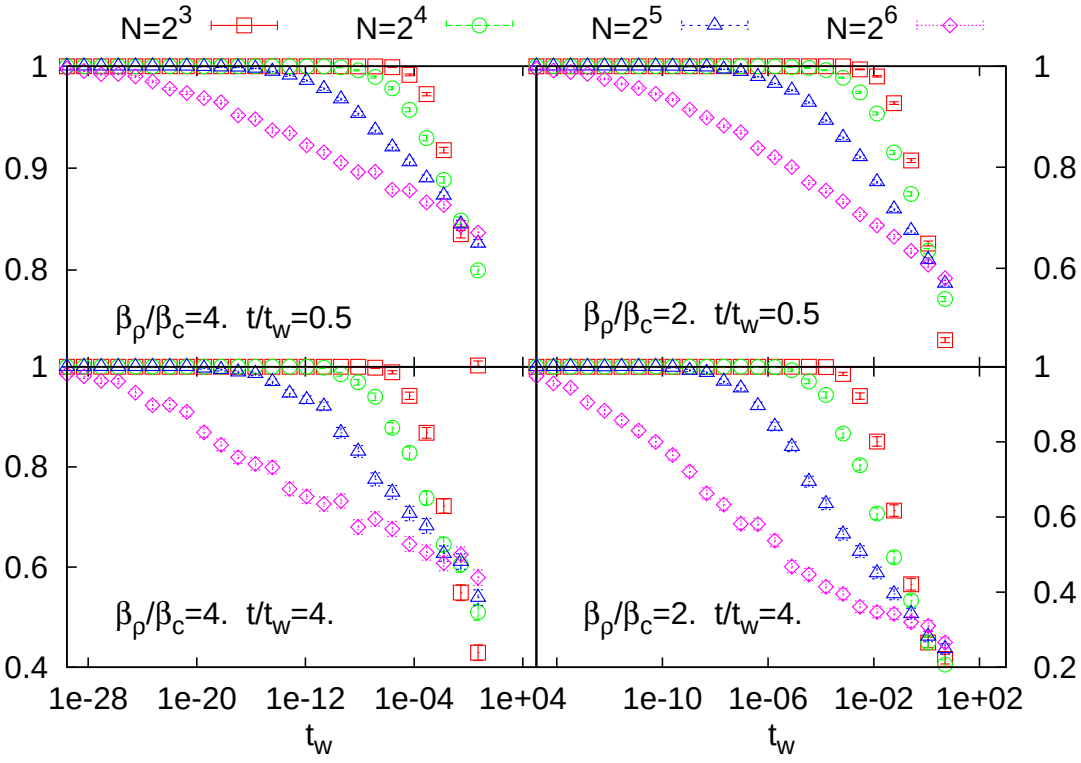

Figure 5.3. $\Pi_N^\varepsilon(t_w, t)$ *vs.* t_w for t/t_w fixed.

case has been generalized to the probability that the overlap between the configuration at time t_w and the one a time $t_w + t$ is larger than ε. The threshold ε should distinguish whether the system has changed state ($q < 1 - \varepsilon$) or not ($q > 1 - \varepsilon$). In the thermodynamic limit ε can be every value between 0 and 1, extremes not included, since $P(q) = (\delta(q) + \delta(1 - q))/2$. However, at finite size the minimum of $P(q)$ between the two peaks is near $q = 0.5$ thus a good choice for the threshold ε is $\varepsilon = 0.5$ (see [83] for the $P(q)$ of the p-spin model with $J_{ijk} = \pm 1$ with probability $1/2$). For this reason, we observed the probability that the overlap between the configuration at time t_w and the one a time $t_w + t$ is larger than 0.5. We studied systems of sizes $N = 2^3, 2^4, 2^5$ and 2^6 where N is the number of spins. We averaged over 1000 realizations of the disorder.

$\Pi_N^\varepsilon(t_w, t)$ *vs.* t_w obtained for different sizes with fixed $w = t/t_w$ (i.e. $\Pi_n^\varepsilon(t_w, wt_w)$) is shown in Fig.5.3. The x-axis is the rescaled time variable: the time of real simulations corresponds to $t_w e^{\gamma N}$ and $(t + t_w)e^{\gamma N}$. For large systems, the decay of Π_N^ε is much slower than the one in small systems. However, contrary to the REM-like case, the large time trend does not allow to recognize any asymptotic value for the

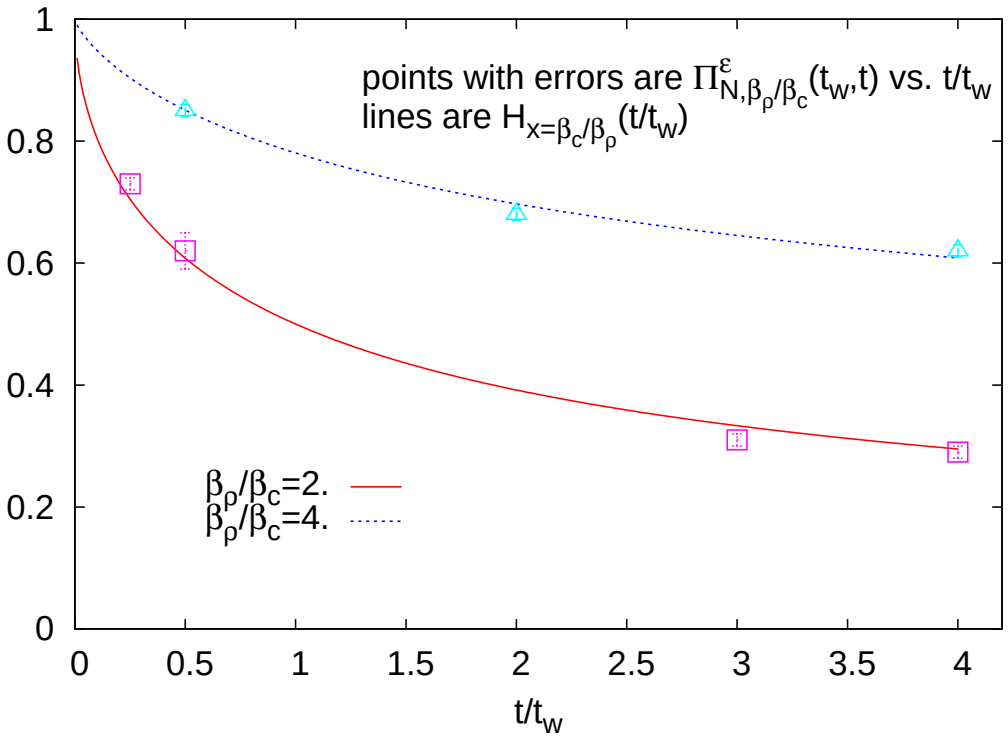

Figure 5.4. $\Pi^{\varepsilon}_N(t_w,t)$ *vs.* t/t_w for $t_w = t^*_w$.

large systems we simulated. Even for the largest system considered, the plateau is not present.

We could not find the large time behaviour of the $\Pi^{\varepsilon}_N(t_w,t)$ functions if we did not compare the decays of the $\Pi^{\varepsilon}_N(t_w,wt_w)$ of different system sizes. In each panel of Fig.5.3 we noted the intersection between different curves of the $\Pi^{\varepsilon}_N(t_w,t)$ decrease. They cross at a time that we call t^*_w. The crossing point of the $N=2^3$ and $N=2^4$ curve is roughly the same as the crossing point of the $N=2^4$ and $N=2^5$ curve and so on. This point does not change with increasing N. Enlarging the system size, $\Pi^{\varepsilon}_N(t_w,wt_w)$, for $t_w < t^*_w$, approaches the $\Pi^{\varepsilon}_N(t^*_w,wt^*_w)$ value from above and, for $t_w < t^*_w$, grows approaching $\Pi^{\varepsilon}_N(t^*_w,wt^*_w)$ from below. For this reason, we infer that for larger system sizes, too large to be simulated, the $\Pi^{\varepsilon}_N(t_w,t)$ would tend to the constant value $\Pi^{\varepsilon}_N(t^*_w,wt^*_w)$.

We want to remark the difference between the trend of $\Pi(t_w,t)$ in REM-like trap model and the trend of $\Pi^{\varepsilon}_N(t_w,t)$ in p-spin model. In the former case the decreasing $\Pi(t_w,t)$ forms a plateau in correspondence to its asymptotic value. In the latter case, for larger systems, the decrease of $\Pi^{\epsilon}_N(t_w,t)$ as function of the rescaled time variable starts earlier and it is slower. However, there is not any plateau. The only way to fix the asymptotic value can be obtained comparing the $\Pi^{\epsilon}_N(t_w,t)$ trends at different sizes. This means that, even if the asymptotic values in both cases agree with the arcsine law, different mechanisms rule the way the weak ergodicity breaking is approached.

Estimates of the $\Pi^{\varepsilon}_N(t^*_w,wt^*_w)$ at each crossing point t^*_w for the values of $\beta_\rho/\beta_c =$

2 and 4 and some values of w are plotted in Fig.5.4. We superimpose the H_x functions with $x = \beta_\rho/\beta_c$ and we find a very good agreement between numerical data and theoretical expectations.

We performed the same procedure using a p-spin model with different coupling constant. The model is defined like in (4.54) with $J_{ijk} = \pm 1$ drawn with equal probability ($p_+ = 0.5$ and $p_- = 0.5$) [83]. We obtained the same result as in the Gaussian case. The particular distribution of the J_{ijk} does not influences the aging mechanism. The parameter which influences the aging results is the variance of the distributions.

5.3 Aging in Metropolis dynamics

In previous sections, we always considered the non-standard dynamics defined in (4.48) and (4.51). We numerically recovered the exact result of [78–82]. The Bouchaud's trap model can describe aging in REM and p-spin models.

A very interesting issue is the extension of this paradigm to the more common Metropolis dynamics. To this aim, we simulated the Bouchaud's trap model with Metropolis dynamics.

The definition of the Metropolis dynamics is the following: an elementary change in the initial configuration is proposed, in our case this change is a single spin flip. The energy difference ΔE between the final and the initial configuration is computed. The probability to accept the elementary change proposed is

$$p_M = \min(1, \exp(-\beta \Delta E)) \; . \tag{5.1}$$

If $\Delta E < 0$ the change is surely accepted since in (5.1) $\min(1, \exp(-\beta \Delta E)) = 1$.

Both these kinds of dynamics lead to the Boltzmann equilibrium measure. They also give the same dynamical result in the case of deep states surrounded by high barriers. Indeed low energies corresponds to very high values of the trapping time using (4.51) and the large barriers prevent the Metropolis dynamics from jumping away during a large number of steps of the dynamics.

However, there is one great difference: in (4.51) the final configuration does not influence the dynamics: at each step, only the depth of the initial configuration traps the system. The final configuration will play its role only at the next step. The dynamics is a sequence of steps only correlated by the single spin flip rule or not correlated at all (trap-model). The energy landscape around the initial configuration of each step is completely disregarded. On the contrary, in Metropolis dynamics, the probability to change configuration does depend on the final configuration: the surrounding energy landscape makes the difference. Three configurations at the same free energy level but in different positions in the landscape (e.g. a local minimum, a local maximum, or a saddle) will lead to the same trapping time in case of the first non-standard dynamics and we will have completely different results using the Metropolis dynamics.

The Metropolis rule provides a more detailed description of a physical dynamics. The independence from the surrounding in non-standard dynamics means

that subsequent steps of the dynamics are not correlated. This is crucial for the mathematical proof in [78, 79, 81]. We can however study the case of Metropolis dynamics using numerical simulation. The results of the numerical approach are given in the following section.

5.3.1 The REM-like trap model

The application of the Metropolis dynamic rule, Eq.(5.1), on the Bouchaud's REM-like trap model (defined in (4.10) and (4.11)) has been performed for $\beta = 2$ and 4 and for systems with M from 2^3 to 2^{10}. We averaged over 1000 samples. The limit 2^{10} has been obtained in the following way: larger and larger systems has been simulated up to those such that the uncertainty of $\Pi(t_w, t)$ has become higher than the difference $|\Pi_{M=2^{i-1}}(t_w, t) - \Pi_{M=2^i}(t_w, t)|$.

Figure 5.5 shows the $\Pi(t_w, t)$ at fixed $w = t/t_w$. As in the case of the trap model with non-standard dynamics the large t_w limit is visible in large enough systems ($M = 2^{10}$). A fit with a constant of the large t_w data for large M gives the large t_w and t behaviour of $\Pi(t_w, t)$. The same procedure has been performed for $\beta = 4$. The results are in Fig.5.6. They are in very good agreement with the expected arcsine law $H_x(w)$.

We conclude that, in the case of Metropolis dynamics, as in the non-standard dynamics in (4.48), the trap model belongs to the class of aging described by H_x.

We remarked that different mechanisms govern the large system size limit of the dynamics in the REM-like trap model and in the p-spin model. We can ask whether the change in the dynamic rule influences the recovering of the large size limit. Despite a quite evident noise affect the data, the REM-like trap model with Metropolis dynamics shows the emergence of a plateau. Hence, the large size limit shows the same qualitative features as in the case of a non-standard dynamics.

A further very interesting step of this study is to verify whether the p-spin model with Metropolis dynamics shows the arcsine law during the aging regime. If it is true, the universality class of the arcsine law aging would be further extended. On a theoretical level, the p-spin model with the Metropolis rule presents a very correlated dynamics since

- a single step of the dynamics involves a single spin flip
- energies of similar configurations are correlated
- the jump between two configurations depends on both of them.

The arcsine law for the p-spin model in the case of non-standard dynamics has been recovered. However we saw that the large size limit was qualitatively different from the case of the REM-like trap model and slightly harder to detect.

The dynamics of p-spin with the Metropolis rule is even more correlated. We do not know whether this can change the aging regime. Numerical investigations about this point are in progress. We still do not have any conclusive results at the moment.

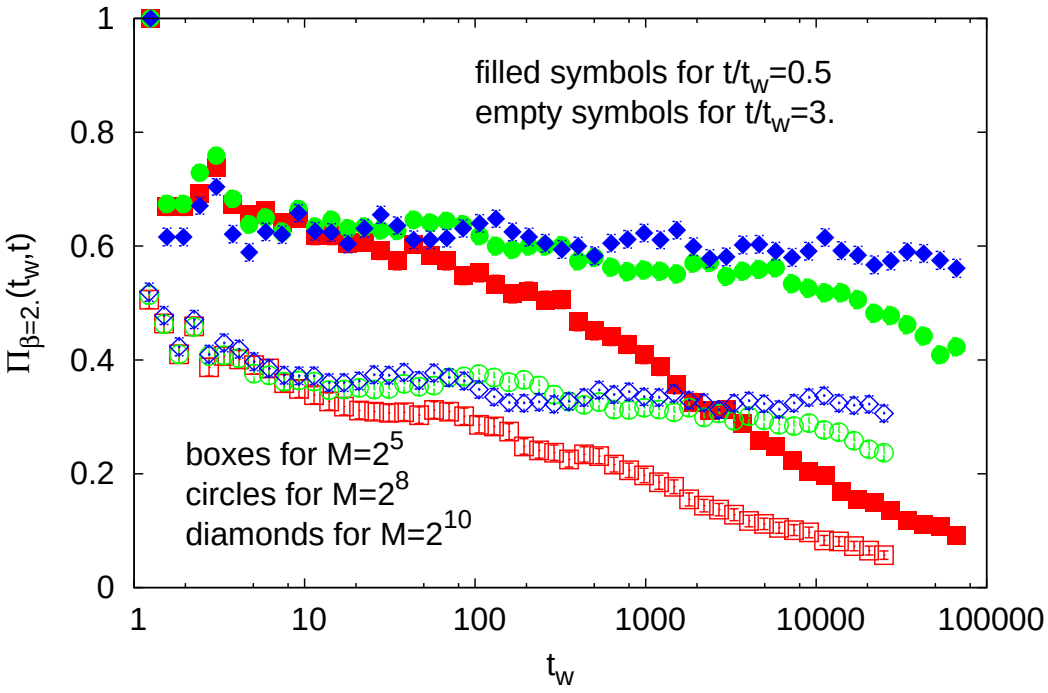

Figure 5.5. $\Pi(t_w, t)$ *vs.* t_w for t/t_w fixed.

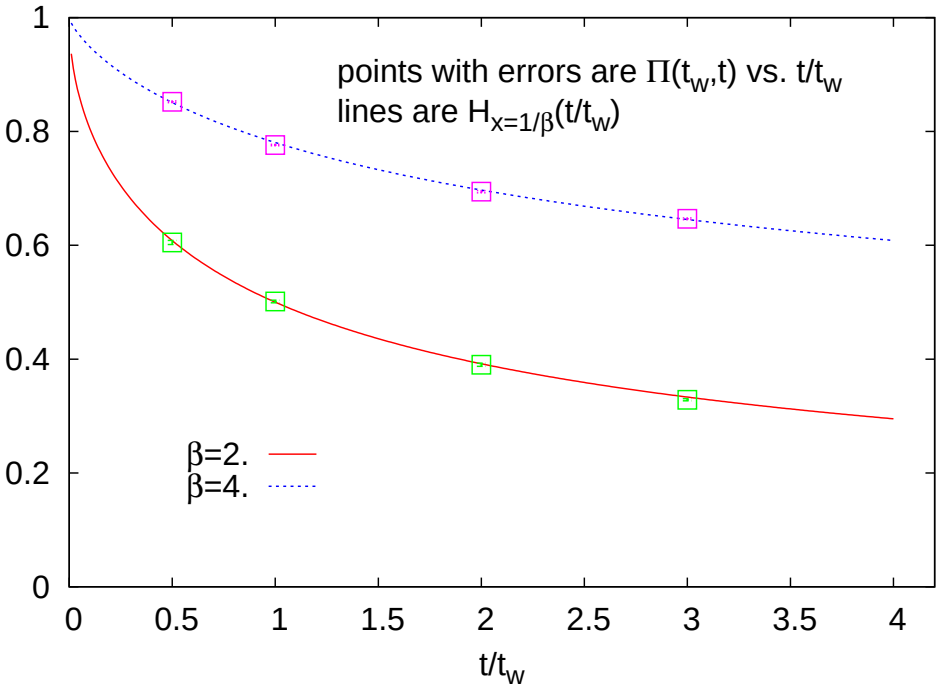

Figure 5.6. $\Pi(t_w, t)$ *vs.* t/t_w for large M and large t_w.

Chapter 6

Conclusions

This thesis reports the results of equilibrium and non-equilibrium studies of the slow dynamics in disordered systems.

The first part was devoted to the problem of the slowing down of the equilibrium dynamics at low temperature in glass-forming liquids. The aim of the work was to test the Mosaic scenario, which is one of the pictures explaining the arrest of dynamics at low temperatures. The Mosaic scenario assumes the existence of many metastable states, each one characterized by a different kind of amorphous order. The landmark of any multi-state scenario as the Mosaic is the existence of a surface tension. Yet, a measurement of the surface tension in glass-forming liquids was still lacking. We therefore focused on the surface tension between amorphous states.

We first study interfaces between configurations corresponding to the local minima of the potential energy, i.e. the inherent structures. These minima are the nearest ones to the low temperature equilibrium configurations. The interfaces between inherent structures, built with the formation of a spherical excitation, showed a nonzero energy cost. A well-defined scaling of the interface cost with the size R of excitations was found. Despite some roughening effects, which are only relevant at small sizes, the interface cost in $d = 3$ grows as the square of the excitations size, i.e. the exponent that governs the interface cost growth is $\theta = 2$. The prefactor of R^2 in the energy cost provides a zero temperature estimate of the surface tension between amorphous states.

The surface tension is found to decrease with temperature increasing. The presence of a nonzero surface tension is the landmark of the presence of different states, thus its decrease indicates that the sharp distinction between different states is loosening. It would be interesting to fix the temperature above which the multi-state scenario is not valid any more. However, temperature is not the right parameter to single out such transition. A better choice is the energy density of the inherent structures. The surface tension value shows a nearly linear decrease when it is plotted as a function of the inherent structure energy. In this case, the energy value at which it becomes zero is sharply defined. Remarkably, such spinodal energy is very close to the threshold energy, the level of the landscape which marks the saddle-minima transition.

Quite a clear picture of the multi-state scenario emerges: at low temperature the partition of the phase space in states dominates the equilibrium dynamics of the system. The amorphous metastable states pay a finite cost (the surface tension is nonzero) when they are put in contact. As the temperature is raised, the dynamics is dominated by broader and broader minima. They can rearrange to match with each other, paying a smaller and smaller interface cost. The surface tension becomes zero exactly when the equilibrium dynamics is not dominated by minima any more and saddles take over.

The surface tension we find has distribution that is broader the higher the temperature. This result confirms a non-sharp version of the Mosaic theory, according to which the presence of states with small enough surface tension allows the decorelation of regions with any size. In other words, a distribution of surface tensions implies a distribution of the size of the rearranging regions. Hence, the crossover between small regions highly influenced by the surrounding and large independently rearranging regions is not sharp. We found a way to quantitatively compare the broadening of the surface tension distribution with the smoothening of the crossover between correlated and uncorrelated regions. The new version of the Mosaic and our findings are in very good quantitative agreement.

A full temperature analysis of the surface tensions has been also performed. This approach indicates that the findings obtained with the inherent structures studies give a fair estimate of the surface tension. The value of the exponent $\theta = 2$ is also recovered in this case. Moreover, in this more realistic framework we measured the relaxation time of the excitations we created. This study indicates that the relaxation of larger excitations (larger R) requires larger time τ. According to the picture of activated dynamics, we analyzed the scaling of the relaxation time using the exponential functional form, $\tau \sim \exp(R^\psi/T)$. The agreement between the functional form and the numerical results was good and we found $\psi = 1$.

In the Mosaic picture both exponents θ and ψ influence the growing of the relaxation time with lowering temperature. The more general prediction of the Mosaic theory is that the relaxation time growth follows a generalized Voghel-Fulcher-Tamman law with exponent $\alpha = \psi/(d-\theta)$. Several values of these exponents have been suggested in previous works usually finding the result $\alpha = 1$ in accordance with the celebrated Voghel-Fulcher-Tamman fit. Our work also indicates the values of the two exponents: $\theta = 2$ and $\psi = 1$. They have been obtained via completely independent procedures. Yet, we recovered the original Voghel-Fulcher-Tamman law with $\alpha = 1$.

The results, previously described, are schematically listed below:

- existence of a finite amorphous-amorpous surface tension Y
- the interface cost is a power law of the size R of the excitations with exponent $\theta = 2$
- the surface tension decreases with increasing temperature: $Y \downarrow \quad T \uparrow$
- existence of a spinodal energy corresponding to the minima-saddles transition: this spinodal marks the break down of any multi-state description

- the surface tension fluctuates, its distribution sharpens with decreasing temperature: Var$[Y] \downarrow \quad T \downarrow$
- the broad surface tension distribution, $P(Y)$, is in quantitative agreement with the smooth correlation function $q(R)$ in [35]
- the activation barriers increase as a power law of R with exponent $\psi = 1$
- the exponents $\theta = 2$ and $\psi = 1$ give back to Vogel-Fulcher-Tamman law

The second part of the thesis reports the results of our study on aging in spin-glass models. The phenomenological approach to aging provided by Bouchaud's trap model is summed up. This is the paradigm of a universal class of aging that obeys the so called arcsine law. The Random Energy Model and the p-spin model belong to this universality class, provided that a non-standard dynamics rules the system. According to this dynamics, at each step the time to change configuration does not depend on the final configuration. The mathematical proof of such extension of the applicability range of the arcsine law has been given recently. Instead, whether the same models belong to the same universality class in the case of the more standard Metropolis dynamics is not clear.

We started our work studying the non-standard dynamics. We numerically simulated the non-equilibrium dynamics of the Bouchaud's trap model observing the expected aging regime. We also studied the p-spin model with Ising spins and in presence of random couplings drawn according to two different distributions (i.e. the Gaussian distribution and the bimodal distribution). We found that the expected arcsine law emerges also in these cases. Yet, in the p-spin model, we observed that the non-equilibrium dynamics approaches the weak ergodicity breaking limit in a different way compared to the trap model.

Finally we analyzed the trap model using the Metropolis dynamic rule. We observed that in this case neither the way the weak ergodicity breaking is reached neither the arcsine law of aging are influenced by the change in the dynamic rule. Thanks to the second finding we can say that the trap model belongs to the universality class that shows the arcsine law of aging also in case of Metropolis dynamics.

Our results show that the arcsine law has a broader range of applicability than expected.

Chapter 7

Outlook

This last chapter is devoted to list some ideas for further developments of the topics discussed in this thesis.

In the first part of the thesis we have been able to measure a finite surface tension Y and find that it increases with lowering temperature. During our study of the surface tension we only measured the energy part of the interface cost completely disregarding the entropic contribution. It would be interesting to compute the full free-energy cost of the amorphous-amorpous interface. This could be achieved computing the vibrational entropy of the final inherent structure $\mathcal{C}^{IS}_{\alpha_{IS}\beta_{IS}}$. The interface free-energy would indicate whether in the Mosaic picture the value of θ is really 2. Moreover, in this way the actual surface tension value and its increase with decreasing temperature would be obtained. The distribution of the new surface tension results should be also compared to the smooth decay of the overlap in [35].

According to the Mosaic picture the cooperative correlation length ξ_c in glass-forming liquids obeys the relation

$$\xi_c = [Y/(TS_c)]^{1/(d-\theta)} \; . \tag{7.1}$$

This indicates that in the low temperature region, where $S_c \sim T - T_k$, we should have

$$\xi_c \sim (T - T_k)^{-1/(d-\theta)} \; . \tag{7.2}$$

On the other hand, the increase of the surface tension could cause a faster increase of the correlation length, at least not too far from T_c. With regard to this problem, it would be interesting to come back to the measure of the Mosaic correlation length in [34,35] to have an estimate of ξ_c at lower temperatures as to have a better defined trend of ξ_c with T. This could independently indicate the value of the exponent θ. However, for the binary soft sphere model, the crystallization of the system occurs just below the temperatures which have been already studied. At lower temperatures, different mixtures are required to avoid the crystal.

In the Mosaic theory, θ and ψ (which is the exponent ruling the power law of activation barriers with the excitation size) determine the slowing down of the dynamics: at low temperature the relaxation time is $\tau \sim \exp[A/(T - T_k)^{\psi/(d-\theta)}]$.

Determination of these two exponents is a widely debated problem. Adam, Gibbs, and Di Marzio suggested $\psi = 3$ in a picture where $\theta = 0$ by construction. Kirkpatrick, Thirumalai, and Wolynes, in the first version of the Mosaic theory, stuck to the nucleation paradigm and obtained $\psi = \theta$. Wolynes subsequently fixed $\theta = d/2$ by means of a renormalization group argument. In our work, we found $\theta = 2$ and $\psi = 1$. This result is in agreement with the Vogel-Fulcher-Tamman law. Yet, it does not fulfill the inequality $\theta \leq \psi$ of [36]. We think that this is due to the exponentially large number of paths in the phase space along which the system can decorrelate: according to this idea an entropic term should reduce the effective exponent ψ and leave unchanged θ. As reasonable as this idea may sound, it would be important to obtain other independent estimates of the exponents θ and ψ.

A recent idea by J. P. Bouchaud to determine θ and ψ is to look at the decrease of the energy of a glass-forming liquid after a quench from high ($T_i \gg T_c$) to low temperature ($T_f < T_c$). Since the surface tension is nonzero, if the Mosaic picture is valid a finite amount of the energy of the equilibrium configuration at T_f should derive from the interfaces between Mosaic tiles. Hence, if we abruptly decrease the temperature at $t = 0$, the transient to reach the low temperature equilibrium should be ruled by the formation and the enlarging of Mosaic tiles. In this picture the energy decrease would be ruled by the reduction of interfaces as the Mosaic cooperative regions grow in the system:

$$E(t;T) - E_{eq}(T) \sim Y(T)\xi(t)^{\theta} n(t) \tag{7.3}$$

where $n(t) = V/\xi(t)^d$ is the number of the cooperative regions at each time. Hence, the energy decrease depends on the increasing correlation length,

$$E(t;T) - E_{eq}(T) \sim Y(T)\xi(t)^{\theta-d} V \ . \tag{7.4}$$

Within the activation picture, we assume that the time scale for the formation of the tiles is exponential with $\xi(t)^{\psi}$. Thus we can write

$$\xi(t) \sim (T \log t)^{1/\psi} \ . \tag{7.5}$$

This implies that the decrease of the energy,

$$E(t;T) - E_{eq}(T) \sim Y(T)(T \log t)^{(\theta-d)/\psi} V \ , \tag{7.6}$$

is a power law of the logarithm of time with exponent $(\theta - d)/\psi$. Moreover, the transient during which the Mosaic tiles grow with time should stop when $\xi_c(T)$ is reached. Hence, in different thermal hisotries the energy decrease should collapse when plotted in terms of the rescaled variable $(T \log t)^{1/\psi}/\xi_c$ Hence, two pieces of information come from the fit of the energy decrease and from its collapse: the value of $(\theta - d)/\psi$ and the value of ψ. Hence θ and ψ can be obtained. This work is currently in progress.

In the second part of the thesis, studying the aging regime in different spin models, we showed that the applicability of the arcsine law is broader than what was expected. Yet, a difference between the REM-like trap model and the p-spin

model has emerged: they showed two different ways to reach the weak ergodicity breaking limit. It would be interesting to understand why this happens.

Further work, now in progress, aims at extending this aging paradigm to the p-spin model with Metropolis dynamics. If futher extension were confirmed, a very interesting development in this topic would be the search of the arcsine law directly in glass-forming liquids. According to the Mosaic picture, the mean-field paradigm is applicable to finite dimensional systems with N particles only on a local level. A single amorphous state can be defined for regions with length scale smaller than the cooperative length ξ_c. Hence, within these regions the off-equilibrium regime in real space could obey the mean-field paradigm of aging. This idea could be tested by looking for the arcsine law in aging of low temperature liquids with a rescaling of the time variable by a factor $\exp(\gamma\xi_c^d)$ instead of $\exp(\gamma N)$. For this study, the suitable cooperative length is the one already obtained in the equilibrium dynamics [35].

Bibliography

[1] D. Turnbull and J. C. Fisher. Rate of Nucleation in Condensed Systems. *J. Chem. Phys.*, 17:71–73, January 1949.

[2] D. Turnbull. Under What Conditions can a Glass be Formed? *Contemporary Physics*, 10:473, September 1969.

[3] A. Cavagna. Supercooled liquids for pedestrians. *Phys. Rep.*, 476:51–124, June 2009.

[4] A. W. Kauzmann. *Chem. Rev.*, 43:219–256, March 1948.

[5] A. Cavagna, A. Attanasi, and J. Lorenzana. Viscoelasticity and Metastability Limit in Supercooled Liquids. *Phys. Rev. Lett.*, 95(11):115702, September 2005.

[6] A. Attanasi, A. Cavagna, and J. Lorenzana. Elasticity and metastability limit in supercooled liquids: a lattice model. *Philosophical Magazine*, 87:441–448, 2007.

[7] P. G. Debenedetti. *Metastable liquids: Concepts and Principles*. Princeton University Press, 1997.

[8] W. Kob. Supercooled liquids, the glass transition, and computer simulations. *ArXiv Condensed Matter e-prints*, arXiv:cond-mat/0212344, 2002.

[9] R. Richert and C. A. Angell. Dynamics of glass-forming liquids. V. On the link between molecular dynamics and configurational entropy. *J. Chem. Phys.*, 108:9016–9026, June 1998.

[10] T. Geszti. *J. Phys. C. Sol. State Phys.*, 16:5805, 1983.

[11] W. Kob and H. C. Andersen. Scaling behavior in the β-relaxation regime of a supercooled Lennard-Jones mixture. *Physical Review Letters*, 73:1376–1379, September 1994.

[12] W. Kob and H. C. Andersen. Testing mode-coupling theory for a supercooled binary Lennard-Jones mixture I: The van Hove correlation function. *Phys. Rev. E*, 51:4626–4641, May 1995.

[13] W. Kob and H. C. Andersen. Testing mode-coupling theory for a supercooled binary Lennard-Jones mixture. II. Intermediate scattering function and dynamic susceptibility. *Phys. Rev. E*, 52:4134–4153, October 1995.

[14] W. Götze. Recent tests of the mode-coupling theory for glassy dynamics. *Journal of Physics Condensed Matter*, 11:A1–A45, March 1999.

[15] J. H. Gibbs and E. A. Dimarzio. Nature of the Glass Transition and the Glassy State. *J. Chem. Phys*, 28:373–383, March 1958.

[16] G. Adam and J. H. Gibbs. On the Temperature Dependence of Cooperative Relaxation Properties in Glass-Forming Liquids. *J. Chem. Phys*, 43:139–146, July 1965.

[17] M. Goldstein. Viscous Liquids and the Glass Transition: A Potential Energy Barrier Picture. *J. Chem. Phys.*, 51:3728–3739, November 1969.

[18] T. B. Schrøder, S. Sastry, J. C. Dyre, and S. C. Glotzer. Crossover to potential energy landscape dominated dynamics in a model glass-forming liquid. *J. Chem. Phys.*, 112:9834–9840, June 2000.

[19] Sokolov. *J. Non-Cryst. Solids.*, 190:235–237, June 1999.

[20] T. Castellani and A. Cavagna. Spin-glass theory for pedestrians. *Journal of Statistical Mechanics: Theory and Experiment*, 5:12, May 2005.

[21] J. Kurchan and L. Laloux. Phase space geometry and slow dynamics. *Journal of Physics A Mathematical General*, 29:1929–1948, May 1996.

[22] A. Cavagna, I. Giardina, and G. Parisi. Role of saddles in mean-field dynamics above the glass transition. *Journal of Physics A Mathematical General*, 34:5317–5326, July 2001.

[23] A. Cavagna, I. Giardina, and T. S. Grigera. A single saddle model for the bgr-relaxation in supercooled liquids. *Journal of Physics A Mathematical General*, 36:10721–10737, October 2003.

[24] T. S. Grigera. Geometrical properties of the potential energy of the soft-sphere binary mixture. *J. Chem. Phys.*, 124(6):064502, February 2006.

[25] K. Broderix, K. K. Bhattacharya, A. Cavagna, A. Zippelius, and I. Giardina. Energy Landscape of a Lennard-Jones Liquid: Statistics of Stationary Points. *Physical Review Letters*, 85:5360–5363, December 2000.

[26] T. S. Grigera, A. Cavagna, I. Giardina, and G. Parisi. Geometric Approach to the Dynamic Glass Transition. *Physical Review Letters*, 88(5):055502, February 2002.

[27] M. Mézard and G. Parisi. Thermodynamics of Glasses: A First Principles Computation. *Physical Review Letters*, 82:747–750, January 1999.

[28] B. Coluzzi, M. Mézard, G. Parisi, and P. Verrocchio. Thermodynamics of binary mixture glasses. *J. Chem. Phys.*, 111:9039–9052, November 1999.

[29] B. Coluzzi, G. Parisi, and P. Verrocchio. Lennard-Jones binary mixture: A thermodynamical approach to glass transition. *J. Chem. Phys.*, 112:2933–2944, February 2000.

[30] T. R. Kirkpatrick, D. Thirumalai, and P. G. Wolynes. Scaling concepts for the dynamics of viscous liquids near an ideal glassy state. *Phys. Rev. A*, 40:1045–1054, July 1989.

[31] K. Binder. Theory of first-order phase transitions. *Reports on Progress in Physics*, 50:783–859, July 1987.

[32] J.-P. Bouchaud and G. Biroli. On the Adam-Gibbs-Kirkpatrick-Thirumalai-Wolynes scenario for the viscosity increase in glasses. *J. Chem. Phys.*, 121:7347–7354, October 2004.

[33] T. S. Grigera and G. Parisi. Fast Monte Carlo algorithm for supercooled soft spheres. *Phys. Rev. E*, 63(4):045102, April 2001.

[34] A. Cavagna, T. S. Grigera, and P. Verrocchio. Mosaic Multistate Scenario Versus One-State Description of Supercooled Liquids. *Physical Review Letters*, 98(18):187801, May 2007.

[35] G. Biroli, J.-P. Bouchaud, A. Cavagna, T. S. Grigera, and P. Verrocchio. Thermodynamic signature of growing amorphous order in glass-forming liquids. *Nature Physics*, 4:771–775, October 2008.

[36] D. S. Fisher and D. A. Huse. Equilibrium behavior of the spin-glass ordered phase. *Phys. Rev. B*, 38:386–411, July 1988.

[37] C. Cammarota and A. Cavagna. A novel method for evaluating the critical nucleus and the surface tension in systems with first order phase transition. *J. Chem. Phys.*, 127(21):214703, December 2007.

[38] F. Thalmann. Note on the role of the dimensionality in the structural glass transition. *J. Chem. Phys.*, 116:3378–3383, February 2002.

[39] C. Cammarota, A. Cavagna, G. Gradenigo, T. S. Grigera, and P. Verrocchio. Surface tension fluctuations and a new spinodal point in glass-forming liquids. *ArXiv e-prints*, arXiv:0904.1522, 2009.

[40] C. Cammarota, A. Cavagna, G. Gradenigo, T. S. Grigera, and P. Verrocchio. Numerical determination of the exponents controlling the relationship between time, length and temperature in glass-forming liquids. *J. Chem. Phys.*, 131(19):194901, November 2009.

[41] J. D. Stevenson and P. G. Wolynes. A universal origin for secondary relaxations in supercooled liquids and structural glasses. *ArXiv e-prints*, arXiv:0905.2152, 2009.

[42] F. H. Stillinger and T. A. Weber. Packing Structures and Transitions in Liquids and Solids. *Science*, 225:983–989, September 1984.

[43] S. Sastry, P. G. Debenedetti, and F. H. Stillinger. Signatures of distinct dynamical regimes in the energy landscape of a glass-forming liquid. *Nature*, 393:554–557, June 1998.

[44] D. C. Liu and J. Nocedal. On the limited memory BFGS method for large scale optimization. *Math. Programming*, 45:503–528, 1989.

[45] B. Bernu, Y. Hiwatari, and J. P. Hansen. A molecular dynamics study of the glass transition in binary mixtures of soft spheres. *Journal of Physics C Solid State Physics*, 18:L371–L376, May 1985.

[46] B. Bernu, J. P. Hansen, Y. Hiwatari, and G. Pastore. Soft-sphere model for the glass transition in binary alloys: Pair structure and self-diffusion. *Phys. Rev. A*, 36:4891–4903, November 1987.

[47] H. Miyagawa, Y. Hiwatari, B. Bernu, and J. P. Hansen. Molecular dynamics study of binary soft-sphere mixtures: Jump motions of atoms in the glassy state. *J. Chem. Phys.*, 88:3879–3886, March 1988.

[48] J. N. Roux, J. L. Barrat, and J.-P. Hansen. Dynamical diagnostics for the glass transition in soft-sphere alloys. *Journal of Physics Condensed Matter*, 1:7171–7186, October 1989.

[49] G. Parisi. Off-Equilibrium Fluctuation-Dissipation Relation in Fragile Glasses. *Physical Review Letters*, 79:3660–3663, November 1997.

[50] J.-P. Hansen and I. R. McDonald. *Theory of simple liquids*. Academic Press, 1976.

[51] Y. Imry and S.-K. Ma. Random-Field Instability of the Ordered State of Continuous Symmetry. *Physical Review Letters*, 35:1399–1401, November 1975.

[52] T. Halpin-Healy and Y. Zhang. Kinetic roughening phenomena, stochastic growth, directed polymers and all that. Aspects of multidisciplinary statistical mechanics. *Phys. Rept.*, 254:215–414, March 1995.

[53] G. Navasques. Liquid surfaces: theory of surface tension. *Rep. Prog. Phys.*, 42:1131–1186, 1979.

[54] M. P. A. Fisher and M. Wortis. Curvature corrections to the surface tension of fluid drops: Landau theory and a scaling hypothesis. *Phys. Rev. B*, 29:6252–6260, June 1984.

[55] X. Xia and P. G. Wolynes. Fragilities of liquids predicted from the random first order transition theory of glasses. *Proceedings of the National Academy of Science*, 97:2990–2994, March 2000.

[56] M. Dzero, J. Schmalian, and P. G. Wolynes. Activated events in glasses: The structure of entropic droplets. *Phys. Rev. B*, 72(10):100201, September 2005.

[57] S. Franz. First steps of a nucleation theory in disordered systems. *Journal of Statistical Mechanics: Theory and Experiment*, 4:1, April 2005.

[58] D. A. Huse and C. L. Henley. Pinning and roughening of domain walls in Ising systems due to random impurities. *Phys. Rev. Lett.*, 54:2708–2711, June 1985.

[59] E. T. Seppälä, M. J. Alava, and P. M. Duxbury. Extremal statistics in the energetics of domain walls. *Phys. Rev. E*, 63(6):066110, June 2001.

[60] K. P. J. Kytölä, E. T. Seppälä, and M. J. Alava. Elastic manifolds in disordered environments: Energy statistics. *Europhysics Letters*, 62:35–41, April 2003.

[61] P. Réfrégier, E. Vincent, J. Hammann, and M. Ocio. Ageing phenomena in a spin-glass : effect of temperature changes below Tg. *Journal de Physique*, 48(9):1533–1539, 1987.

[62] L. Berthier and A. P. Young. Temperature cycles in the Heisenberg spin glass. *Phys. Rev. B*, 71(21):214429, June 2005.

[63] M. Mezard and G. Parisi. *Spin Glass Theory and Beyond*. World Scientific Publishing Company, 1987.

[64] E. Vincent, J. Hammann, M. Ocio, J.-P. Bouchaud, and L. F. Cugliandolo. Slow dynamics and aging in spin glasses. In M. Rubí & C. Pérez-Vicente, editor, *Lecture Notes in Physics, Berlin Springer Verlag*, volume 492 of *Lecture Notes in Physics, Berlin Springer Verlag*, page 184, 1997.

[65] D. S. Fisher and D. A. Huse. Nonequilibrium dynamics of spin glasses. *Phys. Rev. B*, 38:373–385, July 1988.

[66] G. Koper and H. Hilhorst. A domain theory for linear and nonlinear aging effects in spin glasses. *J. Phys. France*, 49:429–443, March 1988.

[67] K. H. Hoffmann and P. Sibani. Diffusion in hierarchies. *Phys. Rev. A*, 38:4261–4270, October 1988.

[68] P. Sibani and K. H. Hoffmann. Hierarchical models for aging and relaxation of spin glasses. *Physical Review Letters*, 63:2853–2856, December 1989.

[69] J. P. Bouchaud. Weak ergodicity breaking and aging in disordered systems. *Journal de Physique I*, 2:1705–1713, September 1992.

[70] J.-P. Bouchaud and D. S. Dean. Aging on Parisi's Tree. *Journal de Physique I*, 5:265–286, March 1995.

[71] L. F. Cugliandolo and J. Kurchan. Analytical solution of the off-equilibrium dynamics of a long-range spin-glass model. *Physical Review Letters*, 71:173–176, July 1993.

[72] L. F. Cugliandolo, J. Kurchan, and F. Ritort. Evidence of aging in spin-glass mean-field models. *Phys. Rev. B*, 49:6331–6334, March 1994.

[73] L. F. Cugliandolo and J. Kurchan. On the out-of-equilibrium relaxation of the Sherrington-Kirkpatrick model. *Journal of Physics A Mathematical General*, 27:5749–5772, September 1994.

[74] B. Drossel and M. Kardar. Scaling of energy barriers for flux lines and other random systems. *Phys. Rev. E*, 52:4841–4852, November 1995.

[75] J.-P. Bouchaud and M. Mézard. Universality classes for extreme-value statistics. *Journal of Physics A Mathematical General*, 30:7997–8015, December 1997.

[76] B. Derrida. Random-Energy Model: Limit of a Family of Disordered Models. *Physical Review Letters*, 45:79–82, July 1980.

[77] G. Ben Arous and J. Černý. The arcsine law as a universal aging scheme for trap models. *Comm. Pure Appl. Math.*, 61(3):289–329, 2008.

[78] G. Ben Arous, A. Bovier, and V. Gayrard. Glauber dynamics of the random energy model. I. Metastable motion on the extreme states. *Comm. Math. Phys.*, 235(3):379–425, 2003.

[79] G. Ben Arous, A. Bovier, and V. Gayrard. Glauber dynamics of the random energy model. II. Aging below the critical temperature. *Comm. Math. Phys.*, 236(1):1–54, 2003.

[80] G. Ben Arous, A. Bovier, and V. Gayrard. Aging in the Random Energy Model. *Physical Review Letters*, 88(8):087201, February 2002.

[81] G. Ben Arous, A. Bovier, and J. Černý. Universality of the REM for dynamics of mean-field spin glasses. *Comm. Math. Phys.*, 282(3):663–695, 2008.

[82] G. Ben Arous, A. Bovier, and J. Černý. Universality of random energy model-like ageing in mean field spin glasses. *J. Stat. Mech. Theory Exp.*, (4):L04003, 8, 2008.

[83] A. Billoire, L. Giomi, and E. Marinari. The mean-field infinite range p = 3 spin glass: Equilibrium landscape and correlation time scales. *Europhysics Letters*, 71:824–830, September 2005.